5D

PNL-2850 A3

UC-11

Pacific Northwest Laboratory Annual Report for 1978 to the DOE Assistant Secretary for Environment

Part 3 Atmospheric Sciences February 1979

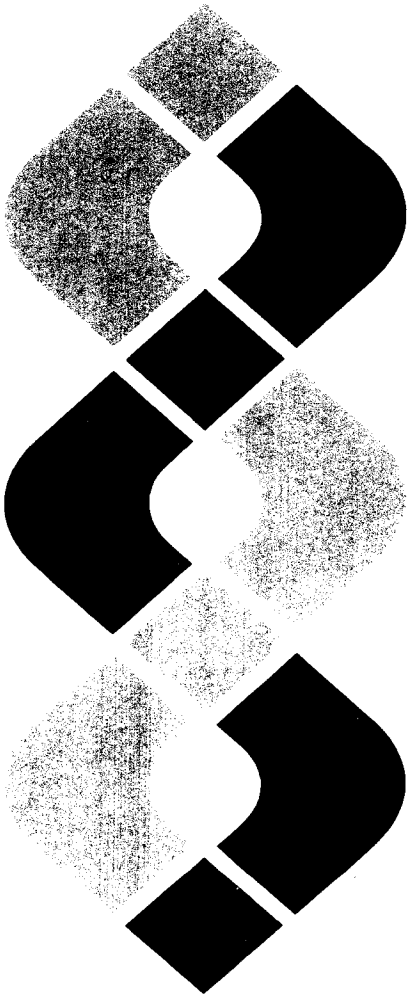

Prepared for the U.S. Department of Energy
under Contract EY-76-C-06-1830

Pacific Northwest Laboratory
Operated for the U.S. Department of Energy
by Battelle Memorial Institute

Battelle

PNL-2850

NOTICE

This report was prepared as an account of work sponsored by the United States Government. Neither the United States nor the Department of Energy, nor any of their employees, nor any of their contractors, subcontractors, or their employees, makes any warranty, express or implied, or assumes any legal liability or responsibility for the accuracy, completeness or usefulness of any information, apparatus, product or process disclosed, or represents that its use would not infringe privately owned rights.

The views, opinions and conclusions contained in this report are those of the contractor and do not necessarily represent those of the United States Government or the United States Department of Energy.

PACIFIC NORTHWEST LABORATORY
operated by
BATTELLE
for the
UNITED STATES DEPARTMENT OF ENERGY
Under Contract EY-76-C-06-1830

Printed in the United States of America
Available from
National Technical Information Service
United States Department of Commerce
5285 Port Royal Road
Springfield, Virginia 22151

Price: Printed Copy $____*; Microfiche $3.00

*Pages	NTIS Selling Price
001-025	$4.00
026-050	$4.50
051-075	$5.25
076-100	$6.00
101-125	$6.50
126-150	$7.25
151-175	$8.00
176-200	$9.00
201-225	$9.25
226-250	$9.50
251-275	$10.75
276-300	$11.00

PNL-2850 PT3
UC-11

3 3679 00047 9198

Pacific Northwest Laboratory Annual Report for 1978 to the DOE Assistant Secretary for Environment

Part 3 Atmospheric Sciences

C. L. Simpson and Staff Members
of Pacific Northwest Laboratory

February 1979

Prepared for
the U.S. Department of Energy
under Contract EY-76-C-06-1830

Pacific Northwest Laboratory
Richland, Washington 99352

PREFACE

The 1978 Annual Report from Pacific Northwest Laboratory (PNL) to the DOE Assistant Secretary for Environment is the first report covering a full year's work under the Department of Energy since it came into existence on October 1, 1977. Most of the research conducted during this period and described in this report was begun under the Energy Research and Development Administration or its predecessor agency, the Atomic Energy Commission. However, several new projects have enhanced the PNL emphasis on environment, health and safety research in the area of synthetic fuels. Preliminary reports on these efforts are spread throughout the five parts of this annual report.

The five parts of the report are oriented to particular segments of our program. Parts 1-4 report on research performed for the DOE Office of Health and Environmental Research. Part 5 reports progress on all other research performed for the Assistant Secretary for Environment including the Office of Technology Impacts and the Office of Environmental Compliance and Overview.

Each part consists of project reports authored by scientists from several PNL research departments, reflecting the interdisciplinary nature of the research effort. Parts 1-4 are organized primarily by energy technology, although it is recognized that much of the research performed at PNL is applicable to more than one energy technology.

The parts of the 1978 Annual Report are:

Part 1: Biomedical Sciences		
	Program Manager - W. R. Wiley	D. L. Felton, Editor
Part 2: Ecological Sciences		
	Program Manager - B. E. Vaughan	B. E. Vaughan, Report Coordinator C. H. Connally, Editor
Part 3: Atmospheric Sciences		
	Program Manager - C. L. Simpson	R. L. Drake, Report Coordinator P. R. Partch/C. M. Gilchrist, Editors
Part 4: Physical Sciences		
	Program Manager - J. M. Nielsen	J. M. Nielsen, Report Coordinator J. S. Burlison, Editor

Part 5: Environmental Assessment, Control,
Health and Safety.

Program Managers - N. E. Carter
D. B. Cearlock
D. L. Hessel
S. Marks — W. J. Bair, Report Coordinator
C. M. Unruh — R. W. Baalman, Editor

Activities of the scientists whose work is described in this annual report are broader in scope than the articles indicate. PNL staff have responded to numerous requests from DOE during the year for planning, for service on various task groups, and for special assistance.

Credit for this annual report goes to many scientists who performed the research and wrote the individual project reports, to the program managers who directed the research and coordinated the technical progress reports, to the editors who edited the individual project reports and assembled the five parts, and to Dr. Ray Baalman, editor in chief, who directed the total effort.

W. J. Bair, Manager
S. Marks, Associate Manager
Environment, Health and Safety Research Program

Previous Reports in this Series:

Annual Report for	
1951	W-25021, HW-25709
1952	HW-27814, HW-28636
1953	HW-30437, HW-30464
1954	HW-30306, HW-33128, HW-35905, HW-35917
1955	HW-39558, HW-41315, HW-41500
1956	HW-47500
1957	HW-53500
1958	HW-59500
1959	HW-63824, HW-65500
1960	HW-69500, HW-70050
1961	HW-72500, HW-73337
1962	HW-76000, HW-77609
1963	HW-80500, HW-81746
1964	BNWL-122
1965	BNWL-280, BNWL-235, Vol. 1-4, BNWL-36I
1966	BNWL-480, Vol. 1, BNWL-481, Vol. 2, Pt 1-4
1967	BNWL-714, Vol. 1, BNWL-715, Vol. 2, Pt 1-4
1968	BNWL-1050, Vol. 1, Pt. 1-2, BNWL-1051, Vol. 2, Pt. 1-3
1969	BNWL-1306, Vol. 1, Pt. 1-2, BNWL-1307, Vol. 2, Pt. 1-3
1970	BNWL-1550, Vol. 1, Pt. 1-2, BNWL-1551, Vol. 2, Pt. 1-2
1971	BNWL-1650, Vol. 1, Pt. 1-2, BNWL-1651, Vol. 2, Pt. 1-2
1972	BNWL-1750, Vol. 1, Pt. 1-2, BNWL-1751, Vol. 2, Pt. 1-2
1973	BNWL-1850, Pt. 1-4
1974	BNWL-1950, Pt. 1-4
1975	BNWL-2000, Pt. 1-4
1976	BNWL-2100, Pt. 1-5
1977	PNL-2500, Pt. 1-5

FOREWORD

The goals of atmospheric research at Pacific Northwest Laboratory (PNL) are to assess, describe and predict the nature and fate of atmospheric pollution and to study the impacts of pollutants on local, regional and global climates. The pollutants being investigated are those resulting from the development and use of four energy resources: coal, gas, oil and nuclear power. In the course of this research, investigative tools are also being developed and atmospheric assessments are being made that will contribute to the development of environmentally sound oil shale, solar and fusion energy resources.

COAL, GAS AND OIL COMBUSTION

The behavior of air pollution resulting from fossil-fuel power plants is being explained. Involved in making this explanation are these factors: the type of pollutants emitted, their transport and diffusion in the air, their physical and chemical transformations during transport, their removal by wet and dry scavenging processes, and their impacts on climate, bodies of water and living species. Since the result of the current and projected coal utilization is the release of large quantities of sulfur dioxide to the atmosphere, current atmospheric research is being conducted primarily in the Multi-State Atmospheric Power Production Pollutant Studies (MAP3S).

FISSION AND FUSION

Concern about long-lived particulates (i.e., plutonium and other radionuclides) released to the environment from fission and fusion plants indicates that the deposition and resuspension of these substances must be studied. For example, because the primary hazard from plutonium is inhalation, its residence in the atmosphere must be clearly defined. Current research, therefore, is evaluating the removal of particulates from the atmosphere by deposition (which limits initial exposure) and any future resuspension from the surface (which continues the potential for inhalation). In addition, the local and regional environmental impacts of pollutant releases from large energy centers (several power plants in close proximity) are being assessed.

OIL SHALE

The mountainous oil shale regions of Colorado, Utah and Wyoming present a particularly difficult air pollution problem because air may be trapped in the valleys of these regions for extended periods of time under certain meteorological conditions. Especially stringent siting requirements, therefore, must be fulfilled to meet State and Federal air quality standards. Adequate models and field measurements of the complex airflow and dispersion conditions in this complex area are not available; they must be developed to assure acceptable siting of oil shale facilities. PNL has undertaken the assessment of the requirements for the proper modeling activities and field measurement programs that will contribute to this very important area of research, as well as to the development of solar and geothermal energy.

The description of atmospheric research at PNL is organized in terms of energy technologies:

- Coal, Gas and Oil
- Fission and Fusion
- Oil Shale

This report describes the progress in FY-1978 for each of these technologies. A divider page summarizes the goals of each area and lists project 189 titles that fund research in the technology as bulleted items.

R. L. Drake
Program Coordinator

CONTENTS

(Listing in parenthesis denotes the sponsoring programs under which the research was done)

1.0 Coal, Gas and Oil

COAL, GAS AND OIL

- **Aerosol and Trace Gas Transformations**
- **Precipitation Scavenging in MAP3S**
- **MAP3S Modeling Studies**
- **Regional Studies**
- **Atmospheric Boundary Layer Studies**
- **Coal Conversion Pollutant Chemistry**
- **DOE/RL Special Studies**

As the use of fossil fuels (especially coal) as an energy source increases, so too will air pollutants, such as sulfur and nitrogen compounds and trace metals, produced by the combustion of these fuels. The analysis of the fate of these pollutants from source to receptor is most urgent so that the nation's energy plan can proceed efficiently and be environmentally sound.

The research activities at PNL are basically related to the MAP3S Program being conducted in the Northeast Quadrant of the United States. They include the data analysis and flight operations based at Muskegon, Michigan; the precipitation chemistry network in the eastern mountains, midwestern plains and coastal areas; the incloud scavenging studies over Lake Michigan; the laboratory analysis of sulfur and nitrogen compounds and trace metals at Hanford; and the trajectory modeling studies being formulated at Hanford. In addition to this work, PNL is conducting extensive field and modeling studies concerned with the diffusion, transformation and deposition of pollutants. The field activities are being conducted in the Milwaukee and Chicago areas, as well as in the Northwest and other areas in the Midwest. The results from the MAP3S and related activities will contribute to our ability to assess the impacts of the country's energy plan.

PNL's field work also includes several studies of the deposition of ozone and respirable and nonrespirable particles. These field studies are leading to an improved formulation for the dry deposition velocity of both gases and particles.

A series of theoretical laboratory tests were conducted during FY-1978 to improve our airborne and ground-based capabilities to measure low concentrations of chemical elements and compounds. For example, the use of ion chromatography for trace element analysis was greatly improved. In addition, the standard NO/NO_x monitor for aircraft research was vastly improved, while an analytical procedure for the determination of C_2 to C_6 hydrocarbons in ambient air was developed.

POLLUTANT TRANSFORMATIONS OVER LAKE MICHIGAN

A. J. Alkezweeny, D. R. Arbuthnot, K. M. Busness,
R. C. Easter, J. M. Hales, R. N. Lee and J. M. Young

An aircraft, a chartered boat, and a constant altitude balloon were used to study pollutant transformations over Lake Michigan in a Lagrangian frame of reference. The experiments were conducted during the summer under strong atmospheric stability where diffusion and dry deposition of pollutants can be neglected.

Since 1976, Pacific Northwest Laboratory (PNL) has been conducting field experiments over Lake Michigan to study the rates and mechanisms of secondary pollutant formations in the Chicago and Milwaukee plumes. Emphasis is placed on the conversion of SO_2 to sulfate. The ultimate goal of the study is to provide parameterized input for use by the Multi-State Atmospheric Power Production Pollutant Studies (MAP3S) modeling community.

During the daylight hours of summer, the surface water temperature of Lake Michigan is usually well below the ambient air temperature. The lake's cooling effect along with the drastic reduction in surface roughness stabilizes off-shore flow, inhibits turbulent mixing and produces nearly laminar flow. Under such conditions, dry deposition and diffusion become very small and can be neglected. Therefore, the changes in the concentrations of reactive species in the main body of the mixing layer should be primarily due to chemical reactions, making it far simpler to determine the rates of these reactions.

During the summer of 1978, several Lagrangian experiments were conducted using the PNL DC-3 aircraft, a chartered boat and a constant level balloon (tetroon). Measurements were made on days during which high-pressure circulation determined the transport winds. A subsidence inversion was usually associated with the synoptic high, and surface flow was generally light with a southwesterly component. Particular emphasis was given to days on which air stagnation occurred.

During the mornings, the boat was used to transport an inflated tetroon to a position downwind of either Milwaukee or Chicago. The release was on the basis of observed and predicted winds in the mixed layer. The DC-3 later took off and rendezvoused with the boat at the selected location. When visual contact between the boat and the aircraft was achieved, a tetroon, balanced to rise to about 500 ft agl, was released from the boat. The boat then followed behind the balloon while collecting samples for SO_2, nitrate, ammonium, and ammonia analysis. In addition, O_3, SO_2, NO/NO_x, light scattering, particle concentration, and aircraft location (longitude, latitude) were measured in real time and recorded on magnetic tape. The aircraft sampling route consisted of 10-mile transects, perpendicular to the tetroon trajectory and at about tetroon altitude. The DC-3 passed over the boat at the middle of each transect.

Figure 1.1 shows a typical tetroon trajectory, which was made on September 6, 1978. Each cross represents the tetroon location at the moment the aircraft crossed its path. Superimposed on the figure are the surface wind speeds and directions reported by several stations around the lake.

Data recorded on magnetic tape and samples collected on filters are being analyzed and results will be reported. The data-processing capabilities at the PNL Muskegon facility have been substantially improved over the past year. An asynchronous hardwire communications link was constructed to enable transfer of data from the aircraft system (seven-track magnetic tape) to the laboratory computer. Enhancements in both hardware and software for the laboratory minicomputer have enabled much of the necessary data reduction and analysis to be performed onsite.

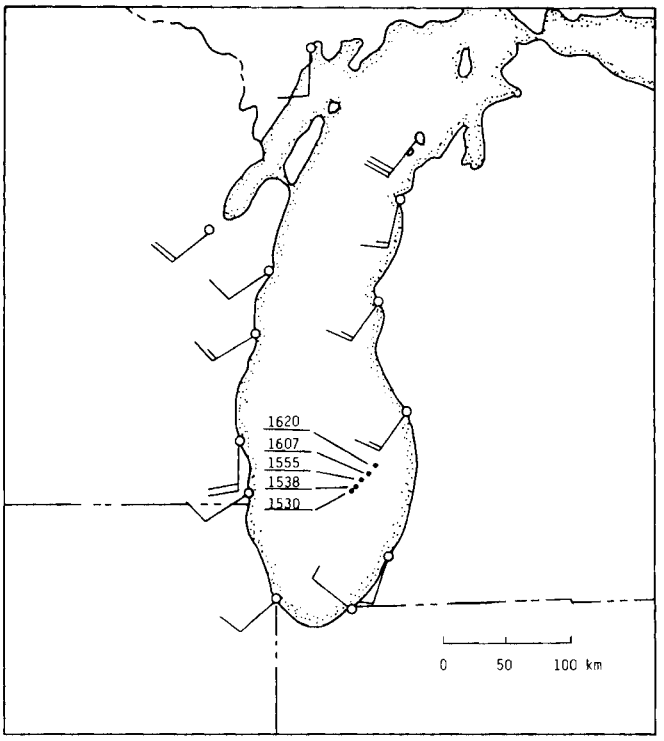

(Neg. 78 B 831-1)

FIGURE 1.1. Lake Shore Winds and Tetroon Trajectory for September 6, 1978, 1400 EDT.

AEROSOL FORMATION IN URBAN PLUMES OVER LAKE MICHIGAN

D. F. Miller[a] and A. J. Alkezweeny

To determine the oxidation rates of SO_2 to sulfate in urban plumes, data from three field experiments, conducted over Lake Michigan, were analyzed and interpreted, using a photochemical smog model. A maximum rate of 4 to 6%/hr was found, and it appeared to occur around noon. Using conservative estimates for the rates of the SO_2 reactions with free radicals, the model predicted maximum rates of 4 to 5%/hr. According to the modeling results, OH and RO_2 radicals were each responsible for about 40% of the oxidation during midday, while HO_2 contributed about 20%.

During the past three years, several field experiments have been conducted over Lake Michigan. In these experiments, the oxidation rates of SO_2 to sulfate in urban plumes were studied, using instrumented aircraft and boats. A sampling program was designed to determine changes with time in the concentrations of sulfate and several reactive species, such as SO_2, NO_x, O_3 and non-methane hydrocarbons (NMHC). The transformation of SO_2 to sulfate has been interpreted using a chemical kinetics code, which was devised to simulate the photochemical reactions

(a) Battelle Columbus Laboratories

believed to have occurred during the sampling period. Only three experiments were analyzed in detail: two involved measurements within the Milwaukee urban plume as it moved eastward across the lake; the third used an urban air mass that passed through Muskegon, Michigan and moved inland in a northeasterly direction.

The SO_2 oxidation rates in the urban plumes were found to be different during these experiments despite similar ozone levels (ranging from 70 to 115 ppb). The maximum rate was 4 to 6%/hr, and it appeared to occur around noon. Using the measured NMHC levels of 0.12 to 0.32 ppmc and conservative estimates for the rates of SO_2 reactions with free radicals, the kinetic simulation of the events predicted maximum rates of 4 to 5%/hr. According to the modeling results, OH and RO_2 radicals were each responsible for about 40% of the oxidation during midday, while HO_2 contributed about 10%.

During one of the experiments in which the Milwaukee plume moved over the lake, the SO_2 oxidation rate in the afternoon was moderate (2%/hr), but the O_3 concentration was quite high (about 100 ppb). The lower-than-maximum oxidation rate accompanied by high ozone has been interpreted as characteristic of a plume's age. Based on these modeling results, when an urban air mass is well aged, the more reactive hydrocarbons seem to be spent, the NO_x levels to be reduced, and most of the SO_2 oxidation to proceed via the peroxy radical (HO_2, RO_2). However, if an influx of primary pollutants, such as NO, occurs, the potential exists for regeneration of OH and for the oxidation rates of hydrocarbons and SO_2 eventually to increase. This explanation accounts for both the increase rate of SO_2 oxidation and the "ozone bulge" that were observed in the path of a power-plant plume within Milwaukee's urban plume.

Using a chemical kinetics code, the model predicted that for SO_2 released at sunup, the conversion to sulfate throughout the day would amount to 25%, assuming zero loss of SO_2 by deposition.

Given the results discussed above, other mechanisms of SO_2 removal seem to be important in limiting the lifetime of SO_2, even in polluted air. Estimates using models are only crude; for better estimates of the factors controlling SO_2 oxidation, the concentration of free radicals directly responsible for the conversion must be monitored.

PNL AIRCRAFT MEASUREMENTS IN THE AMBIENS STUDY

J. M. Hales, R. N. Lee and A. J. Alkezweeny

This report presents a brief description of the Atmospheric Mass Balance Industrial Emitted and National Sulfur (AMBIENS) field study, which was performed in central Indiana during October of 1977. Special emphasis is placed on a description of the Pacific Northwest Laboratory (PNL) aircraft operations.

The AMBIENS field study was a joint laboratory effort conducted under sponsorship of the Multi-State Atmospheric Power Production Pollutant Study (MAP3S). Performed in central Indiana during October of 1977, this project was based conceptually upon a material balance over an area comparable in size to a grid element of typical Eulerian regional pollution models (roughly 100 by 100 km). The various participating groups and their primary functions were as follows: Argonne National Laboratory was responsible for boundary-layer and windfield analysis, dry deposition, and project coordination; Brookhaven National Laboratory for aircraft operations, tracer release and analysis; Pacific Northwest Laboratory for aircraft operations and dry deposition; Stanford Research Institute for lidar operations; and Environmental Measurements, Inc., for correlation spectroscopy (SO_2).

The overall objective of the study was to perform a detailed analysis of atmospheric transport and deposition phenomena to provide the modeling community with information for developing subgrid parameterization techniques. Of particular interest was the subgrid temporal and spatial variability of pollutant concentration. The central Indiana location was chosen for this study because of its flat terrain and absence of local pollution sources, which provided the simplest possible grid element for initial analysis.

The primary objective of the PNL aircraft operation at AMBIENS was to document spatial and temporal characteristics of pollution as it entered and left the grid area. Flights were coordinated closely with the primary Brookhaven aircraft,[a] which flew interlocking patterns with PNL at grid-area boundaries.

Typically, the AMBIENS Control-Center personnel, who performed area forecasts and defined the position of the study element for a given meteorological situation, initiated an experiment. The aircraft performed initial soundings and then flew constant-altitude tracks across the inflow region at various altitudes, which were selected to maximize coverage within the constraints of time and measurement capability. Aircraft measurements included SO_2, O_3, NO/NO_x aerosol light-scattering and size parameters, sulfate and trace elements.

On the basis of wind-transport calculations, the Control Center would determine a time when aircraft would be directed to the outflow area of the grid element and cross-sectional sampling performed. An experiment ended, depending on transport calculations and fuel resources of the aircraft.

A total of four significant budget analyses were performed during the AMBIENS study. Data from these flights are currently being processed for publication.

SUMMARY OF THE PNL AIRCRAFT FLIGHTS DURING THE MAP3S-SURE COOPERATIVE PROGRAM FOR SUMMER 1978

A. J. Alkezweeny, D. R. Arbuthnot,
K. M. Busness, R. C. Easter, and R. N. Lee

A summary of the Pacific Northwest Laboratory (PNL) aircraft flights, which were part of the Sulfur Regional (SURE) Intensive Experiment, conducted during the summer of 1978, is presented, and some preliminary measurement results are reported. The PNL DC-3 and Cessna 411 research aircraft were used on two consecutive days during the experiment to measure regional-scale pollutant problems over the Ohio Valley.

Pacific Northwest Laboratory's (PNL) regional flights during the SURE Intensive Experiment (July 19-20, 1978), which is part of the Multi-State Atmospheric Power Production Pollutant Studies (MAP3S)-SURE cooperative program, were directed at pollutant transport in the Ohio Valley, when mixing-layer winds under the influence of an anticyclone were channeled between a northeast-to-southwest-oriented cold front and the Appalachian Mountain Range. Two aircraft were used in this study: the PNL DC-3 and the Cessna 411. The equipment carried aboard the DC-3 and Cessna 411 and the parameters for which the equipment was used are given in Tables 1.1 and 1.2 respectively. The data from the real-time instrumentation were digitized onboard the aircraft and written onto magnetic tapes.

Figures 1.2 and 1.3 illustrate the two aircraft routes on July 19 and 20, respectively. Each figure includes the time of arrival at each location and the sites of the aircraft spirals. Both aircraft maintained a constant height within the mixing layer during the sampling flights except to accomodate changes in topography. Vertical profiles were obtained at several places along the flight routes by spiraling the aircraft through the boundary layer.

Processing of the magnetic tapes and chemical analysis of the exposed filters from both aircraft are currently underway, and the results of the flights will be reported in detail at a later date. Strip-chart records have been analyzed and have yielded the preliminary observations noted in the following paragraphs.

Early on July 19, the tops of the mixing layers over Fort Wayne, Indiana, and Duncan Falls, Ohio, were about 3500 ft; however, a second spiral over Duncan Falls, taken about 1-1/2 hr later, indicated that the top of the mixing layer had risen to about

(a) A second aircraft was operated by Brookhaven for tracer analysis.

4500 ft MSL. These levels were estimated from the change in the aerosol vertical profiles. In general, the ozone-mixing ratio ranged between 80 and 100 ppb and decreased to about 40 ppb above the mixing layer; although in the Lewisburg, West Virginia area, the ozone level was about 60 ppb. The light-scattering coefficient ranged from 1 to 2 x $10^{-4}m^{-1}$ within the mixing layer, dropping to $\sim$0.35 x $10^{-4}m^{-1}$ aloft.

TABLE 1.1. DC-3 Monitoring Equipment and its Parameters.

Parameter	Instrument	Comments
SO_2	Meloy 285	—
$SO_4^=$	Filter	IPC
$SO_2/SO_4^=$	Filter Pack	Sulfate capture on acid-treated quartz prefilter. Sulfur dioxide captured on base impregnated back-up filter.
NO/NO_x	Teco 14D	—
O_3	Bendix	—
Aerosol	Whitby EAA	0.01 μ continuous mode and size distribution
B_{scat}	MRI Nephelometer	—
Dew Point	EG&G	—
Temperature	Rosemount	—
Turbulence	MRI Universal Indicated System	—
Altitude	Metrodata	—
Position	Global VLF	~0.1 minute precision
Wind Speed	Global VLF	~Kt accuracy above 5 Kt

The top of the mixing layer, southeast of Erie, Pennsylvania, was $\sim$4500 ft MSL as indicated by the nephelometer records, while the mixing layer near Indiana, Pennsylvania, extended to nearly 7000 ft MSL over higher terrain. Ozone levels recorded between Erie and Johnstown were similar to those observed upwind.

TABLE 1.2. Cessna-411 Monitoring Equipment and its Parameters.

Parameter	Instrument	Comment
SO_2	Bubbler	Peroxide oxidation to sulfate
$SO_4^=$	Filter	IPC
$SO_2/SO_4^=$	Filter Pack	Sulfate capture on acid-treated quartz prefilters. Sulfur dioxide capture on base impregnated back-up filter.
O_3	Monitor Lab	—
B_{scat}	MRI Nephelometer	—
Turbulence	MRI Universal Indicated System	—
Dew Point	EG&G	—
Temperature	Metrodata	—
Altitude	Metrodata	—
Position	Metrodata	VOR/DME

On July 20, as the center of the high pressure drifted eastward, the top of the mixing layer increased to an average of 6000 ft MSL. Light-scattering levels were observed to be roughly 50% higher as the southwesterly flow continued to advect moist air into the Ohio Valley. Ozone levels remained nearly the same as the previous day.

The IPC filters exposed during flights between Fort Wayne and Lewisburg have been analyzed for sulfate data. An integrated value of 10.9 $\mu g/m^3$ was observed from Fort Wayne to Duncan Falls on July 19 (see Figure 1.2). Later on the same day, between Duncan Falls and Lewisburg the integrated sulfate level reached 15.3 $\mu g/m^3$.

On July 20, two separate filters were exposed on the portion of the flight from Lewisburg to Duncan Falls. The first sample was collected while the aircraft flew through clouds near Charleston, West Virginia, and yielded a value of 23.8 $\mu g/m^3$. The final portion of the sampling flight was between Duncan Falls and Fort Wayne (see Figure 1.3). The integrated sulfate level reached 25.8 $\mu g/m^3$.

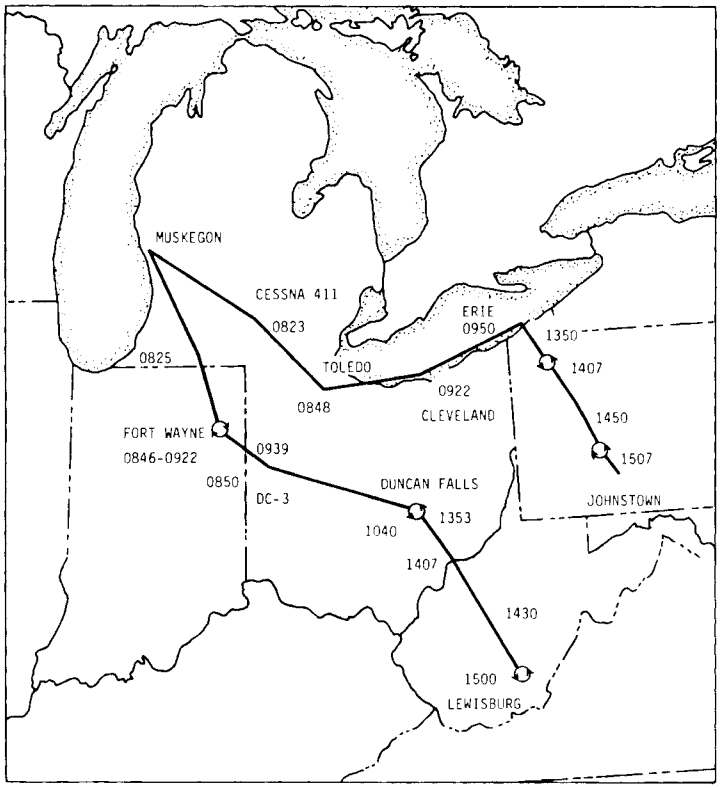

(Neg. 78 6 831-3)

FIGURE 1.2. Flight Plan for July 19, 1978

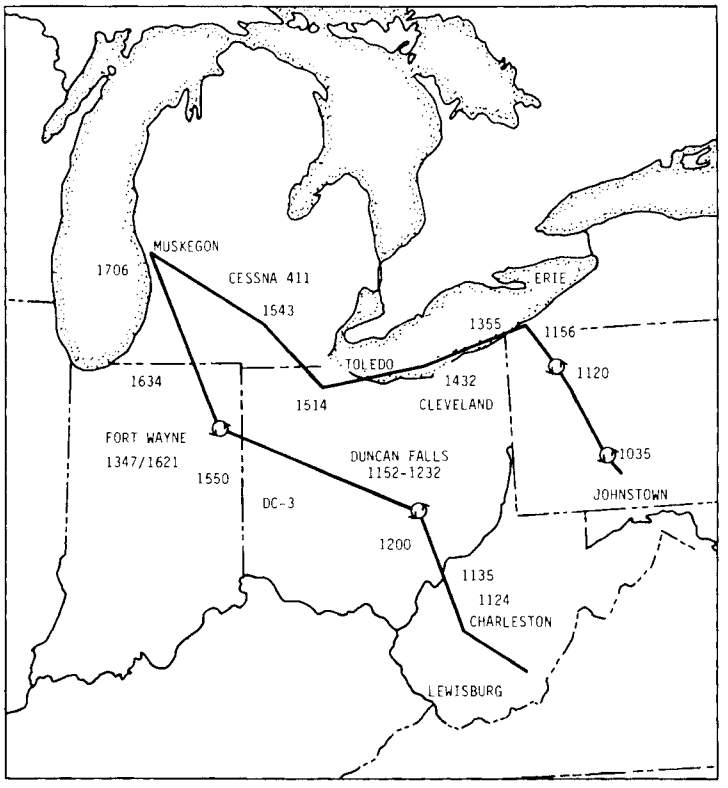

(Neg. 78 6 831-2)

FIGURE 1.3. Flight Plan for July 20, 1978

THE MAP3S PRECIPITATION CHEMISTRY NETWORK

M. Terry Dana, D. R. Drewes, D. W. Glover,
S. D. Harris and J. E. Rothert

The Multi-State Atmospheric Power Production Pollutant Studies (MAP3S) network has reached its final number of eight sites. Four of the sites are providing weekly samples in addition to the regular event samples. Early sulfite data indicate significant levels of this species in the wintertime, while sulfate is at a minimum. Sulfate concentrations peak sharply in the summer, but nitrate is more uniform throughout the year. Collectors from the three major North American networks are being compared in event sampling at the Pennsylvania State site.

With the addition of Oxford, Ohio, during the summer of 1978, the MAP3S network has reached its final number of eight collection sites (see Figure 1.4). The site numbers and cooperating institutions of the second four sites, which have come into operation since October, 1977 are: Site 5 (Illinois State Water Survey); Site 6 (Brookhaven National Laboratory); Site 7 (University of Delaware, Lewes, Delaware) and Site 8 (Miami University, Oxford, Ohio).

The Health-and Safety-Laboratory-type (HASL-type) collectors at sites 1, 2, 4 and 7 were changed to a weekly sampling mode in order to compare weekly average concentrations from the Battelle collector (event samples) with single weekly samples. The U.S. Department of Agriculture NC-141 project network operates with weekly sampling using HASL-type collectors, and it is hoped that appropriate sites of the MAP3S network can become part of this network at the conclusion of MAP3S.

The Pennsylvania State site (3) is the location of a comprehensive collector-comparison study, which began in May of 1978, and is expected to run through May, 1979. At this site, three Battelle, three HASL-type, and three Sangamo collectors (used by the Canadian government network, CANSAP) are being operated, each taking simultaneous event samples. This study should document any differences in collecting ability among the types of collectors used on the major networks in North America. While Battelle is supplying the site and performing most chemical analyses, the ultimate data analysis and reporting will be done by Pennsylvania State University.

(Neg. 78 C 654-1)

FIGURE 1.4. The Final Configuration of the MAP3S Precipitation Chemistry Network

Early results of the careful sampling of sulfite ion, employing infield chemical preservation of sulfite, are shown in Figure 1.5. Through the winter months, sulfite appears to be a significant contributor to the total sulfur deposition in precipitation. However, the concentrations of sulfur in precipitation in the winter are greatly reduced over the summer values (see Figure 1.6). These preliminary, seasonal-trend data (monthly deposition-weighted average concentrations) show a peak in sulfate in the summer (in fact, essentially all acidity in the summer appears to be associated with sulfate) and a decided low in sulfate in the winter. The averages for nitrate, as shown in Figure 1.7, are relatively constant throughout the year, suggesting that nitrate is a greater contributor to wintertime acidity.

A second annual summary of precipitation chemistry data and network progress will be issued as a PNL document early in FY-1979.

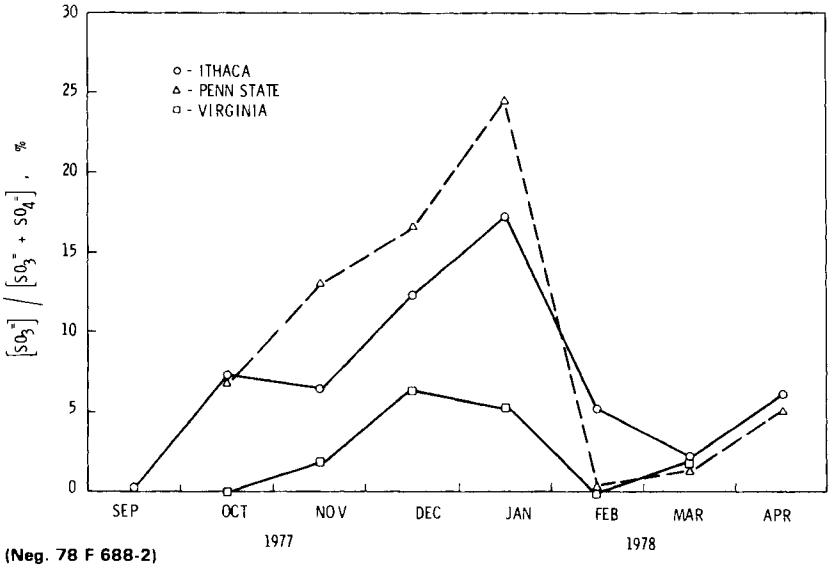

FIGURE 1.5. Monthly Deposition-Weighted Averages of the Ratio of Sulfite Ion Concentration to Sulfite Plus Sulfate

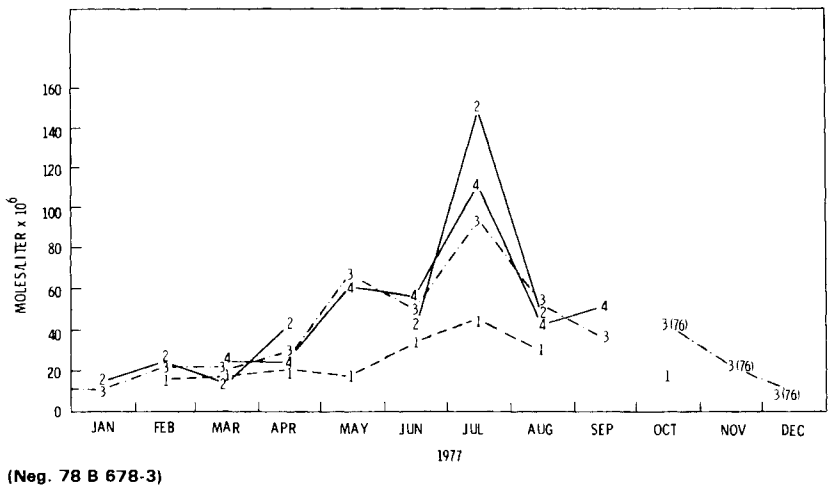

FIGURE 1.6. Monthly Deposition-Weighted Average Concentrations for Sulfate (early data from first four sites)

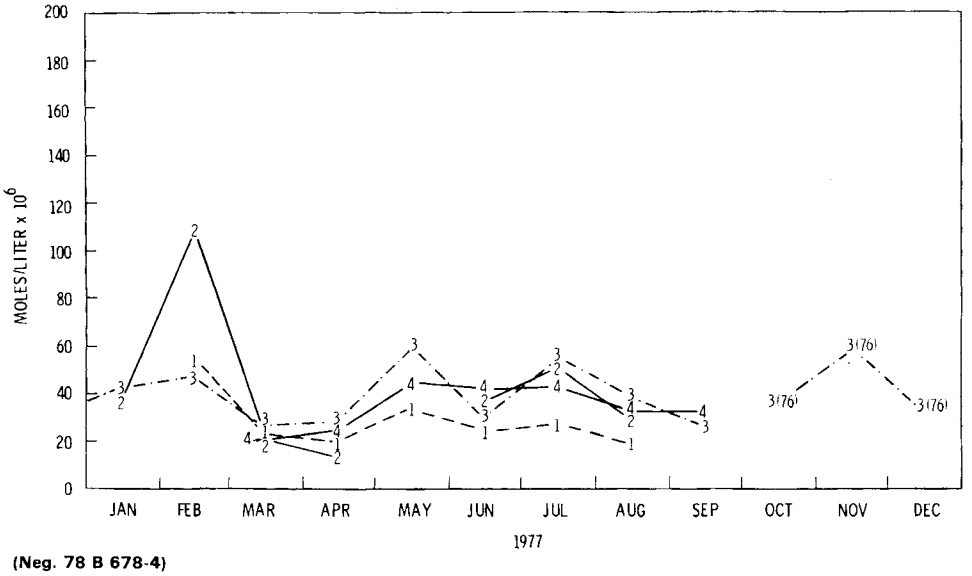

(Neg. 78 B 678-4)

FIGURE 1.7. Monthly Deposition-Weighted Average Concentrations for Nitrate (early data from first four sites)

WET REMOVAL OF POLLUTANTS FROM WINTER SNOWSTORMS

B. C. Scott, N. S. Laulainen and J. M. Thorp

Preliminary aircraft and surface data are presented for the ten storm events sampled in Muskegon, Michigan during the winter of 1977-78. The precipitation chemistry varied widely from site to site and from day to day. Some of the variability can be explained in terms of the primary growth modes of the precipitation particles.

The precipitation scavenging program is designed to examine and to predict the wet transformation and wet removal of pollutants from the atmosphere. To help reach these goals, an extensive sampling program was conducted at Muskegon, Michigan during the winter of 1977-78. The sampling program was intended primarily to examine lake-effect snowstorms, but all precipitation events (lake-effect and/or frontal) were sampled when possible. At present, the data analysis is only partially complete.

During the months of December 1977 and January 1978, ten storm events occurred in which surface precipitation samples were collected. Supplemental aircraft observations were available during eight of these periods. In each storm period, sequential samples of surface precipitation were obtained for chemical analysis at approximately 1-hr intervals at one to three sites. Additional data collected at the surface sites included meteorological observations and replicas of the falling ice crystals for determining growth histories of the precipitation particles.

Simultaneous to the surface sampling, aircraft concentration measurements were obtained for SO_4 aerosol mass, cloud-condensation nuclei, SO_2, O_3 and total ammonia. These clear-air measurements took place in the subcloud layer approximately 500 ft below cloud base. Upon completion of these clear-air observations, the aircraft would sample in the cloud at locations approximately upwind of the surface-sampling sites. Measurements of the concentration of cloud liquid water and the distribution of droplet size were obtained. Replicas of cloud particles and samples of the supercooled cloud water were also obtained for chemical analysis.

Table 1.3 provides a preliminary survey of the aircraft observations. Cloud-water

concentrations during December were considerably higher than they were in January when only one flight detected measurable cloud-droplet water. The sulfate and nitrate concentrations generally ranged between two and ten times more than the concentrations found in the surface water samples. Subcloud air concentrations of sulfate were typically about 3 $\mu g/m^3$ with extreme values of 0.7 and 9.5 $\mu g/m^3$. Between 40 and 85% of the subcloud sulfate appears to have acted as cloud-condensation nuclei in the December storms. The single January storm with detectable cloud-droplet water appears to have activated only 25% of the available sulfate.

TABLE 1.3. Aircraft Observations.

Date	Incloud Altitude, m (msl)	Cloud Water, g/m^3	Cloud Water SO_4, mg/ℓ	Cloud Water NO_3, mg/ℓ	Subcloud SO_4, $\mu g/m^3$	Fraction SO_4 Activated
Dec 2, 1977	1525	0.11	9.8	5.4	2.6	0.41 to 0.81
	1220	0.18	11.7	8.3		
Dec 6, 1977	915	0.28	9.3	8.2	—	—
Dec 7, 1977	1220	0.14	6.5	6.0	1.4	0.55 to 0.73
Dec 10, 1977	915	0.09	6.6	3.0	0.7	0.84
Jan 20, 1978	No Flight	—	—	—	2.8	—
Jan 24, 1978	No Flight	—	—	—	8.3	—
Jan 25, 1978	600 to 1525	0	—	—	9.5	—
Jan 30, 1978	760 to 915	0	—	—	2.7	—
Jan 31, 1978	1065	0.02	29.8	49.5	2.4	0.25
Feb 1, 1978	670 to 915	0	—	—	2.8	—

Table 1.4 presents some of the volume-weighted averages of the sequential samples taken at each sampling site. The sulfate and nitrate concentrations are shown to have varied by a factor of two or more among sites on any given day and by a factor of ten or more from storm to storm. Comparisons among different days illustrate that when nitrate concentrations were high, sulfate concentrations were either high or low; however, when nitrate concentrations were low, sulfate concentrations were also low. Such variability suggests that either the removal mechanisms or the vertical distribution (i.e., the source regions) for sulfate and nitrate are often substantially different. Values of pH for individual samples (not shown in Table 1.4) ranged between 3.78 and 7.09 with the average pH over all storms being near 4.5. Apparently, those samples, which contained less acidic precipitation, consistently contained high concentrations of K, Mg and Ca. Thus, the wind-blown, alkaline soil from shoreline dunes near Lake Michigan and from exposed ground appears to have contributed to the anomalously high pH values. Also of note are the comparisons of pH with nitrate and sulfate concentrations. From sequential samples, the fluctuations in pH appear to be more highly correlated with the fluctuations in the nitrate concentrations than with sulfate fluctuations.

A diagram of the sulfate washout ratio versus precipitation rate is presented in Figure 1.8. Individual samples are plotted and compared to the theoretical predictions arising from analysis of the Muskegon field data taken the previous winter. The open circles represent data collected on days in which no liquid water was detected in the clouds or in which little or no riming (accreting cloud droplets) was detected on the ice particles at the surface. The solid circles represent data collected on days with detectable cloud water or when the majority of the replicated ice particles were rimed.

A large degree of scatter appears about the predicted washout curve in Figure 1.8.

Much of the scatter can be attributed to the open circle data in which the assumptions inherent in the predicted curve are grossly violated. That is, the predicted curve assumes precipitation particles grow mainly by riming, while the open circle data indicate particle growth primarily by vapor deposition onto existing ice crystals.

In addition, the placement of the predicted curve is uncertain at these low precipitation rates because of difficulties in defining cloud-water concentration. Sufficient cloud microphysical data were collected to enable a refined cloud water definition. This definition should further decrease the discrepancy between predicted and observed washout ratios. In spite of these shortcomings, the washout ratio data suggest that the sulfate nucleation-riming mechanism, postulated from previous studies, is the predominant sulfur-removal mechanism in these winter snowstorms.

TABLE 1.4. Surface Precipitation Chemistry Observations.

Date	SO_4, mg/ℓ	NO_3, mg/ℓ	pH
Dec 2, 1977	5.2	3.4	4.5
Dec 6, 1977	1.5	1.1	5.2
	0.7	0.4	5.5
	0.7	0.7	5.2
Dec 7, 1977	4.1	2.8	6.7
	1.3	1.8	4.7
Dec 8, 1977	0.5	2.5	4.3
Dec 10, 1977	0.2	0.4	5.0
	0.3	0.4	5.4
Jan 20, 1978	0.3	0.8	4.8
Jan 24, 1978	8.8	8.0	3.8
Jan 25, 1978	0.6	2.4	4.5
	0.5	2.2	4.4
	0.4	2.6	5.5
Jan 30, 1978	1.6	5.3	4.3
	1.4	5.4	4.3
	2.8	4.9	6.3
Feb 1, 1978	0.6	4.5	4.2
	0.7	5.2	4.4
	0.8	4.1	4.1

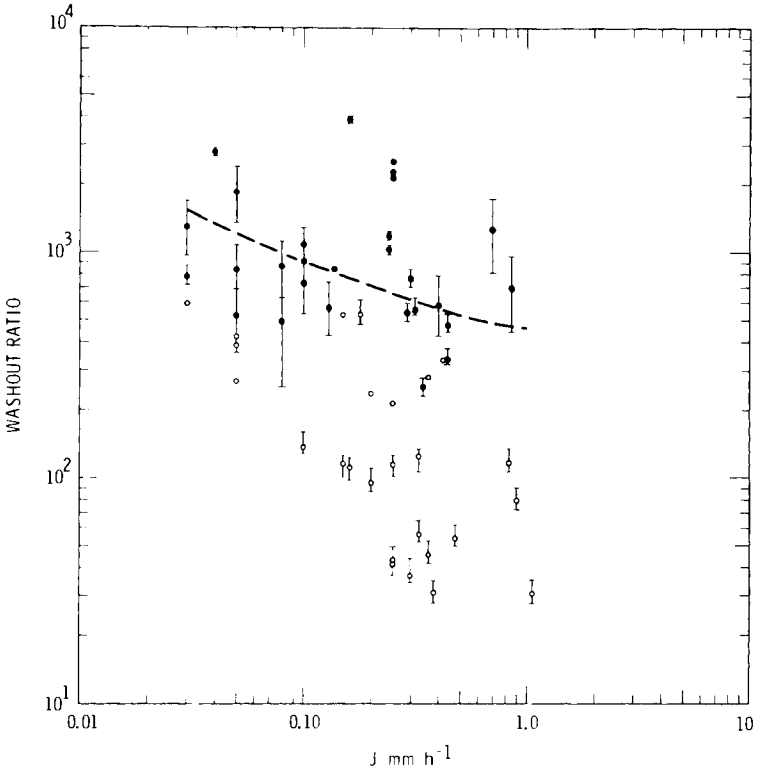

FIGURE 1.8. Sulfate Washout Ratio as a Function of Precipitation Rate (J) for Rimed (•) and Unrimed (o) Snow

THE SULFUR BUDGET DILEMMA?

B. C. Scott

By incorporating storm convergence into the equations describing pollutant transformation and transport, one can readily compute sufficient airborne sulfate concentrations to account for observed concentrations of sulfate in precipitation. Consideration of incloud conversion of SO_2 to SO_4 is not necessary in order to compute the observed SO_4 washout over the Multi-State Atmospheric Power Production Pollutant Studies (MAP3S) region.

In a recent article, MacCracken (1978) argued that substantial SO_2 conversion to sulfate is likely in cloud and precipitation water. The argument is based upon examination of the sulfur budget over the MAP3S region and upon consideration of available sulfate in the air that can be be scavanged. Briefly, the argument is as follows.

The United States sulfur emissions are fairly well known (0.5×10^{12} moles of sulfur/year), and the emission rate is nearly constant throughout the year. The average yearly rainfall that occurs over the 2.5×10^6 km^2 MAP3S network area (1 m y^{-1}) is roughly constant and is approximately uniform from month to month throughout the year.

During the winter months, the precipitation contains about 1.0 mg/l of SO_4; in the summer, roughly 6.0 mg/l. A yearly average SO_4 concentration is near 3.0 mg/l. Thus, during the winter months, about 5% of the emitted sulfur is deposited in precipitation, while in the summer about 30% is removed by rainfall. Averaging over the year indicates that 15% of the emitted sulfur (S) is removed as SO_4.

By selecting appropriate values for the mean residence time of air over the MAP3S region (36 to 38 hr), for the mean fraction (f) of S as SO_4 (0.3), and for a mean deposition rate for SO_2 (0.018 h^{-1}), MacCracken concludes that the fraction of sulfate washed out cannot equal observed values unless incloud conversion of SO_2 occurs.

MacCracken's calculations are, however, extremely sensitive to seasonal variations in the ratio, f, and to the mean air mass residence time, t_R. Table 1.5 and Figure 1.9 illustrate the magnitude of these variations. In addition, there appears to be little physical or mathematical justification for the first-order differential equations selected by MacCracken. What should be considered for problems concerning removal of sulfur is the time rate of change of pollutant concentration in a layer of air. This is particularly important when episodes, such as precipitation events, are being considered.

TABLE 1.5. Average Residence Time and Daily Boundary Layer Wind Speed for Selected Months.[a]

Month	Average Daily Wind Speed, m s^{-1}	Average Residence Time, hr
Jan 1974	14.3	23
April 1974	12.2	27
June 1978	9.3	35
July 1974	7.4	44
July 1978	7.4	45
Aug 1974	6.8	48

[a]Values are based upon radiosonde winds from Pittsburg, PA; Albany, NY; and Huntsville, WVA.

From the basic continuity equation, the concentration of SO_2 or SO_4 can be described as:

$$\frac{\partial n}{\partial t} = - \nabla \cdot n \vec{v} + \nabla \cdot D \Delta n - kn \qquad (1)$$

when n is pollutant concentration, and D is an eddy diffusivity. Defining a diffusion velocity as

$$\vec{v}_D = - \frac{D}{n} \vec{\nabla} n \qquad (2)$$

and integrating Equation (1) over a nondivergent boundary layer of fixed thickness (from the ground to level z) yields

$$\frac{D\bar{n}}{Dt} = n(z) - \bar{n} \; \overline{\nabla_2 \cdot \vec{v}} + n(z) \, v_D(z) - n(o) \, v_D(o) \, / \Delta z - \bar{k} \, \bar{n} \qquad (3)$$

where the vertical velocity at the surface is assumed negligible, and the horizontal fluxes as a result of turbulent eddies and diffusion velocities have been neglected. Here

$$\frac{Dn}{Dt} = \frac{\partial n}{\partial t} + \bar{u} \frac{\partial n}{\partial x} + \bar{v} \frac{\partial n}{\partial y} + \bar{u} \frac{\partial n}{\partial z} \qquad (4)$$

and (the overbar represents a vertical average for the layer).

The diffusion velocity at the top of the layer, $v_D(z)$, should be negligible compared to that at the base and can be neglected. The diffusion velocity at the base of the layer, $f_D(o)$, is commonly called a deposition velocity. To simplify the notation $v_D(o)/\Delta z$ will be set equal to m_2. The term m_2 then represents dry deposition. Here $v_D(o)/\Delta z$ is set equal to m_2.

To further simplify Equation (3) let

$$n(z) = \alpha \bar{n}$$
$$n(o) = \beta \bar{n} \qquad (5)$$

where α is roughly between 0.1 and 0.5, and β is probably between 1 and 5 during the daylight hours and 0.5 to 1.0 at night. Thus, Equation (3) becomes

$$\frac{\bar{D}n}{Dt} = -(\bar{k} + \beta \, m_2) \, \bar{n} - (1-\alpha) \, \bar{n} \, \nabla_2 \cdot \vec{v} \qquad (6)$$

The main difference between Equation (6) and the equation used by MacCracken is the addition of a horizontal divergence term and the inclusion of a weighting factor for dry deposition.

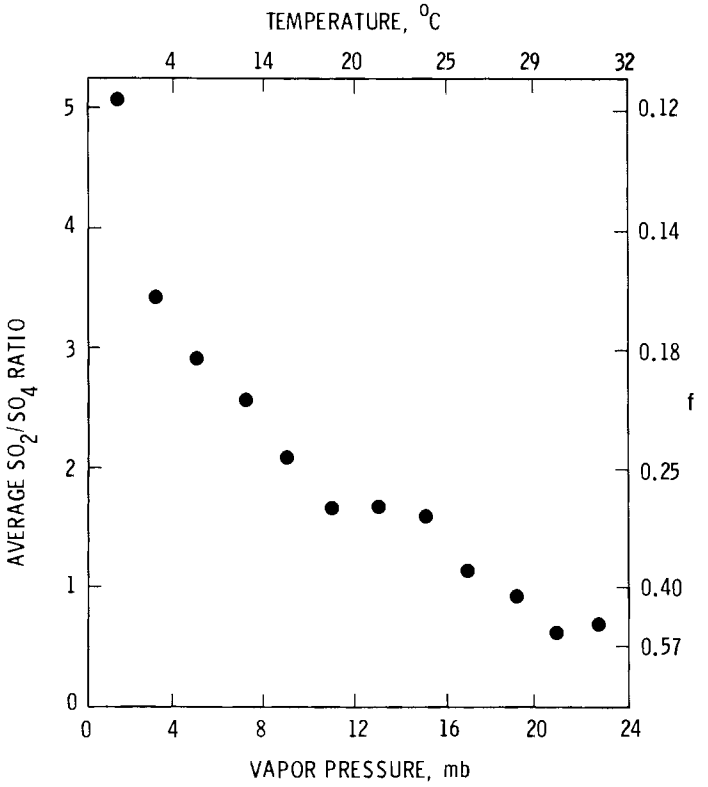

FIGURE 1.9. Average Sulfur Ratio as a Function of Partial Water Vapor Pressure, mb, and Temperature at 50% Relative Humidity

Air frequently encounters a storm circulation some 12 to 48 hr before actual precipitation occurs. During the period of storm circulation influence, the synoptic scale horizontal convergence typically averages near 0.04 h^{-1}. With m_2 on the order of 0.01 h^{-1} and β near 3, the divergence contribution is nearly equal to and opposite in sign to the deposition contribution. Therefore, the mean concentration of a pollutant in a layer not only depends upon transformation and deposition, but also is strongly dependent upon the mean horizontal divergence in that layer.

Incorporating the above estimate of convergence into the m_2 term has the effect of reducing the m_2 term by a factor of two or more from the values used by MacCracken and others. Table 1.6 presents results for different values of (the effective) m_2, which were selected to give close correspondence to the observed percentages of sulfur removed by precipitation. (Effective m_2 is meant to imply the sum of convergence plus dry deposition.) If the sum of the convergence and deposition terms equals about 0.005 h^{-1}, then the observed summer-to-winter variations in sulfate wet removal can be closely reproduced.

To summarize, the percentage of emitted sulfur deposited by precipitation is determined by several parameters. Besides the obvious parameters of chemical conversion rates and dry deposition, there is strong dependence upon the age of the air mass, the duration of the storms, the interval between storms and the magnitude of the convergence associated with the storms. When synoptic scale convergence is taken into account, one need not invoke the possibility of incloud conversion of SO_2 to explain observed surface concentrations of SO_4.

TABLE 1.6. Predicted Variations in Wet Removal of Sulfate as a Function of Mean Air Mass Residence Time (t_R), the Mean Fraction (f) and the Sum of Convergence Plus Dry Deposition (m_2).

Mean Fraction	Mean Air Mass Residence Time, h	Removed m_2 at 0.003 h^{-1}, %	Removed m_2 at 0.005 h^{-1}, %
0.15	22	4.2	4.1
	26	4.9	4.8
0.30	37	13.6	13.2
	39	14.3	13.9
0.50	48	28.7	27.7
	52	30.8	29.6

DERIVATION OF WET REMOVAL RATES FOR SO_2 GAS AND SO_4 AEROSOL

B. C. Scott and M. Terry Dana

If the basic continuity equation is considered, the wet removal of pollutants from the atmosphere can be expressed as the vertical-flux divergence of the pollutant containing precipitation particles. Further, wet removal from a surface boundary-layer can be explicitly stated in terms of a wet-pollutant flux at the surface, provided the layer chosen is thick enough to prevent a pollutant from being carried into the layer from above by precipitation particles. The analysis presented here, which is based upon the time required to grow collector particles to precipitation sizes by accretion of cloud droplets, suggests that the appropriate layer thickness is typically 1200 m or less. Sulfate removal is computed by assuming that the subcloud-sulfate aerosol acts as a cloud-condensation nuclei and is removed by the accretion process. Sulfur dioxide removal is modeled as if it occurred by accretion of droplets by falling snowflakes, or as if it were an equilibrium process for falling water drops. Sulfate wet-removal rates are predicted to be 0 (40% h^{-1}), while SO_2 removal rates are predicted to be 0 (2% h^{-1}).

Models describing wet removal of a pollutant from the atmosphere generally rely on an equation of the following form (see Slinn 1975):

$$\frac{\partial x}{\partial t} = -\nabla \cdot x\vec{v} - \lambda x_{\omega} \qquad (1)$$

(For a complete list of symbols, see nomenclature at the end of this article.)

When using Equation (1) for predicting the wet removal of pollutants, modelers often encounter difficulties because of uncertainties in the value of the wet-removal coefficient, λ. The wet-removal coefficient results from integrating over all sizes of pollutant-containing hydrometeors and is extremely difficult to evaluate. At best, generalized or simplified expressions provide only approximations for the value of λ. In addition, available experimental values, when compared to theoretical estimates, represent both spatial and time averages over the duration of a storm or experiment. As such, they are not directly comparable to the values needed for evaluation of Equation (1).

Typically, modelers need only an expression for determining the wet removal of a pollutant from a layer, that is, the vertical average of Equation (1). Thus, an alternative approach is needed for computing the wet removal of pollutants from the atmosphere: an approach, which relies on a direct calculation of an average, wet-removal rate for the layer being scavenged. The following presents an outline for the procedure required to determine layer-averaged, wet-removal rates for SO_2 gas and SO_4 aerosol.

The wet removal of pollutants is governed by the basic continuity equation

$$\frac{\partial x}{\partial x} = -\nabla \cdot x\vec{v} + \frac{\partial x_p v_f}{\partial z} \qquad (2)$$

If Equation (2) is vertically integrated from the surface (z_o) to a given level (z) and a nondivergent boundary layer is assumed, the following equation results:

$$\frac{D\bar{x}}{Dt} = \frac{(x_p v_f)z - (x_p v_f)z_o}{(z - z_o)} \qquad (3)$$

where terms representing turbulent eddy fluxes and mean atmospheric motions (e.g., pollutant flow out the top of the layer) have been omitted. Then,

$$\frac{D\bar{x}}{Dt} = \frac{\partial \bar{x}}{\partial t} + \bar{u}\frac{\partial \bar{x}}{\partial y_1} + \bar{v}\frac{\partial \bar{x}}{\partial y_2} \qquad (4)$$

The omitted terms in Equation (3) are equivalent in magnitude to the remaining expression, which represents wet removal. The omitted terms must be retained in models determining pollutant concentrations; however for simplicity, only the wet-removal term is being considered.

Equation (3) is most appropriate for application in Eulerian or grid models where predictions of local time changes are desired. However if vertical air velocities are neglected, as is the case for many existing trajectory models (e.g., Johnson et al. 1978, Wendell et al. 1976), then Equations (3) and (4) would also apply to Lagrangian trajectory calculations.

If x_p is expressed as

$$x_p = L_p C \qquad (5)$$

and the precipitation rate is related to L_p and v_f, then Equation (3) can be simplified to:

$$\frac{D\bar{x}}{Dt} = \frac{(jC)_z - (jC)_{z_o}}{z - z_o} \qquad (6)$$

By carefully selecting the height of level z so that the wet pollutant flux at z is zero, then the wet removal of pollutants from the layer of thickness ($z-z_o$) can be evaluated by considering only the pollutant flux at the ground. Currently 1200 m is the best estimate for the thickness, $z - z_o$.

Using the work of Scott (1978) to derive values for C, the following equations are obtained. For sulfate removal by rain and snow,

$$\frac{D\bar{\chi}\,(SO_4)}{Dt} = -0.38\ \chi_g(SO_4)\ J^{0.73} \qquad (7)$$

for SO_2 removal by snow,

$$\frac{D\bar{\chi}(SO_2)}{Dt} = -0.15\ JC_g \qquad (8)$$

and for SO_2 removal by rain,

$$\frac{D\bar{x}\ (SO_2)}{Dt} = -0.83\ JC_g \qquad (9)$$

Here C_g represents ground-level, equilibrium, water concentrations of SO_2, which are a function of SO_2 air concentration pH, and temperature (Hales and Sutter 1973). Equations (7), (8) and (9) are applicable for a surface layer, 1200-m thick; Equation (8) for an assumed cloud-water content of 0.2 g m^{-3}.

Nomenclature

C = mass of pollutant in precipitation water per unit mass of precipitation water, g g^{-1}

C_g = equilibrium concentration in water of SO_2 at the ground, g g^{-1}

j = precipitation rate in mass flux units, g m^{-2} h^{-1}

J = precipitation rate in mm h^{-1}

L_p = precipitation water mass per unit volume of air, g m^{-3}

v_f = fall speed of precipitation particles, m s^{-1}

x = the total mass of pollutant contained within a unit volume of space, g m^{-3} air

$\bar{x}$ = the vertical average of x, g m^{-3} air

x_p = mass per unit volume of air of pollutant contained in precipitation water, g m^{-3}

x_ω = mass per unit volume of pollutant associated with condensed water, g m^{-3}

y_1 = east-west coordinate

y_2 = north-south coordinate

$\bar{u} = \frac{dy_1}{dt}$

$\bar{v} = \frac{dy_2}{dt}$

z = height above ground level

z_o = height of the ground level

λ = a wet-removal coefficient, h^{-1}

χ = equivalent to x

$\bar{\chi}(\ )$ = the vertically averaged concentration of the material in the parenthesis, which is equivalent to $\bar{x}$, g m^{-3}

χ_g = the concentration in the air at ground level, which is equivalent to x_a, g m^{-3}

$\nabla = \frac{\partial}{\partial y_1}\hat{i} + \frac{\partial}{\partial y_2}\hat{j} + \frac{\partial}{\partial z}\hat{k}$

$\vec{v}$ = wind vector

USE OF ION CHROMATOGRAPHY FOR TRACE ANALYSIS OF MAP3S PRECIPITATION SAMPLES

J. E. Rothert

Ion chromatography is ideally suited for trace analysis of precipitation samples, because several ionic species at various concentrations can be analyzed simultaneously with little or no sample preparation. In the rain samples found in the rural, eastern United States, several species can be easily analyzed; however for trace analysis work, seven species (SO_4^{2-}, NO_3^-, Cl^-, PO_4^{3-}, K^+, NH_4^+, and Na^+) are all that are easily separated, using the anion and cation columns.

The Multi-State Atmospheric Power Production Pollutant Study (MAP3S) includes measurement and modeling of fossil-fuel effluent concentrations in precipitation and air in the northeastern United States. To determine precipitation concentrations of sulfur and nitrogen oxides as well as PO_3^{3-}, Cl^-, Na^+, NH_4^+, Ca^{2+}, Mg^{2+}, pH, and conductivity, an eight-site precipitation network has been established in the rural eastern United States. This network includes: White Face Mt., New York; Ithaca, New York; Pennsylvania State University, Pennsylvania; University of Virginia, Charlottesville, Virginia; Brookhaven National Laboratory; University of Delaware, Lewes, Delaware; Illinois State Water Survey; Miami University, Oxford, Ohio. These sites collect rural precipitation on an event basis and ship the samples to Pacific Northwest Laboratory for analysis. The actual sites are not downwind of any close

pollution source; therefore, the data collected are background concentrations and are at trace levels.

Two Durrum Dionex Model 10 ion chromatographs (IC) are used to analyze the precipitation samples for Cl^-, PO_4^{3-}, NO_3^-, SO_4^{2-}, Na^+, NH_4^+, and K^+. Because of its low concentration (often less than 5×10^{-3} mg/ℓ) nitrite is not analyzed with the IC. The other species are analyzed with other techniques including atomic absorption. A Perkin-Elmer Model 56 strip-chart recorder and a Linear Instrument Model 254/MM strip-chart recorder are currently being used to record the chromatographs of the eluated samples and standards.

An ion chromatograph is currently being used to analyze the anions, CL^-, NO_3^-, PO_4^{3-}, SO_4^{2-}. The instrument parameters are 2.1 mℓ/min or a 24% flow rate, a 500-mm separator column, a 150-mm precolumn, and the standard 25-cm suppressor column. The standard eluant, 0.0024M Na_2CO_3/0.003M $NaHCO_3$, is used to eluate the samples. The sample loop volume is 0.1 mℓ.

The 0.3 μmho/cm, the 1.0 μmho/cm, and the 3.0 μmho/cm scales are routinely used in the trace analysis. In order to use the three scales and consistently maintain a smooth baseline, a routine column-cleaning procedure is used. Eluant is never allowed to remain on the separator column overnight or when the pumps are not running. For at least 1/2 to 1 hr each morning, deionized-distilled (DD) water, the conductivity of which is 0.75 μmho/cm, is rinsed through the separator and precolumn with the suppressor column totally bypassed. For another 1/2 to 1 hr, eluant is pumped through the precolumn, separator column, and suppressor column. This procedure is usually sufficient to produce a low-noise, low-drift baseline on a 0.3 μmho/cm scale. Deionized-distilled water is then flushed through the sample loop, approximately 0/nℓ in length, and injected onto the column. A smooth-water baseline with no peaks indicates the IC is clean and ready for use. Before and after each sample or standard, 2 mℓ of DD water are flushed through the sample loop before sample loading and injection on the column. After each day's samples are finished, the suppressor column is either bypassed or regenerated, and the precolumn and separator column are washed again with DD water for at least 1/2 hr. This procedure cleans the columns after each day's use and prepares the columns for use the next day.

Sample preparation is also necessary because of the presence of the negative water peak at approximately the same location as the Cl^- peak. The standards and samples are adjusted to contain the same concentrations of HCO_3^- and CO_3^{2-} as the eluant. The standards are prepared by diluting concentrated standard solutions with eluant. The samples are carefully measured and have a measured amount of concentrated eluant added to them to remove the negative water peak. No other sample preparation is generally needed. Occasionally a sample containing a large amount of solid material is filtered throuth 0.4μ pore size Nuclepore(®) filters before injection.

The concentrations of the standards and samples are measured as a function of peak height. The standard chromatographs are recorded at the same conductivity scales as the samples, 0.3 μmho/cm, 1.0 μmho/cm, and 3.0 μmho/cm. A least squares fit of the standard concentrations as a function of the peak height is used to calculate the sample concentrations from their peak height. The concentrations for each anion vary from event to event and from site to site. The average concentrations, however, are 2 mg/ℓSO_4^{2-}, 3 mg/ℓNO_3^-, 0.2 mg/ℓCl^- and less than 0.02 mg/ℓPO_4^{3-}. The concentrations range from the detection limit on the 0.3 μmho/cm scale of 0.01-0.02 mg/ℓ to 12 mg/ℓSO_4^{2-}, 9 mg/ℓNO_3^-, 2 mg/ℓCl^-, and 0.07 mg/ℓPO_4^{3-}.

The second IC unit is used for NA^+, NH_4^+, and K^+ analysis. The instrument parameters currently being used are 1.8 mℓ/min or a 20% flow rate, the 25-cm separator column, and the 25-cm suppressor column. The eluant currently being used is 0.005M HCl. The sample loop volume is 0.1 mℓ. With the cation IC, the 0.3 μmho/cm scale is used. The 1.0 μmho/cm scale is occasionally used for NH_4^+. The same column cleaning and preparation procedure is used for the cation columns as for the anion columns. The only difference in column preparation is: after regenerating the suppressor column, 6 to 8 hr of pumping eluant through the columns are needed to obtain a smooth baseline. Until the next regeneration cycle, the 1/2-hr period is sufficient for column preparation. The negative water peak does not interfere with any of the three cation peaks, Na^+, NH_4^+, or K^+, being analyzed, so no special sample or standard preparation is needed. The standards are made from diluting concentrated standard solutions with DD water. The samples are analyzed without dilutions or other preparations. Some samples need to be filtered through the Nuclepore(®) filters as with samples on the anion IC. The shut-down procedure is the same for the cation IC as for the anion IC.

The concentrations for the cations vary with event and site. The average concentrations are 0.05 mg/ℓNa^+, 0.3 mg/ℓNH_4^+, and 0.02 mg/ℓK^+. The concentrations range from the detection limit, about 0.01-0.02 mg/ℓ on the 0.3 μmho/cm scale for the three cations, to 0.5 mg/ℓNa^+, 1.0 mg/ℓNH_4^+, and 0.08 mg/ℓK^+.

MAP3S has been in operation for two years. The first IC was purchased at the beginning of MAP3S for anion analysis and has been in constant operation since June, 1976. The separator column was replaced and the pump dismantled for cleaning; otherwise, the IC has worked five days a week for two years. The cation system has been in operation for one year. Outside of a broken sapphire plunger in the pump upon arrival at the lab, the second instrument has also worked daily. Ten to twenty samples per day are run on the anion IC, and 20 to 40 samples on the cation IC. At maximum routine operation, about 200 samples can be processed per month. Although at certain times of the year 200 precipitation samples may be received from the eight sites, this number includes rerunning samples for quality control and analyzing samples from projects other than MAP3S.

PRESERVATION OF NITRITE ION IN SOLUTION

M. Terry Dana

Moderate concentrations of nitrite ion, when added to Multi-State Atmospheric Power Production Pollutant Studies (MAP3S) precipitation samples and distilled-deionized water, decay through oxidation to nitrate very slowly when stored at room or refrigerator temperatures. The decay halftimes range from 44 to hundreds of days under these conditions, but if frozen and rethawed, the concentrations decline very rapidly. Differences in decay rates for precipitation samples may be related to pH or initial nitrate concentration. The method of thawing and number of thaws strongly affect decay rates for frozen samples.

As the predominant acidifying ions, sulfate and nitrate as pollutants of precipitation receive the major attention of the MAP3S research. The degree to which sulfate in water solution has resulted from liquid-phase oxidation of sulfite (or dissolved SO_2) is being investigated in connection with the MAP3S Precipitation Network (PCN), but little attention has been given the NO_2^- to NO_3^- process in the liquid phase (MAP3S 1977). Very little NO_2^- appears in MAP3S/PCN samples; however, no special preservation techniques are employed to preserve it, as is the case with $SO_3^=$. A simple experiment was devised to determine the lifetime of NO_2^- in solution under various conditions. The experiment, besides helping to decide if standard analysis techniques are adequate, can provide valuable insight into NO_2^- to NO_3^- behavior in the atmosphere.

The experiment began by mixing 250-ml aliquots of selected precipitation samples and distilled-deionized (DD) water with easily measurable quantities of $NaNO_2$. Naturally occurring nitrite could not be used, because surviving nitrite concentrations were too low for accurate decay measurements. The samples were then divided into ∿100-ml aliquots in capped 250-ml polyethylene bottles and stored at three temperatures: -15C, +2C, and 25C. Subsequent nitrite analyses, using the Saltzmann (1954) automated wet-chemistry method, determined the history of the decay. These measurements were made at several hours, one day, and then weekly for seven weeks. Selected samples were analyzed for nitrate to confirm that the nitrite decay was due to conversion to nitrate.

Some results of the experiment are given in Table 1.7. Samples A and C were made in DD water, while the rest were actual samples from the MAP3S/PCN. The latter are identified by a number code (MMDDST), where MM is the month, DD the day, S the site number (MAP3S 1977), and T the sample type (irrelevant here). The network samples were selected to represent all the active sites at the time, various initial pH and NO_3^- levels, and a broad time span (winter through spring 1978).

TABLE 1.7. Results of Nitrite Preservation Tests.

Sample[a]	C_o[b]	pH[c]	NO_3^-[c]	$t_{1/2}$, days		
				T = -15C	T = +2C	T = 25C
A	6.4	~5.5	<0.2	~3[d]	e	120
C	5.9	~5.5	<0.2	4-30[d]	e	460
052533	7.1	4.16	26	~0.3[d]	110	81
011135	3.6	4.39	14	f	e	e
012220	2.8	4.86	4.2	f	e	300
011910	4.0	4.87	2.2	f	e	e
121450	3.4	4.13	24	f	e	53
040520	3.9	4.02	35	f	e	67
033170	3.6	4.65	12	f	e	e
050720	3.3	3.77	70	f	e	44
121940	3.4	4.21	22	f	e	100

[a]Sample identification is explained in text (A and C distilled deionized H_2O).
[b]Initial mixed concentration, μmoles/1 NO_2^-
[c]Prior to mixing with NO_2^-, NO_3^- in μmoles/1
[d]Varies widely depending on thawing conditions, etc.
[e]Very long, no measurable decay before 35 days
[f]No data

Where sufficient data permitted, least squares fits to exponential decay were computed.

$$C = C_o \exp(-bt) \qquad (1)$$

where C is the nitrite concentration at time (t), b is a constant and $C_o = C(t=o)$. The time to decay to one-half initial concentration is:

$$t_{1/2} = \frac{-\ln(1/2)}{b} \quad . \qquad (2)$$

These values are listed in the table for cases where the coefficient of determination (r^2) was greater than about 0.85, except where footnoted.

The life of NO_2^- in DD and precipitation samples is remarkably long at room and refrigerator temperature, but is quite short when the samples are frozen. The $t_{1/2}$ values for frozen aliquots are approximate, because the decay rates are strongly affected by number of thaws, method of thawing (e.g., microwave oven versus room temperature), and volume of aliquot. Nitrite in unfrozen aliquots may decay faster for smaller volumes, but available sample volume is insufficient for testing this effect in detail. The decay rates for nitrite in solution differ from those for sulfite (MAP3S 1977) in that frozen samples show a greater rate of conversion for nitrite than the unfrozen nitrite samples. In the precipitation samples, a correlation appears to exist between initial acidity (or NO_3^-) and faster decay, but insufficient samples were done to confirm this.

The implications for laboratory and field sample handling are clear: nitrite samples should definitely not be frozen as a means of preservation. Refrigerator storage is preferable, although a few days at room temperature should not be harmful. In natural conditions, where nitrite is dissolved in cloud or precipitation water, little conversion is likely to take place during the lifetime of cloud or rain drops. When freezing and thawing occur, nitrite can efficiently oxidize, but other data indicate that this probably does not happen to a significant degree. Nitrite concentrations are uniformly low (<0.5 μmoles/l) and NO_3^- levels are roughly constant (10-40 μmoles/l) all year, whereas higher NO_2^- would be expected in the summer if freezing conversion were important. Likewise, NO_3^- would be expected to vary more with the seasons. Assuming poor solubility (compared to that of SO_2) for NO and NO_2 gases, these results do not detract from a hypothesis that NO_3^- in precipitation largely comes from scavenged nitrate particles of HNO_3^- aerosol.

PROCEDURE FOR ALTITUDE COMPENSATION FOR A FLAME-PHOTOMETRIC SULFUR ANALYZER

J. M. Hales, R. C. Easter and R. N. Lee

A calibration scheme, which applies to the Meloy-285 sulfur analyzer, is described. This scheme allows reliable instrument calibration, which automatically compensates for variations in instrument response with altitude.

The Meloy-285 sulfur analyzer utilized for SO_2 measurement onboard the Pacific Northwest Laboratory's (PNL) DC-3 aircraft employs a flame-photometric detector whose signal output is a nonlinear function of concentration. Typically, this output signal is linearized by analog circuitry located between the sensor output and the final output connector of the instrument; this circuitry, however, depends upon establishing a zero output setting (by adjustment of a potentiometer) at zero sulfur concentration. Another property of this instrument is that the zero setting is a function of ambient pressure; thus, when the machine is airborne the baseline continually drifts as altitude varies. This in turn introduces a nonlinearity in the system because of the circuitry described above.

The form of the linearization scheme can be deduced by analysis of the analog circuitry. By inspection of calibration data, however, it is apparent that machine output can be fit accurately to the relatively simple empirical expression

$$y = a[x - z \exp (b(z-x))^{0.59}] \qquad (1)$$

where

y = the actual SO_2 mixing ratio

x = the SO_2 mixing ratio apparent from machine output

a,b = calibration constants

z = machine zero reading (mixing ratio) at altitude h.

The baseline drift with altitude can be expressed with acceptable accuracy by the form

$$z = z_o - \alpha h \qquad (2)$$

where z_o is the baseline reading at zero altitude, and α is a calibration constant.

A computer program was written to read a set of calibration data in the form of x-y pairs, and perform a least squares fit of Equation (1) to obtain the calibration constants a and b. Written in BASIC code, this program is operational on the Muskegon NOVA minicomputer and is being used routinely for local calibration of the Meloy system.

AN ANALYTICAL PROCEDURE FOR DETERMINING C_2 TO C_6 HYDROCARBONS IN AMBIENT AIR

R. N. Lee

A procedure is described for determining light hydrocarbons in ambient air. This method is being used to examine samples collected in Tedlar bags during flights through urban plumes.

Although biogenically derived methane is the major atmospheric hydrocarbon with regard to concentration, the nonmethane hydrocarbons exercise a significant influence on the photochemistry of urban atmospheres. Comprehensive study of these urban systems should include some knowledge of the hydrocarbon composition and its variation in time. The interpretation of concentration trends in the real atmosphere is complicated by diurnal variations in emission rates, differences in reactivity and uncertainties regarding the relative contribution of various sources.

Data interpretation, therefore, rests on assumptions regarding the origin and reactivity of specific indicator compounds. Acetylene, for example, has frequently been used to normalize hydrocarbon concentration data, to indicate the relative contribution of auto exhaust to the polluted air mass, and to estimate the extent of photochemical decay (Calvert 1976; Whitley and Altwicker 1976; Kopczynski et al. 1975). This use assumes that acetylene is a relatively inert member of the photochemical mix and is derived solely from gasoline combustion.

In order to expand the data base for Multi-State Atmospheric Power Production Pollutant Studies (MAP3S) focusing on the Great Lakes region, an analytical protocol has been developed for determining C_2 to C_6 hydrocarbons, which are pollutants derived primarily from auto exhaust and natural gas losses with some gasoline evaporation. This chromatographic procedure is being used to examine air samples collected in Tedlar bags during aircraft sampling missions downwind of areas of major pollutant sources.

Analyses of bag contents are conducted using the system described in Figure 1.10. Hydrocarbons are concentrated from 0.1 to 0.5 liter of filtered air using a U-tube trap packed with Tenax GC absorbent and are immersed in a liquid nitrogen-ethanol bath. Sample injection is performed by backflushing the trap with carried gas, removing it from the cryogenic trap and electrically heating it to 160 to 170°. The column temperature is maintained at -30° during the 4-min desorption period; then the temperature is raised at a rate of 8°/min to a final temperature of 100°.

In order to maintain sample integrity, bags are stored away from direct sunlight and analyzed within 24 hr of collection. Efficient sample capture and transfer has been confirmed for all compounds of interest by performing replicate analyses and plotting peak area versus sample volume.

Figure 1.11 shows a chromatogram for a sample obtained from the Chicago plume. Individual retention times are recorded as well as pertinent analytical conditions and a partial identification of peaks.

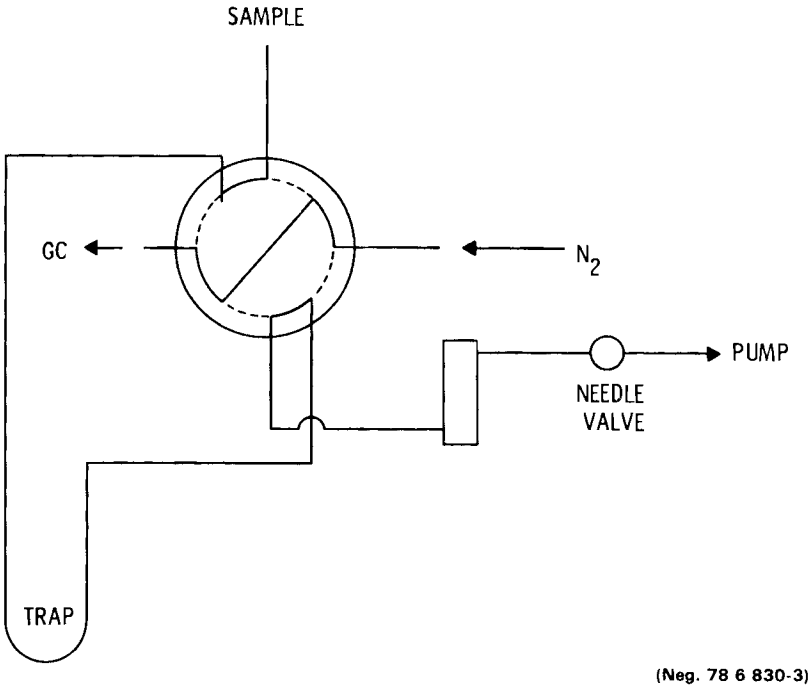

FIGURE 1.10. System for Analyzing Light Hydrocarbon Samples

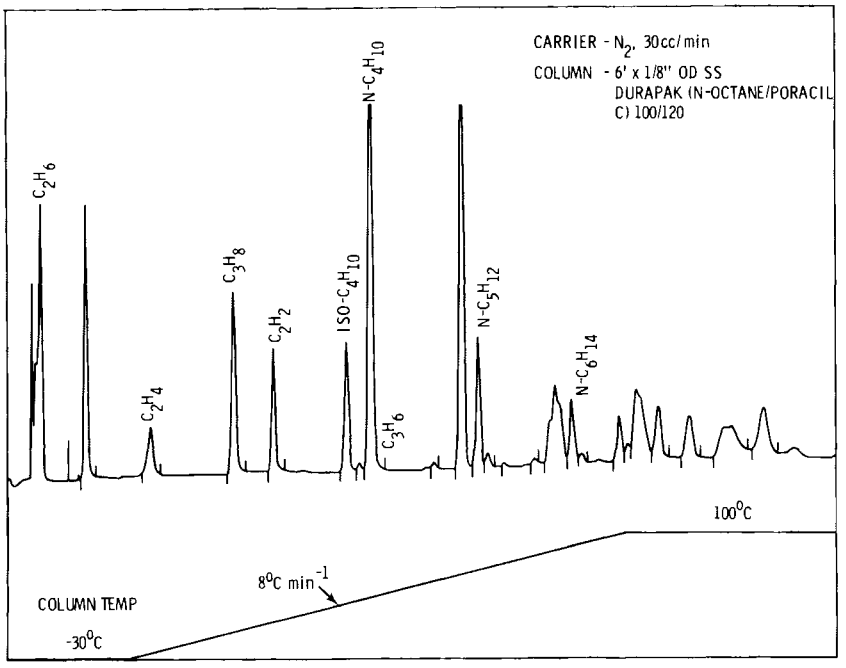

FIGURE 1.11. Chromatogram for a Sample Taken from a Chicago Plume (a) and Column Temperature Program (b)

IMPROVEMENT OF A STANDARD NO/NO_X MONITOR FOR AIRCRAFT RESEARCH

J. M. Hales and K. M. Busness

A standard NO/NO_X analyzer has been modified to improve its sensitivity and specificity. This has resulted in a factor-of-ten improvement in threshold sensitivity level (0.5 ppb).

The commercial NO/NO_X instrumentation previously operating on the Pacific Northwest Laboratory's (PNL) aircraft has been inadequately sensitive and has produced poor baseline resolution. Typical noise levels for these instruments have been in the range of 5 ppb, thus obscuring observation of a great many atmospheric situations of interest in the Multi-State Atmospheric Power Production Pollutant Studies (MAP3S) program. Moreover, because of machine drift and interferences caused by water vapor, definition of the baseline was sufficiently uncertain as to cast considerable doubt on low-concentration results.

For these reasons, one of the two NO/NO_X analyzers available for the aircraft program was modified to improve performance. This analyzer, a Model 642 manufactured in 1974 by REM Scientific, Inc., was modified in the following areas:(a)

- The existing pump was replaced by a larger unit (Welch 1440) to improve vacuum and flow rate.
- The existing photomultiplier tube was replaced by an EMI 965812, which has extended sensitivity into the red-wavelength portion of the spectrum.

(a) We would like to express our thanks to Dr. Donald Steadman of the University of Michigan and to Dr. Chester Spicer, Mr. David Miller and Mr. Darryl Joseph of Battelle-Columbus Laboratories for their helpful suggestions on this matter.

- The existing flow-control orifices were replaced by needle valves to increase flow and allow flow-rate optimization.
- A "Prereactor" system, based upon the design of Dr. Donald Steadman of the University of Michigan, was incorporated into the analyzer.

The flow configuration of the system is shown in Figure 1.12. With this modified configuration, the threshold sensitivity is approximately 0.5 ppb, corresponding roughly to a ten-fold improvement. The second NO/NO_x analyzer (Teco 14D) is to be modified in this manner in the near future, and the combination will be installed on the aircraft for simultaneous $NO/NO_x/HNO_3$ measurements.

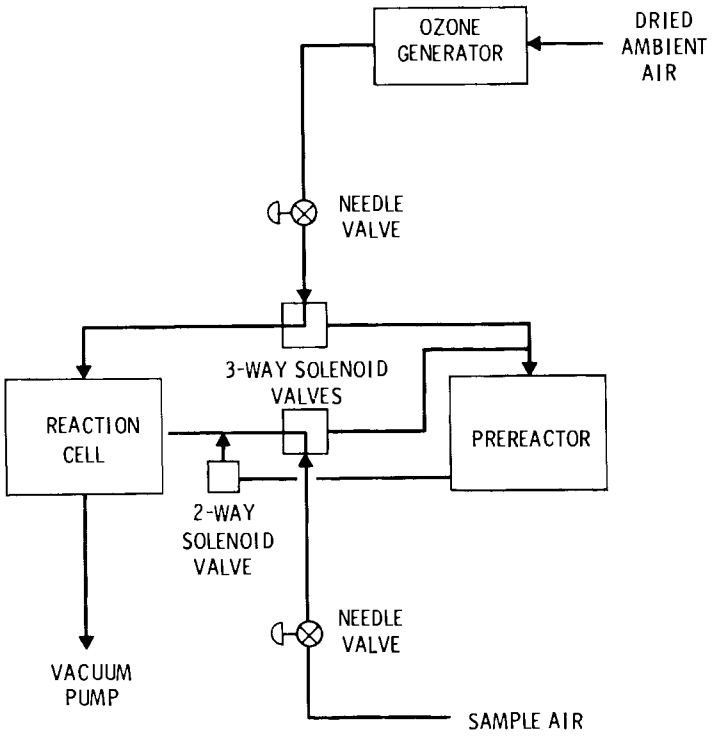

(Neg. 78 6 830-4)

FIGURE 1.12. Flow Schematic of Modified NO/NO_x Analyzer

AIRBORNE AMMONIA MEASUREMENTS IN THE GREAT LAKES REGION

R. N. Lee

An impregnated filter method has been employed to determine ammonia concentrations during aircraft sampling missions in the western portion of the Multi-State Atmospheric Power Production Pollutant Studies (MAP3S) region. Observed ammonia concentrations are less than those generally reported for surface sites in rural areas.

As a natural constituent of the atmosphere, ammonia has received frequent attention from atmospheric scientists because of its significant role in the atmospheric nitrogen cycle, its contribution to the neutralization of acid aerosols and its suggested role in the heterogeneous oxidation of sulfur dioxide (Scott and Hobbs 1967). Atmospheric measurements have led to the general conclusion that natural biogenic processes contribute >99% of the global atmospheric burden. Surface concentrations in nonurban areas of the central United States have been observed to be in the 1.4 to 4.2 $\mu g/m^3$ range, while slightly higher concentrations have been reported for rural sites in Europe (National Academy of Sciences 1977). Concentrations in the tropics have been observed to be twice those typically encountered in the temperate zone.

Anthropogenic sources, while accounting for <1% of the total atmospheric input, are sufficient to produce somewhat elevated levels in the urban atmosphere. Studies in Germany indicate urban concentrations 4 to 5 times greater than those found at rural sites. Sources contributing to these higher levels include waste incineration, domestic heating, fertilizer production and other industrial processes.

Samples collected for ammonia analysis during aircraft programs conducted in the Great Lakes Region have shown ammonia concentration within the mixing layer well downstream of major urban centers. Samples have been collected during spring, summer, fall, and winter months using filters impregnated with oxalic acid (Shendrikar and Lodge, Jr. 1975). The single-filter method originally employed has provided data on the total concentration of atmospheric ammonia. This procedure has recently been modified by placing a prefilter ahead of the impregnated filter in order to achieve a separation of gaseous and particulate species. Exposed filters are extracted with water and analyzed using the colorimetric indophenol method (Lazrus, Lorange and Lodge, Jr. 1968).

The observed concentrations are generally lower than those previously reported at surface sites. Results with the two-filter package indicate an ammonia gas/ammonia aerosol ratio, generally in the 1 to 2 range. Concentration data are summarized in Table 1.8.

TABLE 1.8. Range of Ammonia Concentrations Observed During Flights in the Great Lakes Region, $\mu g/m^3$.

Time	$[NH_3]$ Aerosol	$[NH_3]$ Gaseous	Total
March 1977	—	—	0.69-5.42
July 1977	—	—	0.27-2.93
Oct 1977	<0.2-1.48	0.21-2.66	0.21-3.99
Jan to Feb 1978	0.09-3.13	<0.02-1.29	0.45-3.22

MODIFICATIONS TO MAP3S REGIONAL MODELING PROCEDURES FOR COMPARISONS OF OBSERVED AND PREDICTED POLLUTANT CONCENTRATIONS

D. J. McNaughton

New opportunities for regional model comparisons of observed and predicted pollutant concentrations are arising as a result of data collection by Multi-State Atmospheric Power Production Pollutant Studies (MAP3S) Precipitation Chemistry Network and the Sulfate Regional Experiment (SURE). Data, available and comparable between observations and model calculations, are ambient concentrations of sulfur dioxide and sulfates and precipitation acidity for 24-hr and monthly periods. Complete examination of data has required that physical models and model input and output be modified to produce comparable results with observed data.

Past comparisons of MAP3S models and observed data (Powell et al. 1978) have made use of long-term sulfate concentrations data available from the design phase of the SURE program (Hidy 1975). More refined data that are now available require modifications in the models to allow calculation of both long- and short-term concentrations. No modifications of the long-term puff model were needed for comparisons, but short-term simulations required incorporation of a more complete treatment of turbulent horizontal diffusion and the linear plume segment code.(a) A nonlinear, plume-segment model was also developed, which includes linear scavenging of sulfate particles and nonlinear removal of sulfur dioxide, considering water solubility of SO_2. The solubility calculations require model accounting for plume element superposition in the model.

Past long-term model comparisons to observed data have involved calculation of concentration fields over the grid shown in Figure 1.13. Since the number of emission sources over this area is extremely large, a fraction (61%) of total grid emissions was used to predict the main components of variations in the observed concentration fields. For short-term predictions, concentration fields are less uniform, since no averaging is performed and individual sources become more important. To more efficiently predict short-term concentrations, the model was modified to output predictions for observing station locations (i.e., receptor-oriented predictions) rather than for the entire grid.

With a change in output orientation, input data sets can be modified to include only those emission sources that influence the receptor specified. The procedure for short-term model predictions for each receptor follows:

1) Calculate reversible back trajectories each hour of the observation period for 24 hr (e.g., a 24-hr average observation would require 24 trajectories arriving hourly at a receptor each for 24 hr).

2) Identify the spatial bounds of the envelope (see Figure 1.13) of trajectories.

3) Provide a complete emissions inventory for the regional grid.

4) Based on envelope bounds and source locations, select the subset of the emissions inventory that affects the receptor.

5) Model the case using only those sources that influence the receptor and then average predicted hourly values over the observation period.

Modifying the emission inventory with support programs allows more economical and complete predictions of concentration.

(a) See D. C. Powell, "MAP3S Model Development: Annual Progress" page 1.27 in this report.

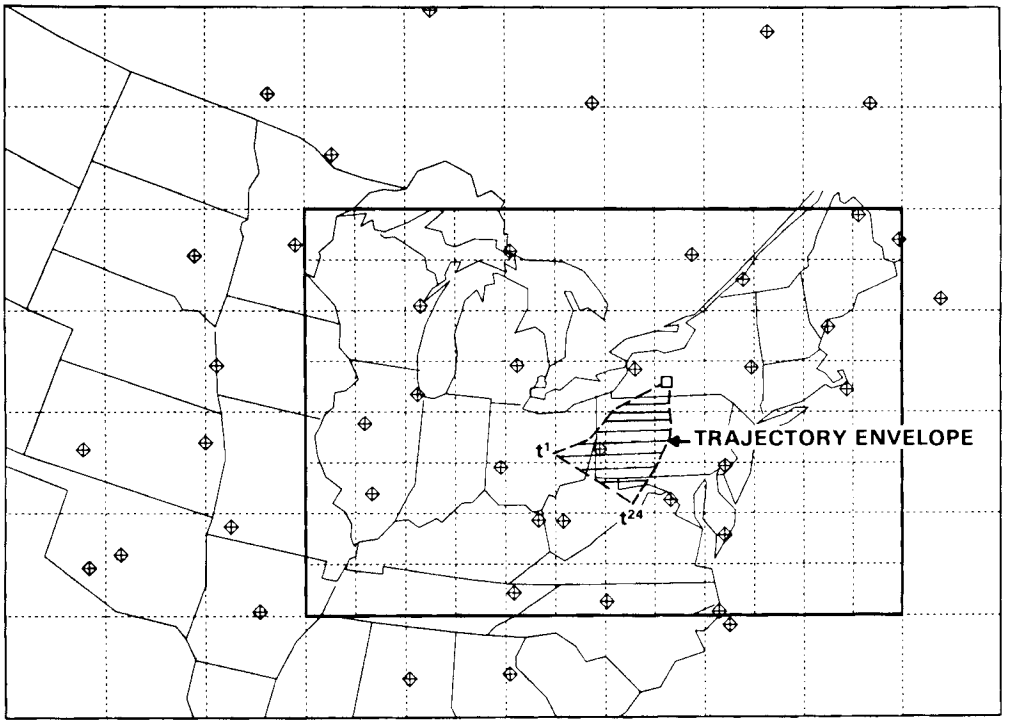

FIGURE 1.13. Long-Term Model Calculational Grid and Short-Term Trajectory Envelope

MAP3S MODELING DEVELOPMENT: ANNUAL PROGRESS

D. C. Powell

The Multi-State Atmospheric Power Production Pollutant Study (MAP3S) modeling capability at Pacific Northwest Laboratory (PNL) now includes the puff model previously reported, a linear plume segment model and a nonlinear plume segment model. The predictions of the puff model are valid only for long-term assessments. The linear plume segment model is adaptable for either short- or long-term calculations. The nonlinear model is intended only for short episodes including precipitation events.

During the past year, MAP3S modeling has been particularly responsive to needs for predictions of both short- and long-term averaged values of concentrations and deposition, using more realistic parameterizations of removal and transformation processes. The prediction of short-term concentration and deposition values has been facilitated by two new plume segment models. One of these models resembles the puff model in its linear treatment of concentrations, while the second uses a nonlinear algorithm for calculation of SO_2 removal, based on work by Dana et al. (1973).

All models use the same input meteorological data, which consist of gridded maps of a single layer of real-time, horizontal, wind components and gridded maps of hourly real-time precipitation. The essential features of all three models are summarized below.

PUFF MODEL

Discrete masses of SO_2 and sulfate are emitted from as many source locations as desired at regular time intervals. Each source is tagged with its individual effective stack height. Trajectory steps

of horizontal advection are calculated over intervals (Δt_a) using the gridded wind data, the values of which are currently specified at intervals of about 170 km. Stability, daytime mixed-layer depth and nocturnal boundary-layer depth are each specified by an invariant diurnal cycle.

Vertical diffusion is Gaussian between constraints above and below. Rate of vertical expansion is a function of stability; thus, the vertical distribution of each puff changes from Gaussian in the early stage of transport to even distributions within the mixed layer. Horizontal diffusion is implicitly assumed to be a function of synoptic scale wind variation only. Horizontal turbulent diffusion is not included.

Removal and transformation are handled separately for each puff by solving in time a set of four ordinary linear equations (Powell et al. 1978). Dry removal is of the source depletion type, but an analytical modification reduces the removal flux to approximate closely that which would be calculated by a surface depletion model.(a)

The deposition velocities for SO_2 and sulfate are calculated from a new algorithm based on a paper by Wesely and Hicks (1977). Since the calculated deposition velocities are functions of surface roughness and stomatal resistance, the program requires gridded values of each. A roughness length has been computed for each square of the sampling grid (linear dimension is 34 km) from an original roughness map.

Wet deposition of SO_2 is a linear function of SO_2 mass and precipitation rate (Powell et al. 1978). Wet deposition of sulfate is modeled after description by Scott (1978) of a bergeron-type storm. The rate is linear in sulfate mass and turns out to be proportional to the five-eighths power of precipitation rate.

The rate of transformation of SO_2 to sulfate depends on:

- type of release; i.e., power plant or urban.
- time of day; a diurnal cycle is used for each release type, both including zero values at night.
- line of transport; whether or not the puff is in the earliest hours of transport, during which time a constant rate prevails for each release type.

For each sampling interval, Δt_s, contributions are calculated from each puff to the sampling grid square the puff is over. Contributions are calculated for ground-level air concentrations and for deposition of SO_2, sulfate and rainfall pH (Powell et al. 1978). The area of the sampling grid square is used mathematically to simulate horizontal diffusion. Therefore, each individually calculated contribution is inversely proportional to a grid square area. The final displayed calculations must be time-averaged over an interval at least several hundred times as long as the sampling interval (Δt_s) if they are to be quasi-independent of grid square area. For this reason, the puff model is suitable for long-term assessments only.

LINEAR PLUME SEGMENT MODEL

The functional difference between the puff model and the linear plume segment model is: the latter may be used for either long-term assessment or short-term episodic calculations. The mathematical difference consists of the use of the Gaussian plume equation (under vertical constraints) with the necessary parameterizations of horizontal diffusion. At the end of each sampling interval Δt (calculations of sampling, advection, and emissions are made over the same interval Δt) a segmented plume is constructed from each source using the successively emitted discrete sulfate masses (see Figure 1.14).

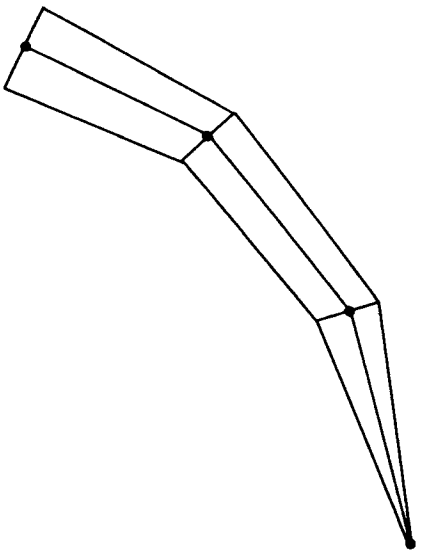

FIGURE 1.14. Schematic Diagram of Segmented Plume Concept

(a) See "Horst" page 1.40 of this report.

The sampling contributions are calculated for a gridded set of points rather than for a grid area. From a given plume segment, contributions are calculated for any sampling point within a distance not farther from the plume centerline than $3\sigma_y$. Both lateral and vertical diffusion rates are functions of stability. Thus, unlike the puff model, each contribution calculated is assumed to be a time-averaged ground-level air concentration or deposition flux valid over the given sampling interval (Δt) at the sampling point to which the calculation applies.

The other features of this model are identical to those of the puff model. The executing time of the linear plume segment model is about three times that of the puff model.

The functional difference between this model and the others is that the nonlinear plume segment model is intended to be used only for short-term precipitation episodes. The mathematical difference is that the wet removal of SO_2 is calculated as a function of water solubility of SO_2, which increases with decreasing SO_2 concentration, with increasing rainfall pH, and with increasing temperature, according to analytical work by Dana et al. (1973).

In order to generate concentration data needed to calculate the changing solubility, the model must keep track of local increases of concentration that result from superimposition of plume segments from plumes originating at different sources. This occurs when a plume from one source passes over the source of another plume as shown in Figure 1.15. Otherwise, this model is similar to the two foregoing models except that constants for deposition velocity and for transformation rate in the nonlinear model are used in their present state of development.

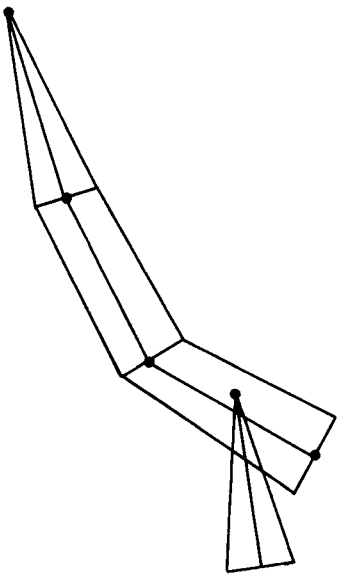

FIGURE 1.15. Schematic Diagram of Segmented Plume Overlap

A CASE STUDY OF ELEVATED LAYERS OF HIGH SULFATE CONCENTRATION

D. J. McNaughton and M. M. Orgill

During studies in August 1976 that were part of the Multi-State Atmospheric Power Production Pollutant Study (MAP3S), Alkezweeny et al. (1977) noted that in the Milwaukee urban plume, layers of relatively high sulfate concentrations occurred at high altitudes with respect to the boundary layer. This paper represents a progress report on studies undertaken to investigate possible causes for a bimodel vertical profile of sulfate concentrations.

Data presented by Alkezweeny et al. (1977) serve as a basis for this study. Data from August 23, 1976, and August 24, 1978, indicate concentrations relatively high in sulfate, at 1000 and 6000 ft, respectively, with lower concentrations at lower altitudes. Concentrations of trace metals also indicate no peaks in the vertical concentration profiles above the surface. Initial studies of the high, elevated sulfate concentrations have centered on the August 23 measurements taken over southeast Wisconsin using synoptic data from the national weather service, emissions data from the national emissions data bank system (EPA), air quality data from the national air surveillance network (EPA), and satellite photographs from the EROS Data Center (U.S.G.S.).

The following describes the synoptic situation for the August 23 to 24 period and presents observations on the study to date as well as plans for future analysis.

The synoptic situation for the August 23 to 24 Lake Michigan experiment is depicted in Figure 1.16. On the day prior to the experimental flight, prevailing visibility throughout most of the Great Lakes was 10 km (6 mi) or less due to haze and fog. During the preceding period, frontal passage was dominated by a stagnating anticyclone typical of one type of high sulfate episode identified by Hidy (1976) and Tong and Batchelder (1978). During the 22nd and 23rd, a weak polar front from Canada moved southward over the Great Lakes area at approximately 22.5 km hr^{-1} (14 mi hr^{-1}) and was located just south of Lake Michigan on the 23rd at 127(07 EST). This weak cold front and associated polar air mass had a tendency to improve the horizontal visibility behind the front, but haze and smoke layers were still reported at higher elevations. Prevailing visibility south of the front was still poor (see Figure 1.16).

A north to south vertical cross section of the frontal system is depicted in Figure 1.17. Above the 950 MB pressure level, the frontal system was located between Chicago and Green Bay. In the lower levels the front appears to merge with the nocturnal temperature inversion layer. Upper-air reports south of the front indicated that the top of the haze layer was between 800-750 MB levels or around 2134 m (7000 ft) MSL. Figure 1.17 indicates that the elevated sulfate layer at 3000 m (10,000 ft), as observed by the Lake Michigan experiment, was located in the frontal transition zone.

Observations of sulfate concentrations of 7 to 9 $\mu g\ m^{-3}$ at high altitude are within the range of typical surface concentrations (Hidy 1976), but their existence above the mixed layer appears possible only by an injection of concentrated sulfate mass into the elevated layers (see Table 1.9). A number of hypothetical mechanisms for this injection are presented:

1) direct emission and subsequent transformation of sulfur dioxide into the layer,

2) broad lifting of a surface layer with high sulfate concentrations,

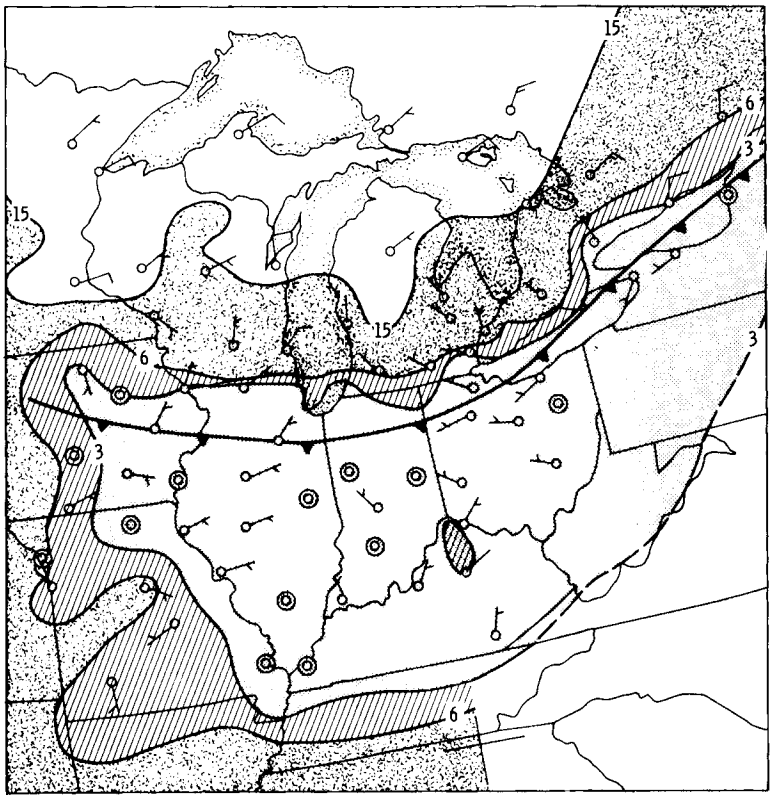

FIGURE 1.16. Surface Synoptic Data and Winds for 2300Z, August 19, 1976 (contours are isolines of prevailing visibility, i.e., 3, 6 and 15 miles)

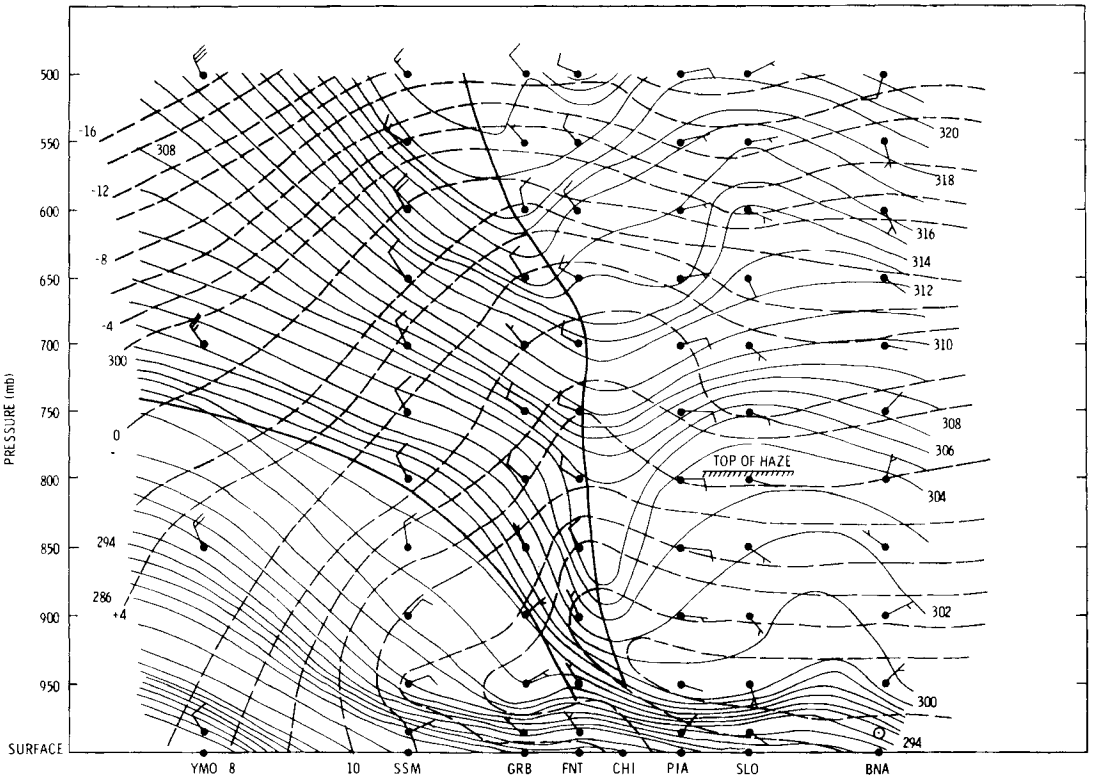

FIGURE 1.17. A North to South Cross Section of Potential Temperature (solid lines) and Temperature for 1200Z, August 23, 1976 (broken lines are isotherms in °C)

3) trapping of sulfate in a stable inversion layer after the suppression of mixing at night or after a frontal passage.

No conclusion, but the following observations, have been made concerning these mechanisms:

- Direct emissions of sulfur oxides at heights greater than 2000 ft are normally expected only in the Upper Ohio River Valley (western Pennsylvania), Ontario, and in Tennessee (Hidy 1976). Considering the character of sulfate formation as a secondary pollutant from sulfur dioxide and the dilution of plumes with distance, concentrations on the order of 10 $\mu g\ m^{-3}$ would be expected within 100 to 200 km of an individual source.

- A broad area of low visibilities (see Figure 1.16) and probably high pollutant concentrations accompanied the stagnative anticyclone preceding the weak but dry frontal passage with the haze layer top near 6000 ft (see Figure 1.17). Local to the observation area, high surface concentrations of both ozone and sulfur dioxide (Table 1.10) drop off rapidly on August 23 as the surface front passes through the area. The surface pollutant layer was either transported out of the area or lifted with the frontal passage. The air in the 10,000-ft layer on August 23 does not appear to be surface air as a result of the low concentrations of trace metals (Table 1.9) measured.

- Pollutants in the deep mixed layer expected in a stagnation situation are normally distributed in a uniform manner except in the immediate vicinity of emission sources. Building of a surface-based inversion may isolate a portion of the mixed layer.

Future studies will make use of trajectory analyses and satellite photographs in an attempt to identify possible source regions. Further analysis of the August 24 cases and other time periods may contribute to identifying the reason for formation of these pollutant layers.

TABLE 1.9. Sulfate and Trace Metals Upwind of Milwaukee.

Date	Altitude in feet	Sulfate, $\mu g/m^3$	Ca, ng/m^3	Mn, ng/m^3	Fe, ng/m^3	Pb, ng/m^3
August 23, 1976	1,500	1.6	239	6.3	159	7.1
	10,000	7.4	28	ND[b]	17	4.4
August 24, 1976	1,500	5.4	3,140	25.6	614	46.0
	6,000	9.0	88	3.4	73	24.0
	8,000	ND	ND	ND	ND	ND
August 29, 1976[a]	1,000 to 6,000	0.3	79	1.7	54.9	3.6
August 30, 1976	5,000	0.9	535	17.3	539	ND

[a]Over Lake Michigan, wind from the north
[b]ND = not detected

TABLE 1.10. Ambient 24-Hour Average Pollutant Concentrations.

	Sulfur Dioxide, $\mu g\ m^{-3}$				Ozone, ppm			
Date	Raling	Milwaukee	Waukesha	Chicago	Raling	Milwaukee	Waukesha	Chicago
8/14/76	52	47	—	62	—	—	—	—
8/19/76	—	—	—	—	0.094	0.077	0.052	0.027
8/20/76	60	36	—	52	0.087	0.060	0.051	0.029
8/21/76	57	42	—	83	0.105	0.061	0.050	0.038
8/22/76	42	26	—	44	0.067	0.060	0.023	0.036
8/23/76	34	18	—	29	0.029	0.019	0.022	0.010

GRAPHICAL INTERPRETATION OF NUMERICAL MODEL RESULTS

D. R. Drewes

Computer software has been developed to produce high quality graphical displays of data from a numerical grid model. The code uses an existing graphical display package (DISSPLA) and overcomes some of the problems of both line-printer output and traditional graphics. The software has been designed to be flexible enough to handle arbitrarily placed computation grids and a variety of display requirements.

Interpretation of gridded data generated by computer (numerical) models is often hampered by the inherent inability of the computer line-printer to display simultaneously several aspects of the situation being modeled. Traditional graphical methods are able to display several of these aspects simultaneously, but are often impeded by the necessary communication link between modeler and graphical artist. Both of these problems, however, are beginning to find their solutions in the recent expansion of computer graphics. Reliable, efficient software packages are now available to produce high quality graphical representations of the results obtained from computer models. Furthermore, the graphical results are available essentially in real time, that is, without having to be interpreted and rendered by an illustrator. Such a technique has been applied to the analysis of results of a computer model that simulates dispersion of atmospheric pollutants from a number of sources at various locations in the western half of the United States.

The model overlays a grid on a map of the region of interest. The sources postulated are then located with respect to this grid, and the model calculates various pollutant concentrations for each grid square. Computer printouts of these values are difficult to interpret since they do not show explicitly the source locations and other geographical information (see Figure 1.18). By sacrificing some of the precision of the direct printout and segregating the results into several categories (say A, B, and C), it is possible to produce a printer plot of "contours" of the concentrations and even to roughly define the geographical information (see Figure 1.19). Even this substantial improvement has basic limitations, however: the source locations cannot be included (except at the expense of other information); the overlaid map is imprecise; and the character spacing on the printer makes the grid appear skewed. The graphical software developed to display these data overcomes these defects and produces a high quality, easy-to-analyze picture (see Figure 1.20) of both the input

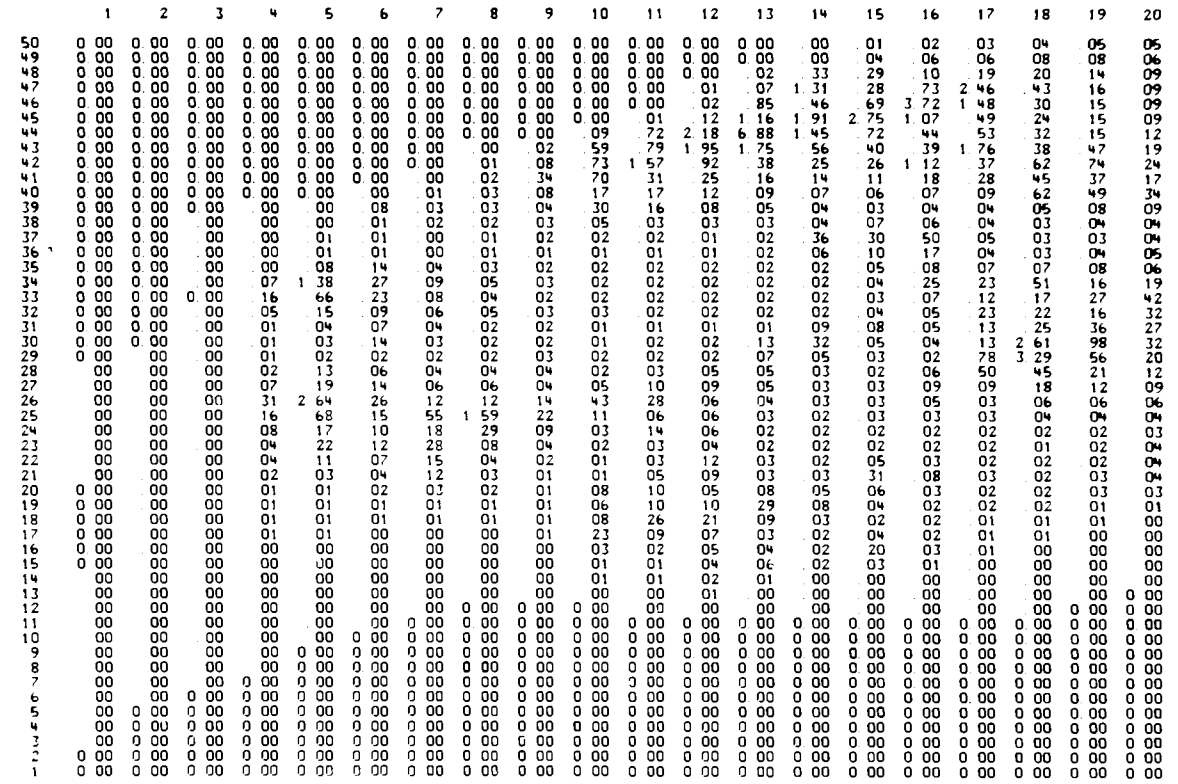

FIGURE 1.18. Numerical Output of Model Results

(source locations and relative sizes), output (concentration contours), and physical relationships (the map basis). Colored analogs, which are especially useful during oral presentations, can also be produced.

The software developed for these displays is not limited to the grid system used for this model. Coordinate strings to define all the state outlines are available. The grid spacing is completely arbitrary, and while the plots are defined relative to the NMC grid,(a) the computation grid may be rotated and translated in any manner desired. Furthermore, the plot may, at the user's option, cover a greater (or lesser) portion of the map than that covered by the grid. Thus, the software is useful for producing graphical displays of gridded numerical data regardless of the geographical orientation of the grid. Because of its modular nature, other pertinent data can also be included, depending on the needs of the user.

(a) Jenne, R. L. "The NMC Octagonal Grid." National Center for Atmospheric Research, Boulder, Colorado.

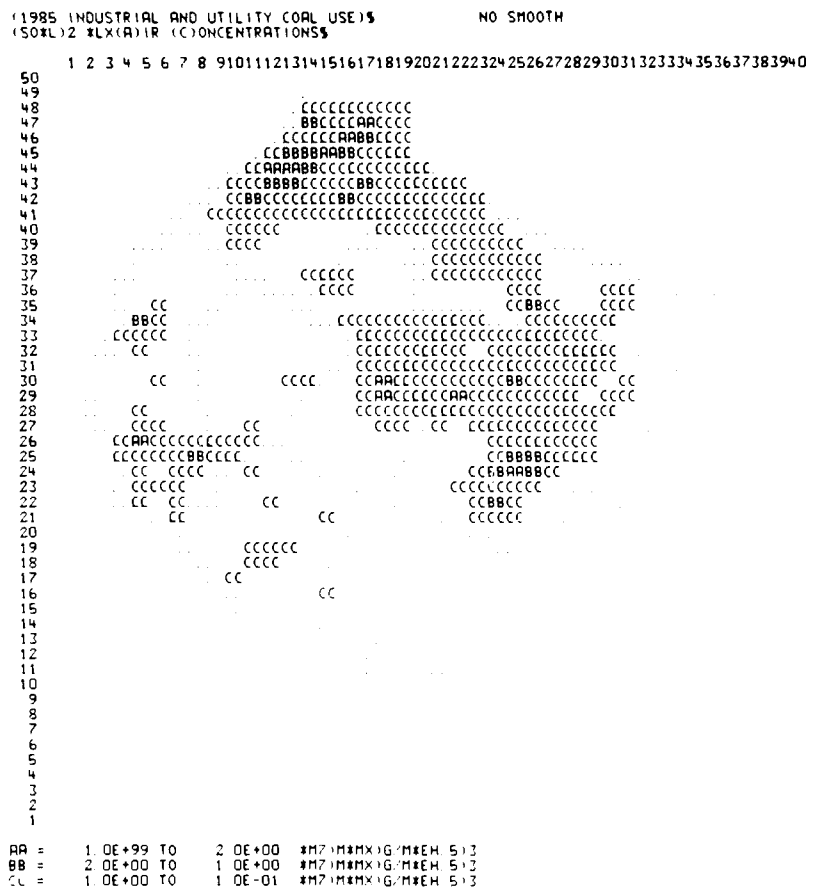

FIGURE 1.19. Printer Plot of Model Results

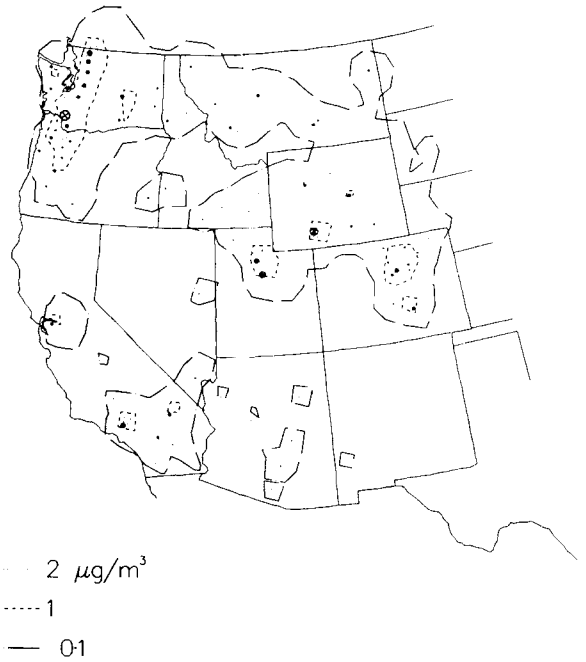

FIGURE 1.20. Contour Plot of Model Results for SO_2 Air Concentrations for 1985 Industrial and Utility Coal Use

DRY DEPOSITION OF ATMOSPHERIC OZONE

J. G. Droppo and J. C. Doran

The dry removal processes of pollutants associated with emissions from fossil-fuel-fired power plants were studied in field tests. Results of ozone dry deposition tests using both an eddy flux method and a profile method are given. These data are needed as input for modeling long-range transport of atmospheric pollutants.

Ozone was selected for study because of its importance as an atmospheric pollutant. The availability of fast response ozone monitors allows direct measurement of the ozone Reynolds flux as well as concentration profiles. The high sensitivity of such instruments allows study of ozone at background concentrations of ozone.

The concentration gradient $\partial C/\partial z$ may be determined as a function of height from measurements of the concentration profile. If an eddy transport coefficient is then assumed, the aerodynamic resistance to transport may be calculated and the surface resistance term determined (Droppo 1976; Garland 1976). The surface resistance may also be determined directly from measurements of the Reynolds flux, $w'C'$, of the pollutant and the pollutant concentration near the surface (Desjardins and Lemon 1974; Wesely et al. 1977). The ratio of $w'C'$ and $\partial C/\partial t$ then provides a value for the eddy diffusivity K_C. While some evidence exists that the diffusivity for heat, K_H, is more appropriate than that for momentum, K_M, the question has not been totally resolved (Dyer and Hicks 1970; Galbally 1971).

Measurements were taken at two sites: one in western Washington and one in eastern Washington. The experimental techniques and procedures were developed at the former site, but the availability of additional apparatus and superior fetch at the latter site made it a more attractive choice.

The terrain at the eastern Washington site was a relatively flat, uniform desert with sparse sagebrush and various grasses being the main vegetation. An acceptable fetch was available in most directions for several kilometers, and a roughness length of $\sim$4.5 cm was estimated from a number of wind and temperature profiles. Winds were determined using three-component Gill anemometers located at heights of 1.22, 4.72 and 18.3 m. Thermistor temperature probes were located at the same heights.

As many as three chemiluminescent ozone monitors were used simultaneously during data collection periods. A factory modified instrument, with a response time of approximately one second, was used to record ozone fluctuations at the top of an 18.3-m tower. Air was drawn in at that height through a teflon line connected to a pump. A double tee arrangement (Figure 1.21) enabled the ozone in the line to be sampled by the monitor that was located near the pump. Reynolds fluxes of ozone were computed from fluctuations in concentration and vertical wind speed at the 18.3-m level.

Two roving sample lines were used to record the ozone concentration profiles. The lines were positioned so that one inlet was located at a height of 0.76 m when the other was at 15.2 m. The intake lines switched positions periodically to compensate for possible systematic errors. The relative calibration of the two instruments

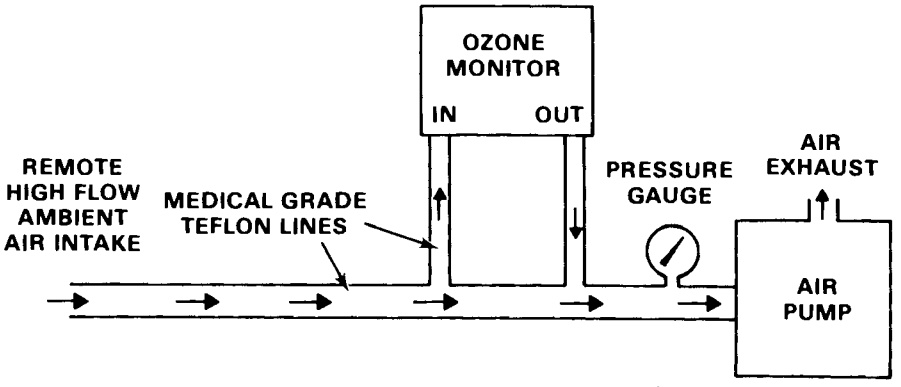

FIGURE 1.21. Schematic Diagram of Ozone Monitor Intake Systems

was checked before and after each data period (∿1 hr) by moving the two intakes to the same height and recording concentrations for several minutes.

Examples of the measured wind, temperature and ozone concentration profiles are shown in Figure 1.22 for slightly unstable conditions and in Figure 1.23 for moderately unstable conditions.

In determining surface resistances to ozone transport, several assumptions are made. First, the roughness length for momentum flux, z_0, is an appropriate height at which to determine the resistance for ozone. Second, the surface and atmospheric resistance terms may be added in series so that the total resistance is given by the sum of these two contributions, $R_T = R_a + R_s$. The surface term, R_s, is simply treated as a residual after the atmospheric contribution, R_a, has been removed. Thus, R_s used here may contain a stomatal resistance contribution as well as any resistance to transfer across the surface layer of air in contact with a vegetative surface (Wesely and Hicks 1977).

From measurements over the semi-arid terrain of eastern Washington, a surface resistance value for ozone of 290 ± 150 s/m was found. This agreed well with results from measurements over a grassy field in western Washington, where the surface resistance was found to be 270 ± 160 s/m.

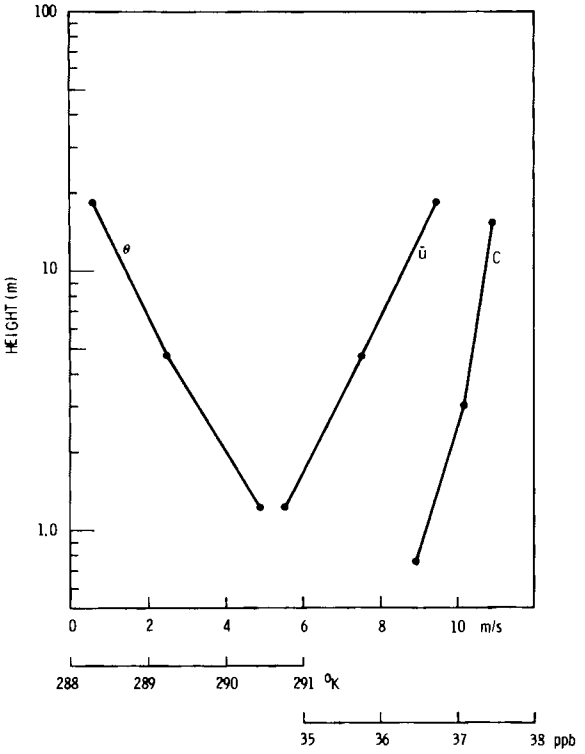

FIGURE 1.22. Measured Ozone Concentrations, Wind and Temperature Profiles in Slightly Unstable Conditions

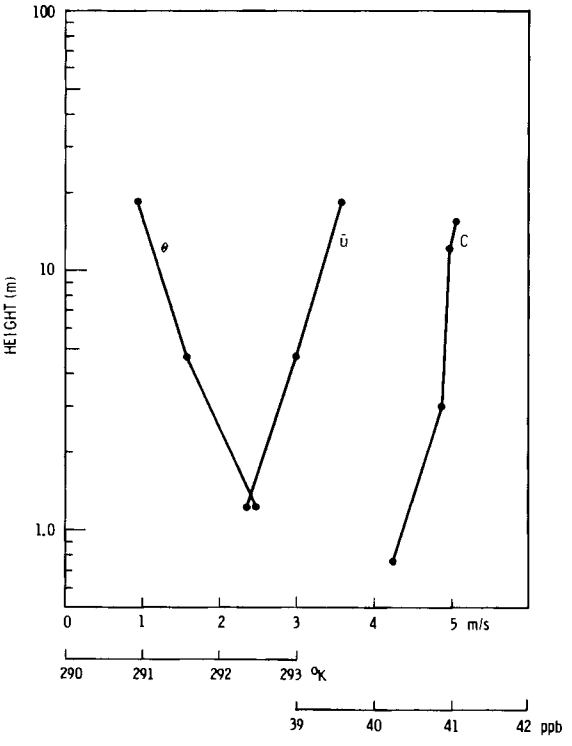

FIGURE 1.23. Measured Ozone Concentrations, Wind and Temperature Profiles in Moderately Unstable Conditions

The eddy diffusivity for any quantity is defined as the ratio of the flux to the concentration gradient. Determining ozone eddy diffusivity requires accurate specification of the very small ozone concentration gradients to allow comparison with values for heat and momentum.

A straight line of the form $C = a + b \ln z$ was fitted to the ozone profiles, and similar fits were made to the velocity and temperature profiles as well. An estimate of $\partial C/\partial z$ at z = 10 m is then given by b/10, and $K_C \approx \text{Flux}(O_3)/(\partial C/\partial z)$. Similar calculations were carried out for velocity and temperature, and some results are summarized in Table 1.11.

TABLE 1.11. Estimated Values of Momentum (K_M), Diffusivity for Heat (K_H) and Eddy Diffusivity (K_C) at 10 m.

Run	K_M, m²/sec	K_H, m²/sec	K_C, m²/sec
1	3.29	3.87	3.63
2	3.32	3.58	4.42
3	1.90	2.99	3.80
4	1.73	2.27	4.65
5	1.48	4.31	2.59

From these values, the ratio K_C/K_M is found to be 1.77 ± 0.62 while K_C/K_H = 1.22 ± 0.54. A value of unity would be expected for one of these ratios if the transport mechanisms for ozone were identical with that for momentum or heat. The significantly better agreement with the eddy diffusivity for heat suggests that it is the more appropriate value.

Surface resistance values for ozone have been measured at two sites and were found to agree well with each other. The combined measurement of concentration profiles and eddy fluxes is a useful technique in transport and resistance studies. Results obtained from these indicate that the eddy diffusivity for ozone is more similar to that for heat than to that for momentum.

PROFILE MEASUREMENTS OF AEROSOL DEPOSITION

J. C. Doran and J. G. Droppo

A field test program, which assesses the accuracy of the gradient profile method of determining deposition velocities, is described.

The gradient method of deposition velocities has proved useful in the study of dry removal of gases, such as SO_2 and O_3 (e.g., Garland 1976). Measurements of particulate deposition by this technique are considerably more difficult, but reported results (Droppo 1977) suggest that the approach is feasible. One of the major objections to this method is that the expected small values of deposition velocity would result in exceedingly small gradients that would not be sufficiently well resolved by available measuring and analysis procedures. However, recent results (Wesely et al. 1977; Hicks and Wesely 1978) indicate that deposition velocities for small particles may be higher than previously anticipated; thus, the gradient method becomes more attractive.

Critical to the successful application of this method is the relative accuracy with which concentration differences between various heights can be measured. A careful study of this aspect of the problem has, therefore, been undertaken.

A 12.2-m tower was erected and used to mount the holder and filters that sample the ambient air. Eight filters were mounted on the tower, and they were divided into two groups of four. Each filter in a group was connected to a common pressure manifold by 1.9-cm I.D. flexible tubing. The manifold was used to equalize the pressure in each of the lines so that identical flow conditions for each filter might be established. In actual practice, minor variations in the filter holder geometries resulted in different flow rates. These rates, however, were monitored by Roots meters located at the manifold, which ensured that the meter readings were recorded at the same pressure for each line. This made pressure corrections unnecessary. The manifold itself was attached to three pumps, which were used to draw air through the lines. An independent set of pumps, meters and manifold were connected to the second group of filters. Figure 1.24 shows a schematic diagram of the arrangement.

The two lower levels of two filters each were each fixed in position on the tower at heights of 1.2 m and 2.6 m, respectively. The upper two pairs of filters could be raised and lowered by means of a cable, rope and pulley assembly. In the lowered position, the heights were 2.85 m and 3.16 m; in the raised position, they were 5.26 m and 11.7 m. This feature allowed the filters to be changed when the holders were in the lower position, thereby eliminating the need for extensive tower climbing to carry out the experiments.

Thus far, several calibration runs have been carried out with the filter holders in their lowered position, and one run has been done with the filters raised. The filters are currently being analyzed for sulfur concentration using x-ray fluorescence. Further experiments in this area are contingent upon evidence that the required concentration accuracies have been realized in these initial tests.

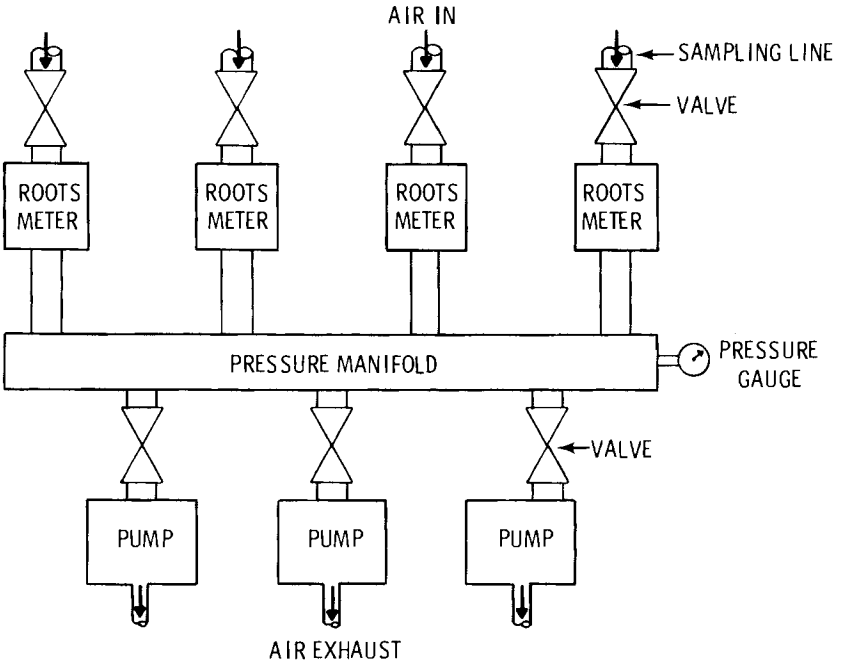

FIGURE 1.24. Schematic Diagram of Flow Measurement and Regulation System

A SIMPLE CORRECTION TO THE SOURCE-DEPLETION MODEL

T. W. Horst

A simple correction, based on gradient-transfer theory, is proposed to correct the source-depletion, diffusion-deposition model for the deposition-caused vertical contaminant profile. The resulting predictions compare very well with those of the surface depletion model.

The common source-depletion method of correcting a Gaussian diffusion model for dry deposition is biased in its predictions of ground-level airborne contamination and of deposition flux (Horst 1977). Nevertheless, the source-depletion model is quite attractive due to its computational simplicity. A modification of the source-depletion model, based on gradient transfer theory, is proposed and the resulting predictions are shown to compare very well with the correct solution as computed by the surface-depletion model.

The source-depletion model accounts for dry deposition by reducing the source strength (Q) as a function of downwind distance, without altering the vertical distribution of contamination. Thus, if the contaminant is well mixed to a height (Δz), the bulk concentration is

$$\bar{C} = \frac{Q(x)}{u\Delta z} \quad . \tag{1}$$

The deposition flux is assumed to be $v_d\bar{C}$ and conservation of mass then requires

$$Q(x) = Q_o \exp\left\{-\int_0^x \frac{v_d}{u\Delta z}\,dx'\right\} \quad . \tag{2}$$

The errors of the source-depletion model result from its neglect of the deposition-caused concentration profile near the surface. For a horizontally uniform situation and a nonsettling contaminant, this profile is:

$$C(z) - C(z_*) = v_d C(z_*) \int_{z_*}^{z} \frac{dz'}{K(z')} \tag{3}$$

where K(z) is the eddy diffusivity of the contaminant, $C(z_*)$ is the contamination at ground level, and $v_dC(z_*)$ is the correct deposition flux. Hence, Equation (2) is corrected by multiplying the deposition velocity (v_d) by the ratio $C(z_*)/\bar{C}$, which can be obtained from Equation (3).

$$\bar{C} \equiv \frac{1}{\Delta z}\int_{z_*}^{\Delta z} C(z)\,dz$$

$$= \frac{C(z^*)}{\Delta}\int_{z_*}^{\Delta z}\left[1+v_d\int_{z_*}^{z}\frac{dz'}{K(z')}\,dz\right] \tag{4}$$

At locations close to the source the contaminant is not well mixed in the vertical. The source depletion model assumes the crosswind-integrated, ground-level contamination to be

$$\frac{Q(x)}{Q_o}\,C_o(z_*) = \frac{Q(x)\,\exp(-h^2/2\sigma z^2)}{\sqrt{\pi/2}\;u\;\sigma_z} \tag{5}$$

where h is the source height and σ_z is the standard deviation of the diffusion plume in the vertical. Since $h^2/2\sigma_z^2$ goes to zero at long distances from the source, a comparison of Equations (1) and (5) suggests the use of Equation (4) with $\Delta z = \sqrt{\pi/2}\;\sigma_z$ to also correct the source depletion model close to the source. Thus,

$$C(z_*) = C_o(z_*)\left[\frac{C(z*)}{\bar{C}\;(\Delta z = \sqrt{\pi/2}\;\sigma_z)}\right]\frac{Q(x)}{Q_o} \tag{6}$$

and

$$Q(x) = Q_o \exp\left\{-\int_o^x \frac{v_d\,\exp(-h^2/2\sigma_z^2)}{\sqrt{\pi/2}\;u\;\sigma_z}\left[\frac{C(z_*)}{\bar{C}}\right]dx'\right\} . \tag{7}$$

Figure 1.25 compares the predictions of Equations (4) and (6) for the ratio $[C(z_*)/Q(x)]/[C_o(z_*)/Q_o]$ to the predictions of the surface depletion model (Horst 1977 and 1978a). Since the uncorrected source-depletion model predicts a value of one for this ratio, the proposed correction is very good, especially for $\sigma_z/h \geq 1$ where almost all of the deposition occurs.

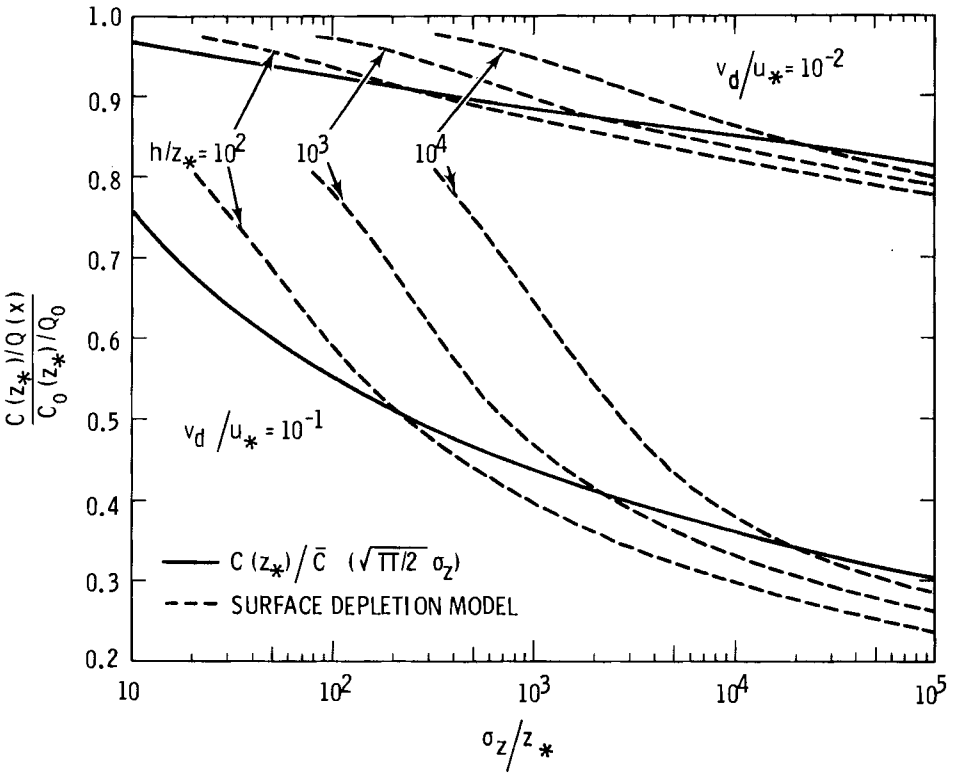

FIGURE 1.25. A Comparison of Normalized Ground-Level Concentrations Predicted by the Corrected Source-Depletion Model and by the Surface-Depletion Model

STUDIES OF MATERIALS FOUND IN PRODUCTS AND WASTES FROM COAL-CONVERSION PROCESSES

M. R. Petersen and J. S. Fruchter

Researchers at Pacific Northwest Laboratory (PNL) have been investigating materials from synthetic fossil-fuel processes. During this past year, solids from the Lignite Gasification Pilot Plant and samples from the Solvent Refined Coal Pilot Plant (SRC-II mode) have been analyzed for organic and inorganic constituents. Observations on these samples are summarized.

The objectives of this program are to identify and to quantify the constituents occurring in products, effluents, and emissions from coal-conversion processes that warrant consideration in the development of control measures. Sampling and analyses of materials from a coal gasification and a coal liquefaction plant have been completed during this year, and some findings are summarized below.

Lignite Gasification (CO_2 Acceptor) Process

Before the Lignite Gasification Pilot Plant was shut down in September 1977, PNL obtained some samples of feed coal, gasifier and regenerator fines, and spent limestone acceptor for research purposes. These samples were analyzed using instrumental neutron activation analysis (INAA) and

x-ray fluorescence (XRF) for many major and minor elements. The results of these analyses are shown in Table 1.12. Some of the more volatile elements, such as arsenic and bromine, tend to partition onto the fines. Because the coal ash tends to accumulate on the acceptor, many elements found on the spent acceptor came from the coal. The gasifier fines indicated that the coal ash and the measured concentrations were higher in many elements than in the acceptor. The regenerator fines found during recalcining the acceptor were also high in most elements.

Solvent Refined Coal Process

During this year, the Solvent Refined Coal Pilot Plant at Fort Lewis, Washington, completed a series of runs in the SRC-II mode. This mode of operation produces a low-sulfur fuel oil. During one of their mass balance runs, samples of feed coal, product distillates, solid wastes, effluent water, and offgases before flaring were collected.

TABLE 1.12. Inorganic Element Concentrations in Solid Samples from Coal Gasification Process, in ppm by Weight Except as Noted.

	Feed Coal		Gasifier Fines		Lime (Spent Acceptor)		Regenerator Fines	
Element	INAA	XRF	INAA	XRF	INAA	XRF	INAA	XRF
Na	0.40% ± 0.01		0.24% ± 0.01		640 ± 30		0.41% ± 0.1	
Si		5800 ± 1650		—		<1.4%		<2.7%
P		<1300		1.05% ± 0.19		3.4%		2.8%
S		0.60% ± 0.05		1.65% ± 0.14		9100 ± 1040		3.7%
Cl		<160		<380		<500		1000 ± 400
K		55 ± 15		470 ± 60		<300		3500 ± 300
Ca		1.61% ± 0.10		12.7% ± 0.9		47%		35.9% ± 24
Ti		550 ± 40		2590 ± 180		1200 ± 90		4300 ± 280
V				100 ± 30				114 ± 25
Cr	9.5 ± 0.2		32 ± 1	28 ± 2	28 ± 7		82 ± 5	85 ± 10
Mn		31 ± 1		170 ± 13		202 ± 15		180 ± 17
Fe	0.27% ± 0.01	0.290% ± 0.020	2.07% ± 0.05	228% ± 0.14	1.15 ± 0.01	1.337% ± 0.09	1.67 ± 0.2	1.8% ± 0.1
Co	1.4 ± 0.1		9.6 ± 0.2		4.2 ± 0.1		24.8 ± 0.4	
Ni	4.9 ± 0.6	5.7 ± 0.5	42 ± 5	44 ± 3	53 ± 8	60 ± 5	68 ± 8	67 ± 6
Cu		7.8 ± 0.3		67 ± 5		50 ± 4		69 ± 7
Zn		5.7 ± 0.3		38 ± 3		59 ± 4		58 ± 4
As	1.2 ± 0.1	1.3 ± 0.1	22.5 ± 0.5	8.6 ± 1.4	4.6 ± 0.1	5.2 ± 0.8	8.3 ± 0.3	7.6 ± 0.7
Se		1.91 ± 0.06		3.0 ± 0.4		2.8 ± 0.6		13.5 ± 1.1
Br	1.09 ± 0.08	1.0 ± 0.1	5.7 ± 0.3	4.8 ± 0.5	3.1 ± 0.1	2.4 ± 0.5	27.1 ± 0.4	28 ± 2
Rb	<2	1.3 ± 2	5.1 ± 1.0	5.7 ± 0.6		3.4 ± 0.7		17 ± 1
Sr		296 ± 5		940 ± 60		840 ± 40		1540 ± 70
Sb	0.26 ± 0.04		1.8 ± 0.3		0.32 ± 0.06		0.88 ± 0.15	
Ba	320 ± 40		1080 ± 120		300 ± 40		1350 ± 110	
La	24.8 ± 0.2		18.8 ± 0.2		9.2 ± 0.2	24.8 ± 0.3		
Hf	5.2 ± 0.3		2.2 ± 0.1		0.68 ± 0.04			2.6 ± 0.1
Pb		3.1 ± 0.2		8.6 ± 1.4		<3.8		27 ± 2
Th	1.5 ± 0.1		6.9 ± 0.1		3.2 ± 0.1		9.8 ± 0.2	
U	4.4 ± 0.4		2.6 ± 0.3		2.8 ± 0.2		4.4 ± 0.4	

The distillates were analyzed for selected polynuclear aromatic hydrocarbons (PAH). These gas chromatograph/mass spectrometry analyses were performed using argon chemical ionization in selected ion mode with a nematic crystal column. The concentrations of the PAH compounds found in the samples are listed in Table 1.13. The data were obtained from just one set of samples and may not necessarily reflect values that may occur under different process conditions. The observed concentrations were dependent on the boiling ranges of the distillate cuts and were found to be highest in the heavy distillate (boiling range 288°-454°C).

TABLE 1.13. Concentration of Selected PAH Compounds in Distillates from SRC-II Process, in ppm by Weight.

	Chrysene	Perylene	Benzo(e)pyrene	Benzo(a)pyrene
Light Distillate	0.2	—	—	0.028
Middle Distillate	3.0	—	2.3	1.0
Heavy Distillate	326	12	356	115

Mercury measurements were made in the offgas stream from the SRC-II process and are shown in Table 1.14. Because of uncertainties in the volume of gas in this process, we were unable to determine whether or not all of the mercury could be accounted for in this stream. The mecury was apparently removed by the sulfur recovery unit at the plant, as no mercury could be detected downstream from this unit or in the sulfur. The scrubber solution was found to contain considerable concentrations of mercury. Several arsenic species were also measured in the offgas stream.

TABLE 1.14. Mercury in Gas Samples from SRC-II Process.

	Total Mercury Concentration
Untreated Process Gas	20 ng/ℓ
Scrubbed Process Gas	<0.4 ng/ℓ
Scrubber Solution	2600 ng/ℓ

Some collected data are shown in Table 1.15. This table shows major and trace element data for samples of feed coal, mineral residue, product solids and liquids, process liquids, particulates, and effluent gases taken from the coal liquefaction plant. Figure 1.26 shows mass balances for six elements in the solid product mode. The balances are only approximate since operating parameters are varied from run to run. Except for mercury, titanium, and bromine, most elements appear to remain with the mineral residue. In the case of bromine, approximately 84% remains with the product, whereas approximately 56% of titanium remains with the product. In the case of mercury, 89% is unaccounted for in the solid and liquid products and is presumably emitted in the process offgas.

These studies will continue at the SRC plant in both SRC-I (solid product) and SRC-II modes, and samples that can be compared with stored materials will be collected and analyzed. With these data, some projections can be made on the composition of possible effluents from the proposed SRC demonstration plant in West Virginia.

TABLE 1.15. Inorganic Element Content of Solid Samples From Coal Liquefaction-Refined Solids Process, in ppm Except as Noted.

	Feed Coal (Solids Process)		Mineral Residue (Solids Process)		Solid Product		NBS Coal SID.	
Element	INAA	XRF	INAA	XRF	INAA	XRF	INAA	XRF
Na	180 ± 4		3150 ± 60		8.8 ± 1.5		420 ± 20	
Cl		276 ± 30		1020 ± 50			850 ± 150	
K	1200 ± 0.02	1000 ± 100		1.16% ± 0.05	115 ± 20		0.27% ± 0.02	
Ca		0.069 ± 0.010		1.15% ± 0.05				0.42% ± 0.05
Ti		620 ± 20		2300 ± 200		520 ± 30	0.11 ± 0.02	0.13 ± 0.02
V	29 ± 2	25 ± 3		180 ± 20		10 ± 1	35 ± 4	38 ± 4
Cr	18 ± 2	17 ± 2	150 ± 3	161 ± 10	7.5 ± 2.1	6.0 ± 2.2	19 ± 2	18 ± 2
Mn	35 ± 2						42 ± 6	
Fe	2.29% ± 0.12	2.10% ± 0.15	13.3% ± 0.5	14.5% ± 0.3	270 ± 30	300 ± 40	0.81% ± 0.05	0.78% ± 0.035
Co	5.2 ± 0.02		30 ± 1		0.26 ± 0.04		5.2 ± 0.1	
Ni	21 ± 2	23 ± 1	120 ± 5	115 ± 5	6	2.1 ± 0.2	16 ± 2	14 ± 2
Cu		10 ± 1		126 ± 10		0.8 ± 0.1		15 ± 2
Zu	26 ± 2		120 ± 15	138 ± 20	8.1 ± 0.5	7.2 ± 0.8	37 ± 3	32 ± 3
As	19 ± 1	17 ± 2	77 ± 5	75 ± 5	3.11 ± 0.15	1.8 ± 0.2	5.7 ± 0.5	6.1 ± 0.5
Se	3.6 ± 0.2		20 ± 2	15 ± 3	0.17 ± 0.03	—	3.3 ± 0.3	3.1 ± 0.4
Br	3.6 ± 0.3	3.9 ± 0.3	4.9 ± 0.4	5.2 ± 0.4	4.7 ± 0.4	4.8 ± 0.4	17 ± 2	17 ± 2
Rb	13 ± 1	15 ± 1	82 ± 10	96 ± 5		0.4	19 ± 2	18 ± 1
Sr	59 ± 15	140 ± 10	310 ± 30	325 ± 15	0.96 ± 0.16	2	170 ± 20	150 ± 20
Sb	1.4 ± 0.1		7.4 ± 0.3		0.066 ± 0.009		3.7 ± 0.3	
Ba	46 ± 5		240 ± 25		0.14 ± 0.03		390 ± 40	
La	8.9 ± 0.5		46.8 ± 1.2		0.10 ± 0.02		10.5 ± 0.2	
M	0.44 ± 0.02		2.3 ± 0.2		0.05 ± 0.005		0.97 ± 0.09	
Mg	0.16 ± 0.01		0.005		0.020 ± 0.005		0.12 ± 0.02	
Pb		8 ± 1		42 ± 3		1		11
Th	1.9 ± 0.1		9 + 1		0.19 ± 0.03		3.4 ± 0.3	
U	1.1 ± 0.1		7.3 + 0.3		0.54 ± 0.05		1.6 ± 0.2	

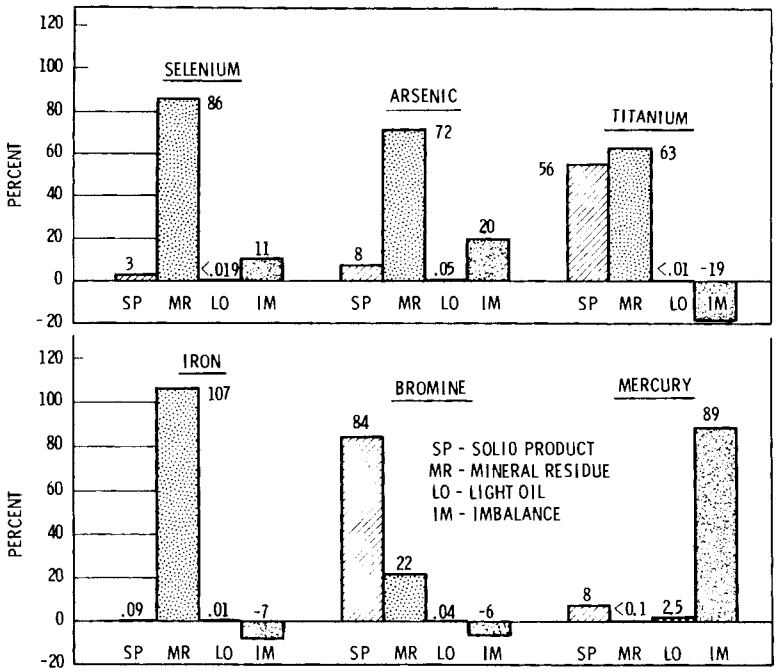

FIGURE 1.26. Balances for Six Elements in a Coal Liquefaction-Refined Solid Process

A SPECTROSCOPIC TECHNIQUE FOR MEASURING ATMOSPHERIC CO_2

G. M. Stokes and R. A. Stokes

As part of a continuing effort to identify areas in which astronomical techniques and data may be profitably applied to atmospheric problems, both new and archival solar spectra have been collected to prepare for an analysis of their use for studying the changes of the atmospheric CO_2 burden. This analysis has resulted in the initiation of an observing program using the Fourier Transform Spectrometer (FTS) of the McMath Solar Telescope at Kitt Peak National Observatory (KPNO). This program is generating spectra, the quality of which should not only aid the archival CO_2 study but also lead to analyses of other trace gases.

Man's annual consumption of fossil fuels has grown by a factor of 50 during the roughly 120 years spanning the transition from a pre-industrial culture to today's highly industrialized society. Our current increase in the consumption rate is about 4.3%/yr, and it is estimated that the earth's atmosphere now contains 85×10^9 tons more now than in 1860, mostly as a result of burning fossil fuels (Baes et al. 1976; Keeling et al. 1976).

Carbon dioxide has a significant effect on the average temperature of the earth's surface and lower atmospheric layers as a result of the gas's large infrared opacity, which produces a "greenhouse effect." Because of the CO_2 content the earth's average surface temperature is now 35 K higher than the bolometric temperature of the earth as seen from space. Clearly, further increases in atmospheric CO_2 concentration can be expected to raise the earth's average surface temperature even to the extent of overwhelming other mechanisms that give rise to natural climatic fluctuations.

A measurement of CO_2 abundance based on solar absorption spectroscopy taken at the turn of the century is important for two reasons. It would provide independent corroboration with other results, which have placed the increase of the atmospheric carbon dioxide abundance in the twentieth century at about 10%, and it would provide a measurement very different from that used in carbon dioxide research to date. In particular, the absorption method measures the total column of carbon dioxide in the atmosphere between the observer and the sun, rather than a local value that may be subject to the vagaries of local conditions.

In the past year, the present research program has focused on: evaluating the required accuracy of any technique designed to contribute to the historical study of the carbon cycle and determining abundances. The accuracy requirements for carbon dioxide abundance studies were estimated in several ways. In particular, over and above any long-term change in the CO_2, there appears to be an annual variation in CO_2 concentration. At Mauna Loa this variation amounts to approximately 1% of the total CO_2 abundance (Keeling et al. 1976).

Since the older spectroscopic data was not accumulated with the goal of either detecting or correcting for seasonal effects, this annual variation must be viewed as a source of noise in the measurement that eventually will limit the accuracy of the technique. Therefore, the goal of the analyses of archival data need only be a fractional accuracy of between 1 and 2%. However, any new measurement effort must meet the time resolution requirement and should be as accurate as possible.

The analysis of the abundance of an atmospheric constituent using absorption spectroscopy is in principle extremely simple. Invert the relationship

$$I_\nu = I_{o\nu}\, e^{-\tau_\nu} \qquad (1a)$$

where

$$\tau_\nu = \int N(\ell)\, \phi_\nu(\ell)\, P(\ell)\, d\ell \qquad (1b)$$

and solve for the abundance of the element N. In Equation 1a, line absorption is referred to, such that I_ν is the observed intensity at frequency ν in the line, $I_{o\nu}$ is the intensity of the sun's radiation at the top of the atmosphere and τ is the optical depth. Equation 1b represents optical depth as integral along the path from the observer to the top of the atmosphere. The three terms in this equation are: $N(\ell)$ the number density of the atom or molecule of interest, $\phi_\nu(\ell)$ the line profile function, and $P(\ell)$ the population factor of the ground-level of the absorption. Each of these is a function of position in the

atmosphere making the inversion problem quite difficult in practice.

The data that are now in hand for analysis are given in Table 1.16. In Figure 1.27, the epochs of four major landmarks in solar absorption spectroscopy are shown on a diagram that also gives the historical production of carbon as a result of man's activities (Baes et al. 1976).

The first two areas of concern in the analysis of the data have been line identification and continuum placement. Using a line identification scheme contained in the REDUCER data reduction package, developed by Kitt Peak National Observatory, as a starting point, a method that automatically gives the wavelengths of lines found in a digitized spectrum has been developed. This scheme is extremely important since the spectral region chosen for analysis, the 1 to 2.5 micron region, contains well in excess of 10,000 lines, more than 7,000 of which originate in the earth's atmosphere. The second step in the analysis is the placement of the solar continuum that is the reference level against which the strength of the telluric absorption lines is measured. The continuum placement scheme is now being tested on the two sets of Hall data (Table 1.16) and some Fourier transform spectra recently taken at Kitt Peak National Observatory.

TABLE 1.16. Spectral Data Being Prepared for Analysis.

Data, Observer and Location	Wavelength Range, μ	Date
Spectral Atlas (Mohler et al, Mt. Wilson)[a]	0.84 to 2.52	1950
Spectral Atlas (Hall, KPNO)[a]	1 to 2.5	1970
Spectral Scans (Hall, KPNO)[b]	1.57 Band of CO_2	1975
Spectral Scans (Hall, KPNO)[b]	1.57 Band of CO_2	1978
FTS Spectra (Stokes, KPNO)[b]	1 to 2.5	1978

[a] See Section 4 for references.
[b] Available from Battelle Observatory, Richland, Wa

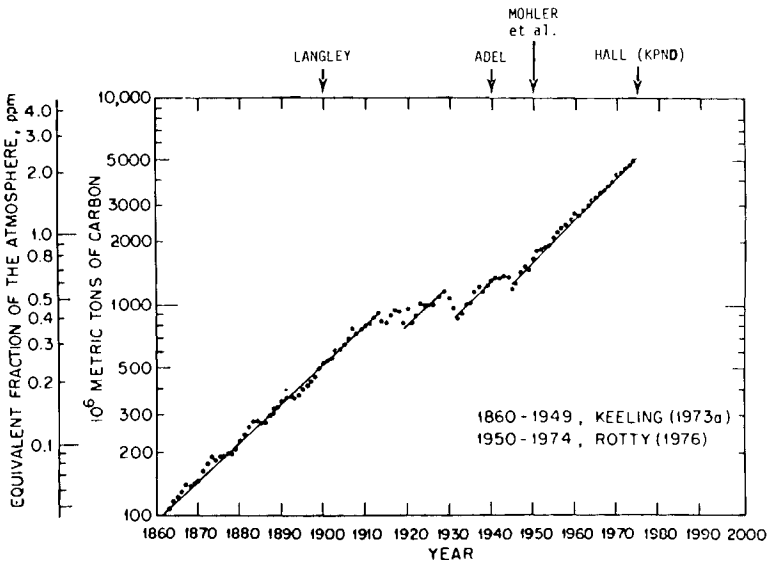

FIGURE 1.27. Epochs of Four Major Solar Spectral Atlases

2.0 Fission and Fusion

FISSION AND FUSION

- **Particle Resuspension and Translocation**
- **Alternate Fuel Cycle Technologies/Thorium Fuel Cycle Technologies (AFCT/TFCT)**
- **Meteorological Effects of Thermal Energy Releases**
- **Atmospheric Boundary Layer Studies**
- **Fallout Rates and Mechanisms**

The major pollutants of concern from the nuclear energy industry are long-lived particles (i.e., plutonium and other radionuclides) and waste heat and water vapor from power-plant cooling systems. Since these pollutants may affect living species and local and regional climate in an adverse manner, field, laboratory and theoretical investigations of their fate are very important to human welfare.

Research activities at PNL include studies of atmospheric diffusion and deposition of material on the earth's surface, resuspension of particulate matter, the transport of drift particles from the effluents of cooling towers, and the regional and global transport of material. Transport studies include the modeling of vertical diffusion and deposition, the determination of the effect of time-averaged precipitation on wet deposition, and the analysis of the redistribution of a layer of HTO by rainfall.

A REVIEW: DEPOSITION AND RESUSPENSION PROCESSES

G. A. Sehmel

A review chapter was written on deposition and resuspension processes for the forthcoming Department of Energy publication, Atmospheric Sciences and Power Production, edited by D. Randerson. The chapter includes eleven tables and thirteen figures summarizing data from 241 references. The conclusions of that review chapter are given.

Mass transfer across the air-surface is important for all toxic materials, regardless of their size. If these materials are respirable, predicting the concentrations that might potentially be inhaled is crucial. These concentrations can be calculated from atmospheric diffusion and transport models that include a boundary condition for mass transfer across the air-surface interface. The problem is that many of these models either have not been validated (Crawford et al. 1978) or have been validated only under limited conditions. Models have not been validated, for instance, for the case of significant air-surface mass transfer. Once these models are validated, deposition velocities and resuspension rates will be available.

Though many experiments have been conducted and theoretical models developed to predict the effects of particle and gas deposition since the literature was reviewed in Atomic Energy--1968 (Slade 1968), our ability to predict surface mass-transfer deposition rates from those field experiments has not improved significantly--with one exception. A model developed from many laboratory experiments developed by Sehmel and Hodgson (1978) so improves our capability to predict deposition velocities that it should be used until more refined and definitive experiments are completed.

Accurate predictions of surface depletion of airborne pollutant plumes from anthropogenic sources require that the best available estimates for dry deposition velocities be used. However, the relative significance of dry deposition is being appreciated only in the recent literature. Earlier deposition experiments focused on the wet removal of nuclear fallout debris from the stratosphere rather than on dry deposition near ground level. The fact that fallout is removed primarily by wet deposition has over-shadowed a more important consideration: the key role of pollutant-release height in determining the relative effectiveness of dry versus wet removal processes. Since most energy sources release pollutants near ground level, studies of dry deposition may be more significant than studies of wet deposition in predicting the removal of pollutants from the atmosphere.

Inadequately controlled experimental variables limited early field experiments. As a result, most field-determined mass-transfer data should be interpreted with qualification. The deposition velocities determined in these field experiments ranged from 10^{-3} up to 20 cm/sec, a range also predicted by Sehmel and Hodgson's empirical model (1978).

The model predicts deposition velocities as a function of particle diameter, friction velocity, aerodynamic surface roughness, and particle density. These predictions emphasize that the distribution of pollutant particle size must also be known. The model predicts a minimum deposition velocity of 0.025 cm/sec. For smaller particles and gases than these with minimum deposition velocity, deposition velocities increase because of Brownian diffusion. For larger particles, deposition velocities increase because of gravity-settling and eddy diffusion.

Resuspension, the other mass-transfer process discussed in the chapter, has been receiving increasing attention within the last several years, as is evidenced in the 1974 conference proceedings (Engelmann and Sehmel 1976) that consider both resuspension and dry deposition. Resuspension can be a continuing problem after toxic materials are deposited on environmental surfaces.

Once the material is on the ground, it will be recycled into the atmosphere and inhaled by man. The chapter demonstrates that resuspension physics is so poorly defined that much research is needed.

One problem is that resuspension coefficients have not been adequately defined. One resuspension coefficient relates airborne concentrations to local surface-contamination levels, but does not describe either the vertical flux from resuspension or the total downwind flux. Any calculation using an "average" resuspension factor must be qualified as uncertain within 2 to 3 orders of magnitude because resuspension factors, which cannot be predicted, have ranged 2 to 3 orders of magnitude even in a single field experiment. The second resuspension coefficient describes the fraction of material resuspended per unit time. Using this coefficient, if the surface contamination level is known, the vertical flux from resuspension is the product of resuspension rates and source concentrations. Resuspension rates measured for both wind and mechanical stresses indicate that mechanical stresses can cause more material to be resuspended at one time than can wind, but that effect is short-lived because mechanical stresses usually last over less time and space.

Deposition and resuspension research results are equally applicable to pollutants from both nuclear and nonnuclear energy sources. Differences in these air-surface mass-transfer processes cannot be distinguished as a function of chemical properties. Dry deposition can be predicted as a function of particle size, but resuspension cannot.

Experimental deposition and resuspension research results are needed to define these transport and mass-transfer processes more adequately. In future studies of these processes, the experiment conditions and experimental techniques must be controlled and defined, and theoretical interpretation of the results validated. Model and experimental validation are the crux and requirement for future research of air-surface mass-transfer processes.

INERT TRACER WIND RESUSPENSION AS A FUNCTION OF WIND SPEED, ATMOSPHERIC STABILITY, AND INITIAL TRACER PARTICLE SIZE

G. A. Sehmel and F. D. Lloyd

Wind-caused resuspension rates are being determined in three different, long-term, inert-tracer field experiments. Chemical results were recently received from an accumulated backlog of air filter samples. Resuspension rates are yet to be calculated from these data.

Wind and mechanical stresses can resuspend respirable pollutant particles from environmental surfaces. Subsequently, resuspended pollutants can become a concern downwind. Although resuspension is known to occur, resuspension physics cannot be adequately described, either for predictive resuspension rate models or for airborne concentration at breathing height above a resuspension source. General predictive models describing physics for environmental surfaces would be even more complex than models describing resuspension of a single particle from a smooth, uniform surface. Environmental surfaces can be described as being generally nonuniform. Resuspension rates are thus required that represent an integrated value over the geometry and vegetative cover of many different, reasonably uniform terrain types.

The present study is directed toward determining resuspension rates averaged over 7.5- to 30-m resuspension fetches at three locations at the Hanford site (Sehmel and Lloyd 1978). The resuspension tracer at each location is an inert tracer, calcium molybdate, which has been deposited at a controlled surface contamination level. Subsequently, wind-resuspended tracer is collected in particulate air samplers located on sampling towers. In each experiment, particulate air-sampling equipment is placed in locations to permit calculation of a resuspended tracer mass balance. From this mass balance, resuspension rates are determined as a function of wind speed increments.

In two experiments, the sampling tower is located at the centers of two circular

areas of 23- and 30-m radii upon which tracer has been deposited. For these experiments, particulate air samplers are always pointed into the wind by wind vanes. At these two sites, resuspended tracer is sampled as a function of wind speed.

The effects of both wind speed and atmospheric stability on resuspension rates are being determined in a third experiment. In this experiment, isokinetic air sampler inlets are fixed towards a 225° direction. These isokinetic air samplers are activated only when the wind direction is within a wind sector of 225±35°.

Additional experiments have been completed at the two circular tracer areas. Chemical analyses have been completed for the tracer content on each filter for these two experiments as well as for a backlog of air filter samples from previous experiments. Chemical analytical results were recently received. However, there has not been sufficient time to analyze these data. Resuspension rates will be reported at a later time.

The third experiment measuring resuspension rates as a function of atmospheric stability, wind speed, and wind direction is being conducted near the Hanford meteorological tower. To date insufficient air sampling time has been accumulated with the required atmospheric stability, wind speed, and direction to expect a detectable tracer content on the sampling filters.

Since data are still needed to predict the effects of atmospheric stability on resuspension, a radionuclide analysis of filter samples from the third experimental site is being considered. The 225±35° wind sampling direction locates the sampling array downwind of the 200-West area during many high-wind speed conditions. This option for measuring detectable radionuclides seems viable since previously airborne plutonium-239 was measured even from the top of the 125-m Hanford meteorological tower (Sehmel 1978d). In that experiment, particulate air samples were collected independent of wind speed and direction.

If this option for radionuclide analysis of the filter samples is exercised, effects of atmospheric stability on airborne concentrations downwind from controlled contaminated areas can be measured as a function of real-time stability. These measurements are preferable to the questionable validity of predicted downwind airborne concentrations from derived diffusion coefficients and atmospheric transport models. Although radionuclide analyses would not permit direct calculation of resuspension rates, the relative airborne radionuclide concentration measured at each wind speed and atmospheric stability would give the relative effects of these parameters on resuspension from the Hanford site.

Results from the present option could be directly related to surface contamination levels if contamination levels and resuspension rates were known or assumed. This modeling effort would require that resuspension rates and contamination levels be determined and model predictions be matched with observed vertical airborne radionuclide profiles at this third experimental site.

Decisions for analyzing filter samples for either tracer or radionuclides will be based in part upon the amount and types of winds experienced this fall at the experimental site. The airborne mass-loading as a function of atmospheric stability and wind speed will always be determined for these data.

AIRBORNE PLUTONIUM AND AMERICIUM CONCENTRATIONS MEASURED FROM THE TOP OF RATTLESNAKE MOUNTAIN

G. A. Sehmel

Airborne plutonium-239+240 and americium-241 blowing from offsite was measured in an initial experiment at the top of Rattlesnake Mountain. Average airborne concentration measured was similar to fallout concentrations. Airborne plutonium concentrations were independent of wind speed for seven wind speed increments between 0.5 and 31 m/sec. In contrast, the airborne americium concentration was a minimum at a wind speed of approximately 7 m/sec. Similarly, the airborne solids concentration in $\mu g/m^3$ was a minimum at an intermediate wind speed increment of 7 to 11 m/sec.

Radionuclide fallout throughout the world is doubtless resuspended continuously by wind and mechanical stresses. To determine airborne concentrations from this resuspension, a field experiment was conducted to determine airborne plutonium and americium concentrations as a function of wind speed and direction. Sampling was conducted at the top of Rattlesnake Mountain, which is the western boundary of the Hanford exclusion site and the highest mountain within the local area. The elevation of the sampling site is 1075 m, which is approximately 875 m above the 200-Area plateau (200-m elevation) of the Hanford site. The sampling site is approximately 17 km west of the Hanford 200-West Area and is approximately 36 km from Richland.

Measurement of airborne radionuclides at this sampling site could give insight into both wind resuspension and the possible delivery rate of stratospheric debris as a function of wind speed. Although both mechanisms could be delivering airborne radionuclides to the sampling location, samples were not fingerprinted to identify the source age.

Airborne solids were collected with a commercial air sampling system,(a) consisting of a cyclone preseparator followed by a standard 20- x 25-cm high-volume fiberglass filter. At operating conditions of 1.1 m^3/min (40 cfm) through the sampling system, the manufacturer's specifications indicate a 6-μm cutoff for the cyclone preseparator. Thus, particles collected on the 20- x 25-cm filter should be principally in the respirable size range.

The experimental sampling array consisted of seven individual sampling systems, each of which consisted of a cyclone preseparator and 20- x 25-cm filter. The seven systems were automatically operated for only wind directions from 205 to 275°. Individual sampling systems were operated for seven different wind speed increments: 0.5 to 3, 3 to 5, 5 to 7, 7 to 11, 11 to 15, 15 to 17.5, and 17.5 to 31 m/sec, respectively. Wind speed and direction were measured at an elevation of 2.1 m.

The inlets to the cyclone preseparators were at a breathing height of 1.7 m. The as-received systems were further modified by the addition of a cyclone inlet closure. The closure covered the inlet until the automatic control signal from the wind speed and direction controller activated a selected sampling system. After sample collection, the net weight of solids collected on the filters was determined. Subsequently, plutonium-239 (i.e., 239+240) and americium-241 analyses were performed by a commercial laboratory.(b)

Airborne plutonium and americium concentrations in $\mu Ci/cm^3$ of air and $\mu Ci/g$ of airborne solids were determined. For these data shown in Figure 2.1, the vertical lines show one sigma limits corresponding to the radiochemical counting statistics. The range of each wind speed increment is shown by a horizontal line through each data point. The dashed lines show the estimated data trends.

The plutonium results are shown on the left side of the figure. The average airborne concentration was 5×10^{-17} $\mu Ci/cm^3$. This average concentration is 0.0008 of the MPC_{168} hr of 6×10^{-14} $\mu Ci/cm^3$ (ERDA 1977). The confidence limits around each data point are larger for the two wind speed increments above 15 m/sec. Sample collection was low for these two samples, since

(a) Model 230CP cyclone preseparator, Sierra Instrument Co., Carmel Valley, California.
(b) LFE Environmental Analysis Laboratory, 230 Wright Ave., Richmond, California 94804.

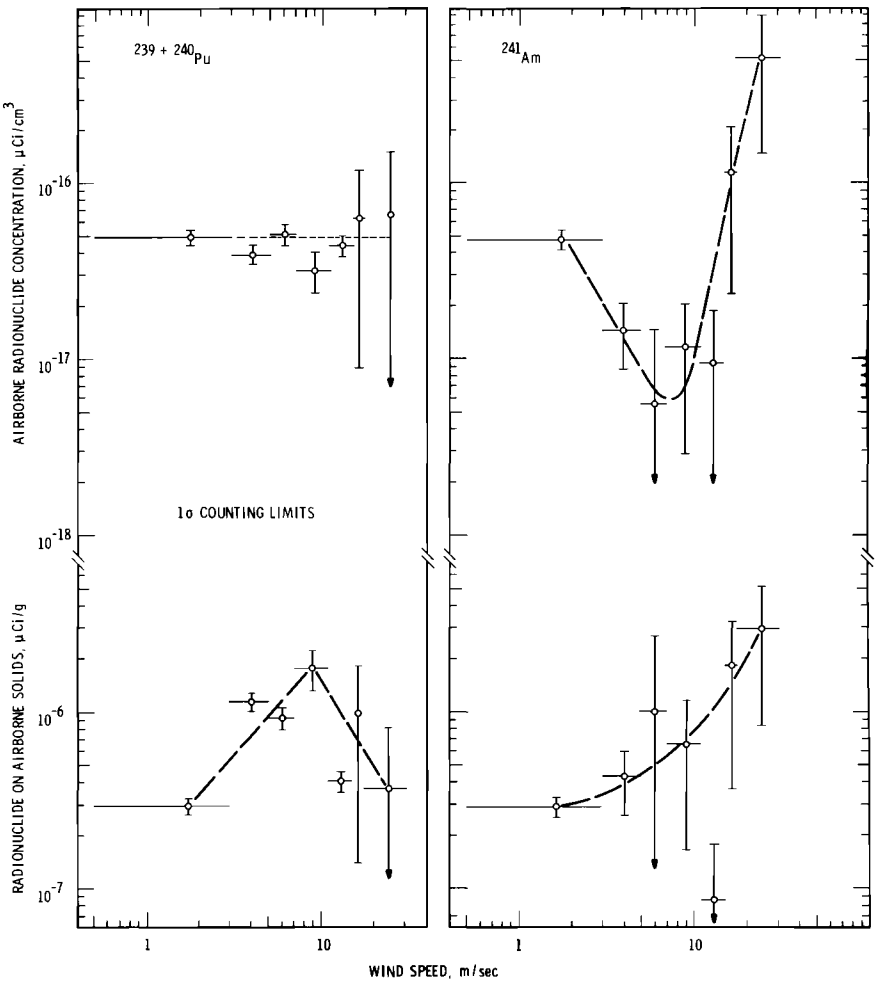

FIGURE 2.1. Airborne $^{239+240}$Pu and ^{241}Am Concentrations in Air and on Airborne Solids Collected at the Top of Rattlesnake Mountain from May 22 to June 22, 1978 when Sampling 205 to 275° Winds Coming from Offsite.

there was relatively little time with wind speeds above 15 m/sec.

The plutonium-239 concentrations in µCi/g on the airborne solids are shown at the bottom of the figure. Plutonium-239 concentrations ranged from 3×10^{-7} up to 1.8×10^{-6} µCi/g. Plutonium-239 concentrations were a function of wind speed. A maximum concentration of 1.8×10^{-6} µCi/g occurred at an intermediate wind speed increment of 7 to 11 m/sec. The reason for this maximum is unknown. However, one might postulate that the relative resuspension availability of plutonium on surface soils as compared to the availability of uncontaminated soil increases as wind speed increases from 0.5 up to approximately 9 m/sec. For higher wind speeds, the relative resuspension availability of uncontaminated surface soils must increase as compared to the availability of plutonium on surface soils.

The data for airborne americium-241 are shown on the right side of Figure 2.1. Airborne americium-241 concentrations ranged from about 6×10^{-18} to 5×10^{-16} µCi/cm^3. An unexpected result was that airborne concentrations at 7 m/sec were about one-eighth of the concentration at 1.75 m/sec (0.5 to 3 m/sec increment). A minimum airborne americium-241 concentration occurred around 7 m/sec wind speed. For higher wind speeds, airborne americium-241 concentrations increased (as drawn) with the 4.6 power of wind speed.

Airborne americium-241 concentrations were a function of wind speed; airborne plutonium-239 concentrations showed no relationship with wind speed. These differences suggest that either source characteristics or transport mechanisms may be significantly different for plutonium and americium. These possibilities are also indicated by comparing radionuclide

concentrations in μCi/g on airborne solids. As the lower right section of Figure 2.1 shows, americium-241 concentrations tended to increase with increasing wind speed. Only the 11 to 15 m/sec wind speed increment shows a significant deviation from this increase. In contrast, as the lower left section of Figure 2.1 shows, plutonium-239 content per gram was maximum at a wind speed of about 9 m/sec.

There seems to be some relationship between the airborne solids concentrations and the americium-241/plutonium-239 ratio. Airborne solids concentrations in $\mu g/m^3$ and the americium-to-plutonium activity ratio are shown in Figure 2.2. For both data sets, a minimum occurs at a wind speed of about 9 m/sec. Airborne solids concentration ranged from about 18 up to 180 $\mu g/m^3$. The airborne solids concentration was nearly identical for the lowest wind speed increment of 0.5 to 3 m/sec and highest wind speed increment of 17.5 to 31 m/sec. However, the minimum concentration of 18 $\mu g/m^3$ occurred for the 7 to 11 m/sec intermediate wind speed increment.

These airborne solids concentration measurements at seven wind speed increments are an extension of our previous measurements at three wind speed increments. Previously, the 3 to 5 m/sec increment was the lowest wind speed for which data were collected. For those experiments, airborne solids concentrations increased for the high wind speeds. For the present data, a wind speed increment from 0.5 to 3 m/sec was also measured. It is this lower increment that is showing an increased airborne solids concentration and, thus, is defining the existence of a minimum at higher wind speeds.

Since the plutonium and americium airborne concentrations show different trends as a function of wind speed, the ratio of airborne and americium-to-plutonium radionuclide concentrations is shown on the lower portion of Figure 2.2. The ratio

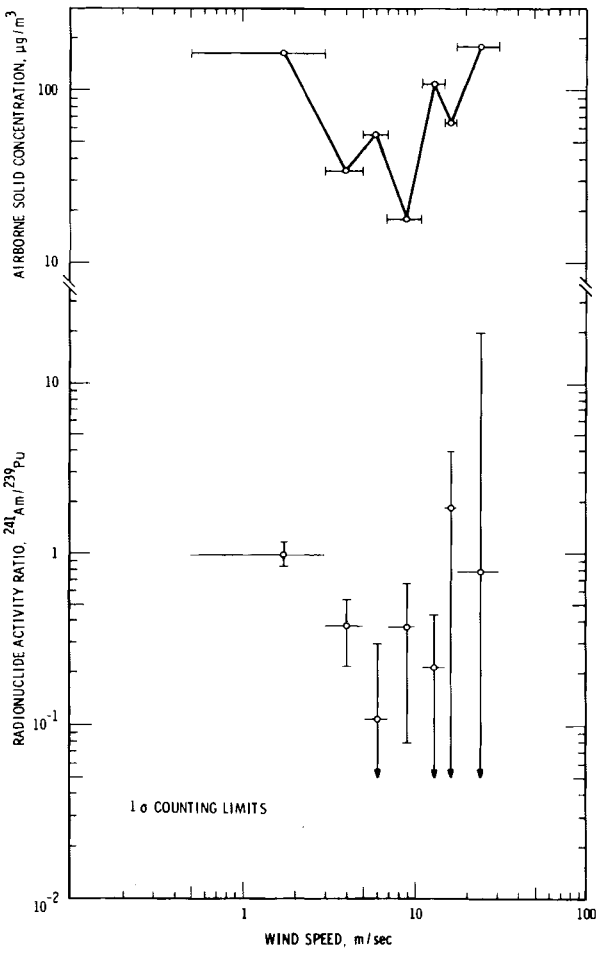

FIGURE 2.2. Airborne Solids Concentration and $^{241}Am/^{239}Pu$ Radionuclide Ratio for Airborne Solids Collected at the Top of Rattlesnake Mountain from May 22 to June 22, 1978 when Sampling 205 to 275° Winds Coming from Offsite.

ranges from 0.1 to 1.8. The calculated one-sigma counting-statistics limits for these ratios are very large (Kempthorne and Allmaraz 1965). Nevertheless, there may be a minimum ratio in the wind speed range of 5 to 15 m/sec. Thus a minimum occurs at an intermediate wind speed for both airborne solids concentrations and the americium-241/plutonium-239 ratio. The underlying causes and reproducibility of these minima are still under study.

This experiment is being repeated with the experimental inclusion of airborne particle size discrimination. The sampling system now consists of the cyclone preseparator as well as a particle cascade impactor in front of the 20 x 25-cm filter. This second experiment was begun in July 1978 and is still operating.

PLUTONIUM RESUSPENSION

G. A. Sehmel

A second experiment near the Prosser barricade in the Hanford area confirmed that airborne plutonium was being blown in from offsite by southwesterly winds.

Plutonium resuspension could occur as a result of resuspension from accumulated surface sources arising from fallout deposition from areas offsite of Department of Energy (DOE) facilities. To determine this fallout resuspension, field experiments were conducted near the Prosser barricade of the Hanford area about 19 to 20 km southeast (130° to 160°) of the fuel-processing areas.

Previously, airborne plutonium-239 concentrations were measured (Sehmel 1977 and 1978) near the Prosser barricade during April 21 to June 29, 1976, when southwest winds blew from offsite between 190° and 260°. Airborne plutonium was sampled with particle cascade impactors, which collect respirable particles, and rotating cowl collectors, which collect nonrespirable particles by gravity settling (Sehmel 1978c). Airborne plutonium-239+240 concentrations, $\mu Ci/cm^3$, on respirable particles and airborne plutonium-239+240 fluxes in μCi (m^2 day) on nonrespirable particles were reported.

Airborne plutonium-239+240 concentration ranged from about 10^{-18} to 10^{-16} $\mu Ci/cm^3$. The plutonium was collected on all particle cascade impactor stages. Data were reported for collection on the 3 plus 7 μm impactor stages, 1 plus 2 μm impactor stages, and the backup filter. Airborne plutonium-239+240 concentrations increased as powers of wind speed: μ1.1 to μ9.3.

The concentration of plutonium-239+240 per gram of airborne soil was also determined. For respirable particles, plutonium-239+240 concentrations ranged from 1.3×10^{-7} to 1.0×10^{-6} μCi/g with an average of 4.0×10^{-7} μCi/g of airborne solids. For nonrespirable particles, the plutonium-239+240 concentration ranged from 1.3×10^{-7} to 2.1×10^{-7} μCi/g.

EXPERIMENT

The sampling experiment was repeated from August 12, 1976 to January 11, 1977, to confirm this initial experiment. Airborne solids were collected within particle cascade impactors located at heights of 0.3, 2.0 and 5.8 m above ground. The air was sampled only if the wind was blowing from offsite towards the Hanford area from 190° to 260°. Respirable particles were sampled with particle cascade impactors for wind speed increments from 3 to 5, 5 to 7, and 7 to 11 m/sec measured at a height of 1.5 m. Since the cowl inlet was always open, all southwest winds were continuously sampled for nonrespirable particles with the rotating cowl, inertial, collection system.

Samples were weighed after collection, and subsequently selected samples were combined for plutonium analysis in order to increase the radiochemical sensitivity. Plutonium analyses were performed by a commercial lab[a] by total dissolution electrodeposition and alpha spectroscopy.

RESULTS

Airborne plutonium concentrations in $\mu Ci/cm^3$ as well as airborne solid concentrations are shown in Figure 2.3. Data are

(a) LFE Environmental Analysis Laboratory, 230 Wright Avenue, Richmond, California 94804.

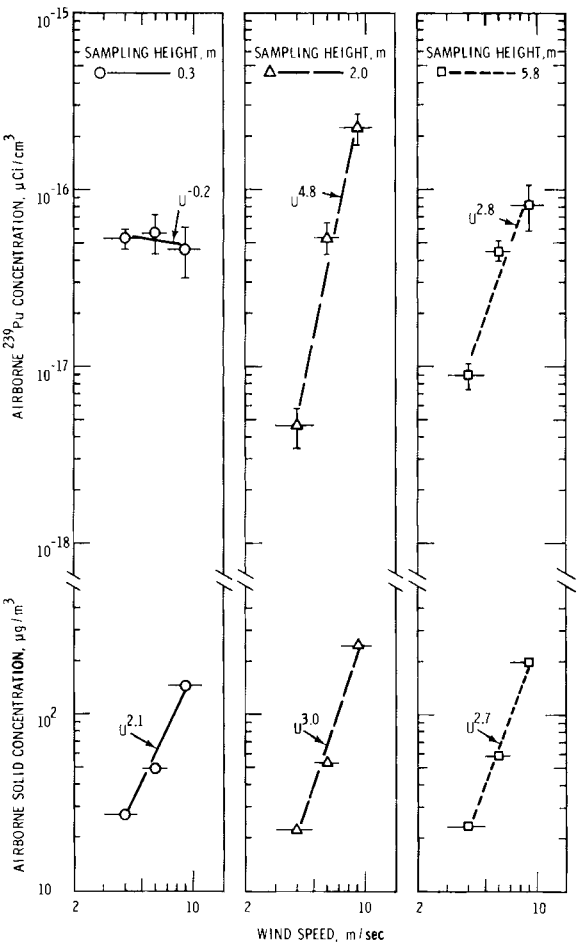

FIGURE 2.3. Airborne ^{239}Pu Concentrations and Soil Loadings for Total Samples Collected Within Particle Cascade Impactors near Prosser Barricade at Hanford from August 12, 1976 to January 11, 1977 when Sampling 190 to 260° Winds Coming from Offsite.

shown separately for each sampling height of 0.3, 2.0, and 5.8 m. For these data, the range of each wind speed increment is shown by a horizontal line through each data point. The vertical lines show the limits for one sigma, corresponding to the radiochemical counting statistics. Also shown are lines, calculated by least squares, through the data points. The wind speed dependency is shown as an exponent on the wind speed velocity (U), measured at 1.5-m height. Airborne concentrations ranged from 4×10^{-18} up to a maximum of 2×10^{-16} µCi/cm^3. This maximum concentration is 0.3% of the MPC(168 hr) of 6×10^{-14} µCi/cm^3 (ERDA 1977). As shown in Figure 2.4, these measured airborne concentrations are within the range measured for fallout at Richland, Washington and Point Barrow, Alaska.

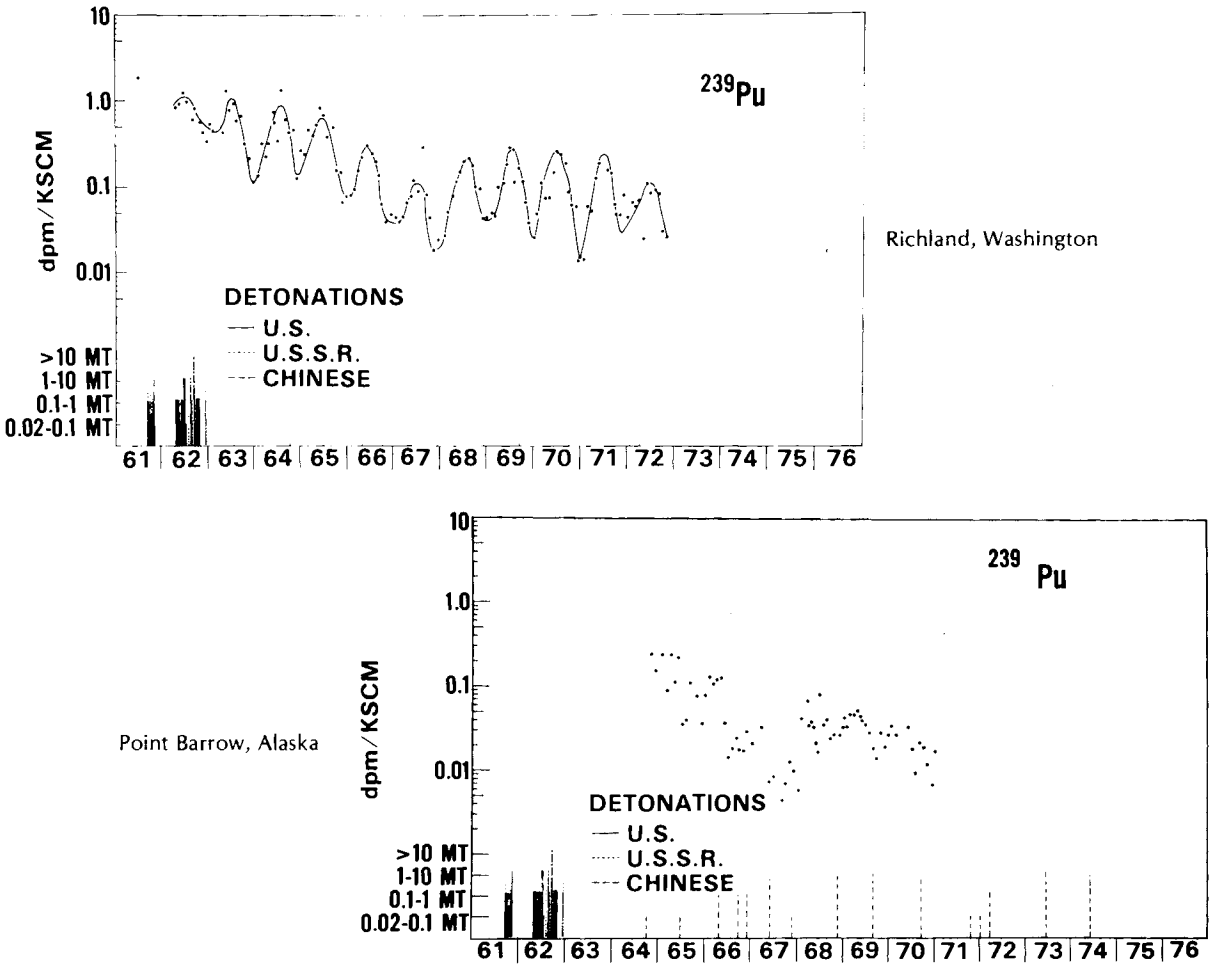

FIGURE 2.4. Plutonium 239+240 Concentration in Surface Air.

At the lowest sampling height of 0.3-m, the airborne plutonium concentration was nearly constant at about 5×10^{-17} $\mu Ci/cm^3$ for all wind speeds. Although the plutonium concentration remained constant, the bottom portion of the figure shows that the airborne dust loading increased with the 2.1 power of wind speed.

In contrast to the 0.3-m height, plutonium concentration at the 2-m and 5.8-m heights increased with increasing wind speed. The airborne concentrations in $\mu Ci/cm^3$ for the 2-m sampling height are shown in the central section of the figure. Airborne plutonium concentrations were 4.6×10^{-18} $\mu Ci/cm^3$ for the 3- to 5-m/sec wind speed increment. At this lowest wind speed increment, the airborne plutonium concentration at the 2-m height was one order of magnitude less than the plutonium concentration at the lower elevation of 0.3-m for all wind speeds. As a possible explanation of the data, a decrease in airborne plutonium concentration with height would be expected for a local resuspension source. In contrast, the airborne plutonium concentration at a 2-m sampling height is about four times greater than that at the 0.3-m height for the highest wind speed increment from 7 to 11 m/sec. This increased airborne plutonium concentration with height at high winds suggests that resuspension results from an upwind source with deposition occurring between the source and sampling location.

At the 2-m sampling height, airborne plutonium concentrations increased with the 4.8 power of wind speed, while the airborne solids concentration increased with the 3.0 power of wind speed. For the largest sampling height studied (5.8-m), the airborne plutonium concentration and airborne solids concentration both increased with the wind speed to the 2.7 to 2.8 power.

Airborne plutonium concentrations in $\mu Ci/g$ of airborne material were also determined. In Figure 2.5, the plutonium-239 $\mu Ci/g$ is shown at each sampling height as a function of wind speed. For the lowest

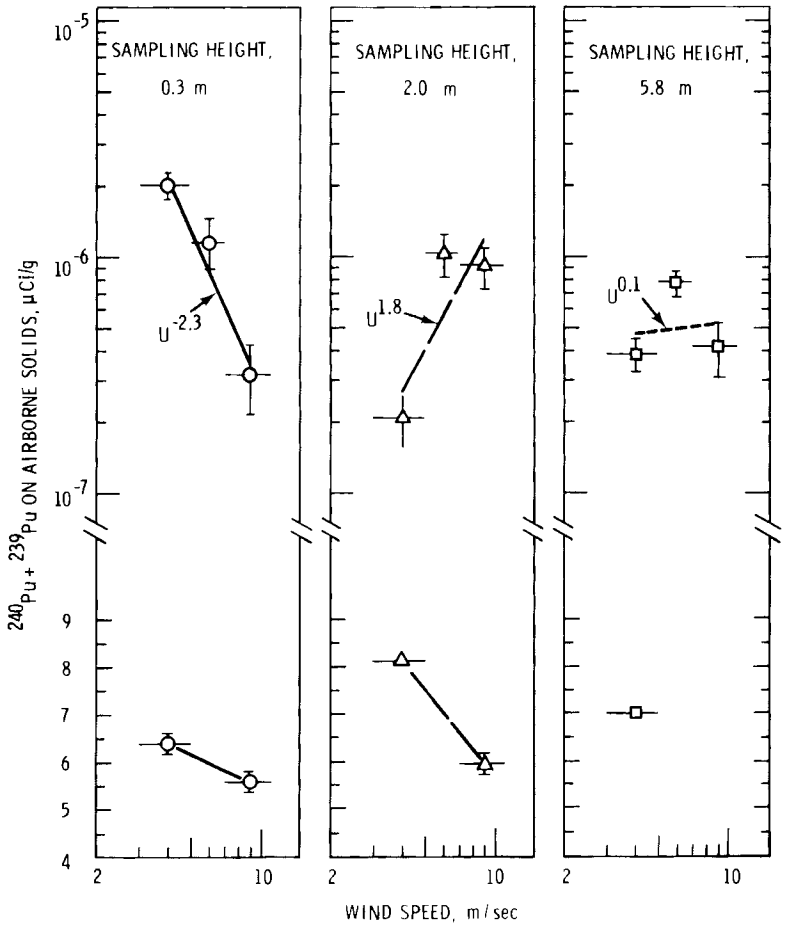

FIGURE 2.5. Plutonium 239+240 Concentrations on Airborne Soil for Total Samples Collected Within Particle Cascade Impactors near Prosser Barricade at Hanford from August 12, 1976 to January 11, 1977 when Sampling 190 to 260° Winds Coming from Offsite.

sampling elevation level of 0.3-m, the plutonium concentration in μCi/g on airborne soil decreased with speed to the negative 2.3 power. The underlying cause of the decreased μCi/g with increasing wind speed is unknown. A possible explanation for this decrease in μCi/g could include either locally uncontaminated soil being resuspended at higher wind speeds or uncontaminated soils being transported from upwind. In contrast, at a sampling height of 2.0-m, the plutonium concentration on the airborne soil increased with the 1.8 power of wind speed. This relationship might be explained by a resuspension process proportional to U^3 and a subsequent airborne plume dilution proportional to 4^{-1}. Thus, the exponent 2 is nearly equal to the experimental exponent of 1.8.

A third dpm/g pattern is shown by the data from the highest sampling elevation level of 5.8 m. For this height, the μCi/g was nearly constant for the lowest and highest wind speed increments with a maximum μCi/g occurring at the middle wind speed increment. The reason for this maximum is unknown. However, a maximum might have also occurred for the intermediate wind speed at the 2.0-m height.

For nonrespirable particles setting within the cowl, plutonium-239 concentrations in μCi/g and fluxes in μCi/(m^2 day) are shown in Table 2.1. The plutonium concentration per gram associated with these nonrespirable particles was always less than that associated with respirable particles.

Airborne plutonium fluxes in μCi/(m^2 day) for these nonrespirable particles were calculated for two time periods. Horizontal-flux calculations were made both for the total time that winds were simultaneously between 3 and 11 m/sec and with wind direction between 190° and 260° and for the total time that cowl-air samplers were in the field. When the shorter period (3 to 11 m/sec and 190° to 260° winds) was used, horizontal plutonium fluxes ranging from 1.56×10^{-7} to 3.28×10^{-7} μCi/(m^2 day) were calculated.

TABLE 2.1. Plutonium$^{239+240}$ Transport on Nonrespirable Particles from Offsite near the Prosser Barricade on the Hanford Reservation from August 12, 1976 to June 11, 1977.

	Pu on Airborne Solids		Airborne Pu Nonrespirable Flux, Ci/(m^2 day)	
Sampling Height, m	dpm/g	μCi/g	Only for 190 to 260° Winds, 3 to 11 m/sec	For Total Field Time
0.1	0.22	1.0×10^{-7}	1.56×10^{-7}	1.30×10^{-8}
2	0.23	1.1×10^{-7}	1.89×10^{-7}	1.57×10^{-8}
5.8	0.39	1.8×10^{-7}	3.38×10^{-7}	2.82×10^{-8}

The relative plutonium transport for respirable versus nonrespirable particles was not directly measured, since the cowl inlet was open and large particles could be trapped within the cowl at all wind speeds. The direct measurement would have required closure of the cowl inlet during the nonsampling periods. Nevertheless, an estimate was made for the relative plutonium transport on respirable and nonrespirable particles. The calculations required that the air velocity be uniform for all sampling heights, that anisokinetic sampling corrections be negligible and nonrespirable material be collected only between 3 to 11 m/sec winds for directions between 190° and 260°.

For comparison with the flux of nonrespirable particles, the average respirable particle concentration is multiplied by the average wind speed, 4.6 m/sec, to get the average flux of respirable particles. The average flux of respirable particles and the flux of nonrespirable particles are then compared to determine the percentage of plutonium transported on respirable particles. These calculations suggest that from 95.6 to 99.3% of the plutonium was transported on particles of respirable size.

TECHNICAL PROGRESS IN THE ALTERNATE FUEL CYCLE PROGRAM - II

W. E. Davis and W. J. Eadie

A U.S. scale assessment model developed at Pacific Northwest Laboratory (PNL) was used in an annual assessment for simulated releases from Carlsbad, New Mexico; Morris, Illinois; and Brookhaven, New York in 1975. The estimated concentration of pollutants and deposition were sent to Savannah River to be used to determine the effects of a release from each site.

With the increasing number of light-water reactors, approximately 60 in the United States in 1976 and 100 being built, the number of spent-fuel elements from these reactors will increase. A study in progress is attempting to evaluate the environmental effects of reprocessing these spent-fuel elements. Part of the study is determining the doses to man from the release of pollutants to the atmosphere during reprocessing. PNL's U.S. scale assessment model has been selected to describe the transport, diffusion and deposition of pollutants from a simulated release during reprocessing (Davis, Eadie and Powell 1978). Air concentration and surface deposition values calculated from this simulation will be used to estimate doses to man.

PNL's model is the same one described in last year's annual report (Davis, Eadie and Powell 1978). The model operates on a fixed two-dimensional advection grid, where the dimensions of each square are 2° latitude and 2° longitude for an 18 x 17 grid.

The winds used for advection are the mean winds from radiosonde sites for a layer 300 to 1500 m above the surface, except for Brookhaven, New York. The winds, measured every 12 hr, are then interpolated to a grid using an interpolation scheme based on a distance-squared weighting function. The hourly values are calculated by linear interpolations in time. The advection of the parcels is provided by trajectories using winds bilinearly interpolated from the grid points. No allowances are made for vertical transport in the model.

The only change made in the model this year was the inclusion of a gridded mixing-depth field for use in the Brookhaven, New York assessment. The reason for using a field of gridded mixing height is that there were large gradients of mixing heights from over land to over water in the region of the release point (Holzworth 1964). This variation, if not accounted for, would cause large errors in the estimated surface concentrations. The winds, likewise, were averaged over a depth in keeping with the mean mixing depth in the vicinity of Brookhaven, New York.

In the simulations, pollutants were released at a height of 62 m and at a rate of 1 Ci/sec. Estimates were made about the depth of the mixing layer from averages of the monthly values of mixing depth (Holzworth 1964). Figures 2.6 to 2.10 show the results of these simulations for Carlsbad, New Mexico; Figures 2.11 to 2.15 for Morris, Illinois; and Figures 2.16 to 2.20 for Brookhaven, New York (BNL).

In general, there are three groups of five figures for each of the three annual assessment sites. Figures 2.6,2.11 and 2.16 show air concentrations with no deposition. Figures 2.7, 2.12 and 2.17 show air concentration with a dry deposition velocity of 1 cm/sec used in the assessment. Figures 2.8, 2.13 and 2.18 show air concentrations with a dry deposition velocity of 1 cm/sec and a washout ratio of 5×10^5 used with hourly gridded precipitation in the assessment. Figures 2.9, 2.14 and 2.19 and Figures 2.10, 2.15 and 2.20 show the total dry deposition and total wet and dry deposition, respectively.

There are discernible differences among the no-deposition air concentrations for three sites (Figures 2.6, 2.11, 2.16). For Carlsbad, New Mexico (Figure 2.6), the 1×10^{-10} Ci/m^3 isopleth indicates three directions with a northerly/southerly and southwesterly wind component evident. In Figure 2.11 the strong westerly component of the wind has influenced the air concentration pattern for Morris, Illinois. In the Brookhaven, New York assessment (Figure 2.16), a northwesterly wind component is evident in the air concentration pattern.

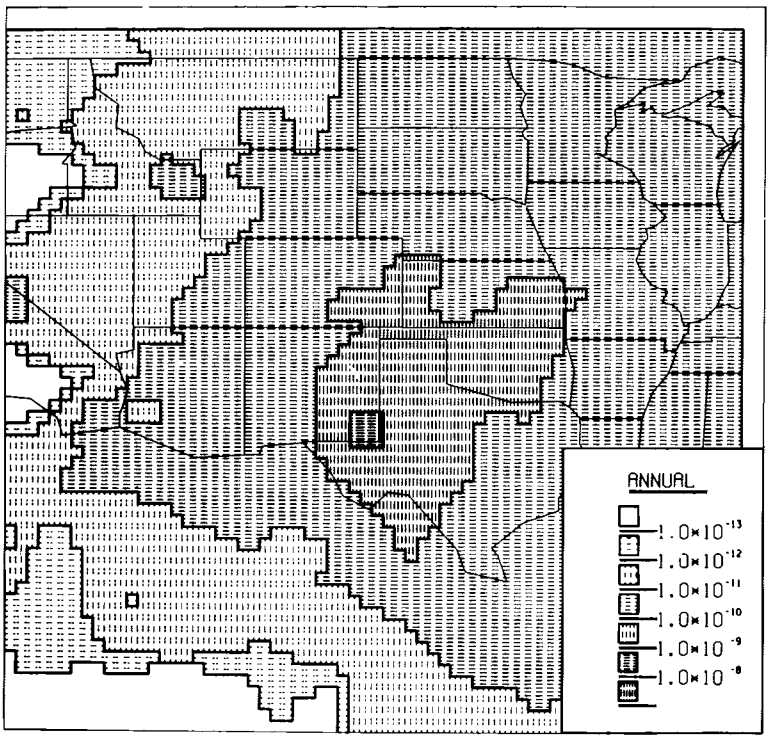

FIGURE 2.6. Surface Air concentrations for 1975 for Simulated Release from Carlsbad, NM, of 1 ci/sec with No Deposition. Height of release was 62 m. Lines of concentrations are for Ci/m^3.

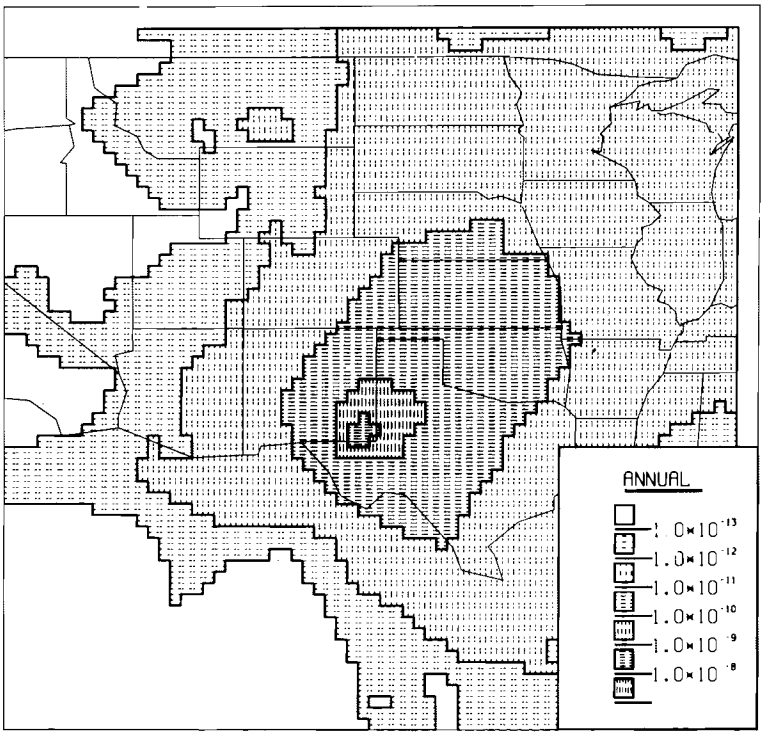

FIGURE 2.7. Surface Air Concentrations for 1975 for Simulated Release from Carlsbad, NM, of 1 Ci/sec with a Dry Deposition Velocity of 1 cm/sec (See Figure 2.6)

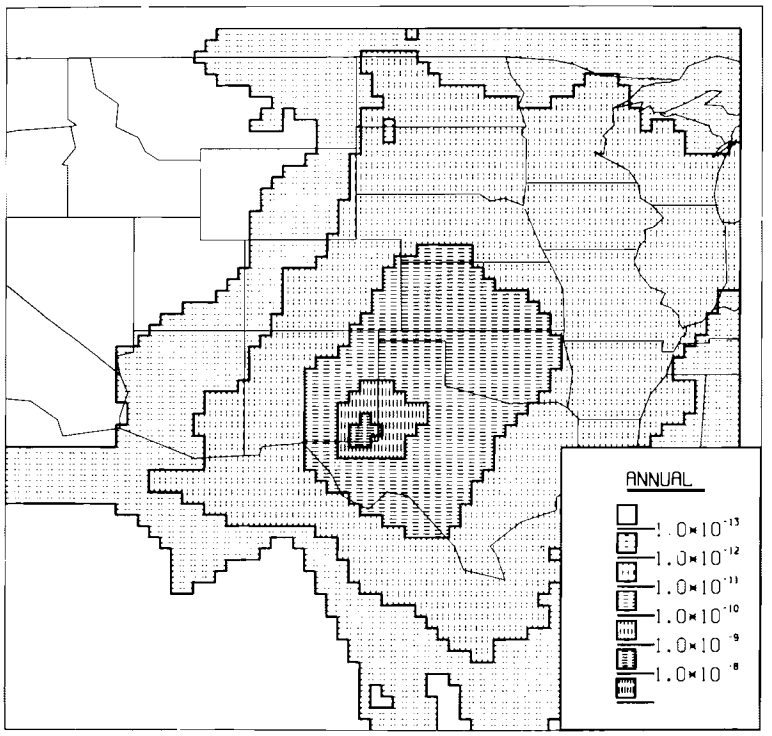

FIGURE 2.8. Surface Air Concentrations for 1975 for Simulated Release from Carlsbad, NM, of 1 Ci/sec with a Dry Deposition Velocity of 1 cm/sec and Washout Ratio of 5 x 10^5 with the Use of Hourly Precipitation (See Figure 2.6)

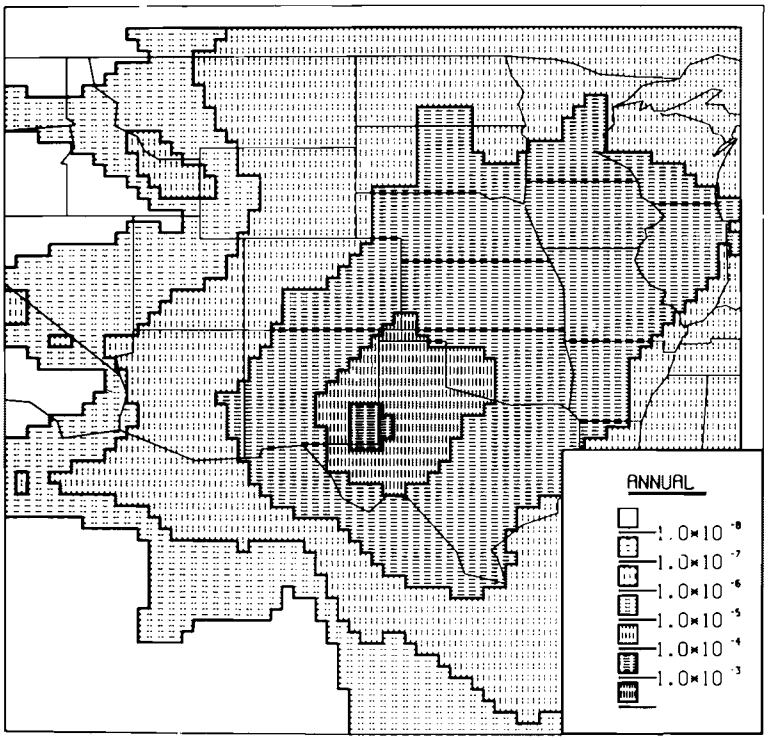

FIGURE 2.9. Ground Deposition for 1975 from a Simulated Release from Carlsbad, NM, of 1 Ci/sec with a Dry Deposition Velocity of 1 cm/sec. Lines of deposition are for Ci/m².

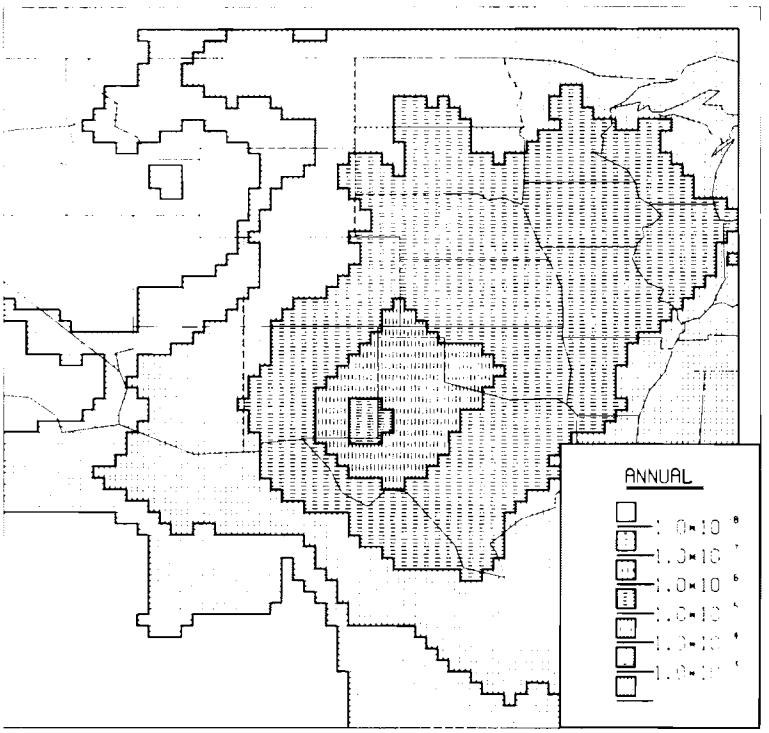

FIGURE 2.10. Ground Deposition for 1975 from a Simulated Release from Carlsbad, NM, of 1 Ci/sec with a Dry Deposition Velocity of 1 cm/sec and a Washout Ratio of 5 x 10^5 with the Use of Hourly Precipitation (See Figure 2.6)

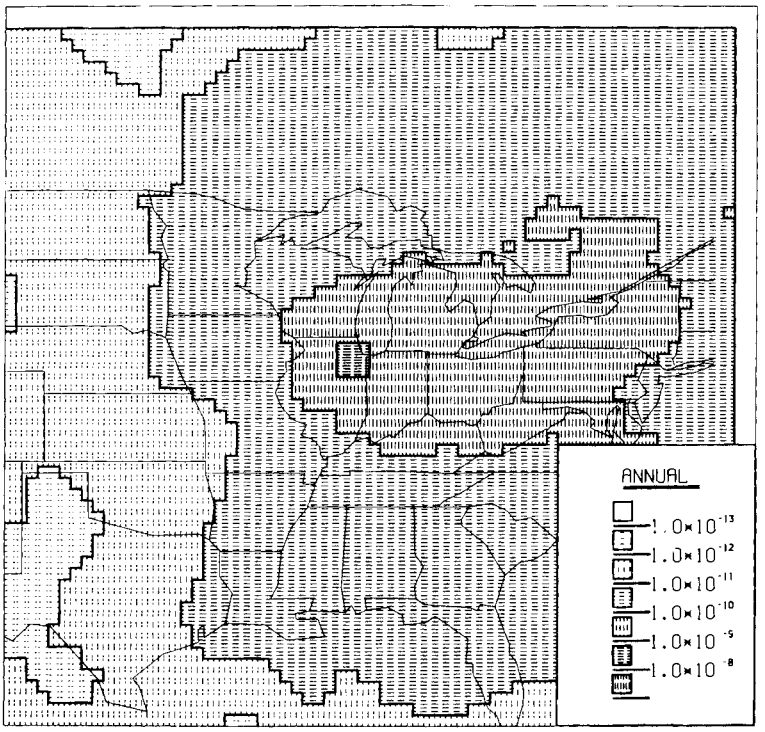

FIGURE 2.11. Surface Air Concentrations for 1975 for Simulated Release from Morris, IL, of 1 Ci/sec with No Deposition. Height of release was 62 m. Lines of concentrations are for Ci/m³.

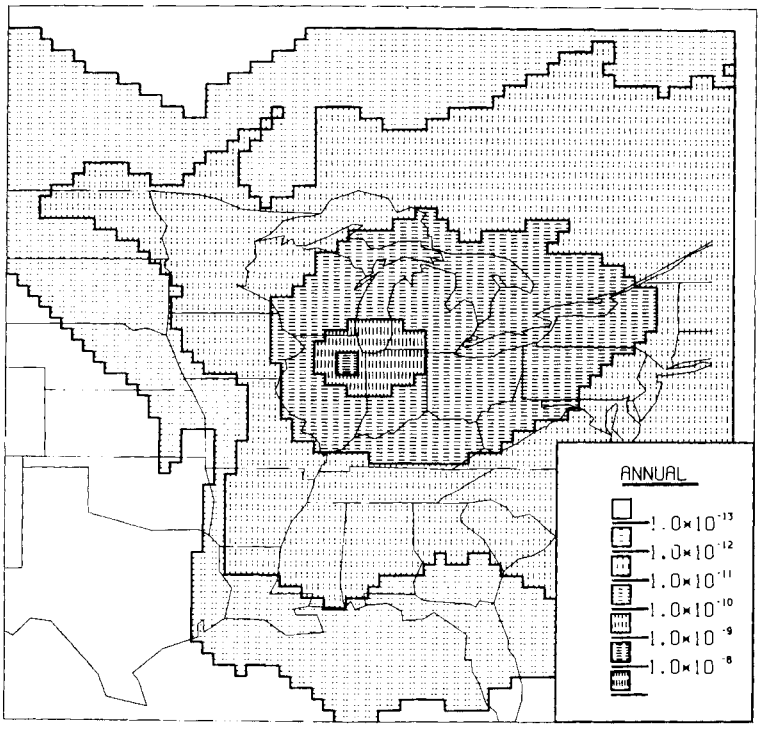

FIGURE 2.12. Surface Air Concentrations for 1975 for Simulated Release from Morris, IL, of 1 Ci/sec with a Dry Deposition Velocity of 1 cm/sec (See Figure 2.11)

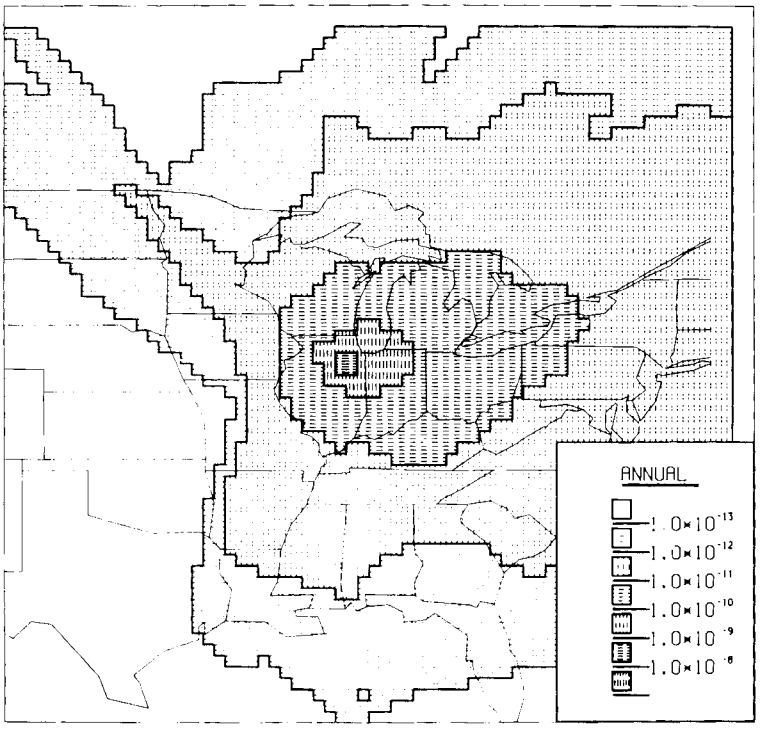

FIGURE 2.13. Surface Air Concentrations for 1975 for Simulated Release from Morris, IL, of 1 Ci/sec with a Dry Deposition Velocity of 1 cm/sec and Washout Ratio of 5 x 10^5 with the Use of Hourly Precipitation (See Figure 2.11)

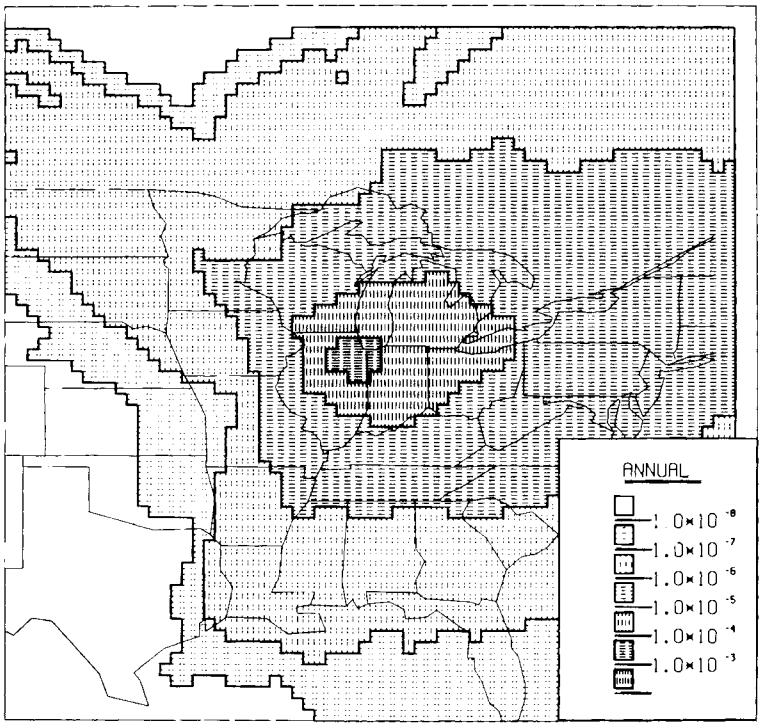

FIGURE 2.14. Ground Deposition for 1975 from a Simulated Release from Morris, IL, of 1 Ci/sec with a Dry Deposition Velocity of 1 cm/sec. Lines of deposition are for Ci/m^2 (See Figure 2.11)

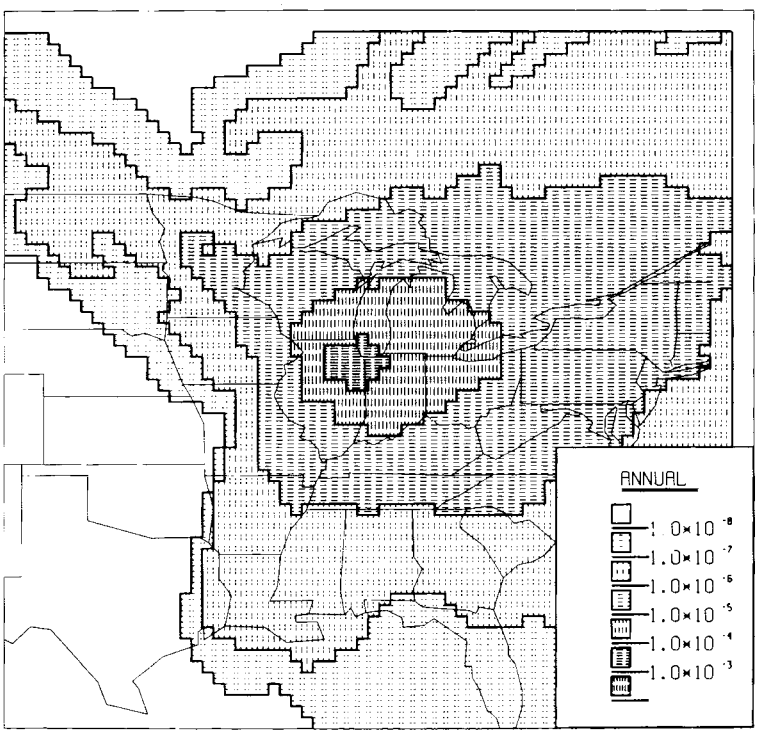

FIGURE 2.15. Ground Deposition for 1975 from a Simulated Release from Morris, IL, of 1 Ci/sec with a Dry Deposition Velocity of 1 cm/sec and a Washout Ratio of 5 x 10^5 with the U of Hourly Precipitation (See Figure 2.11)

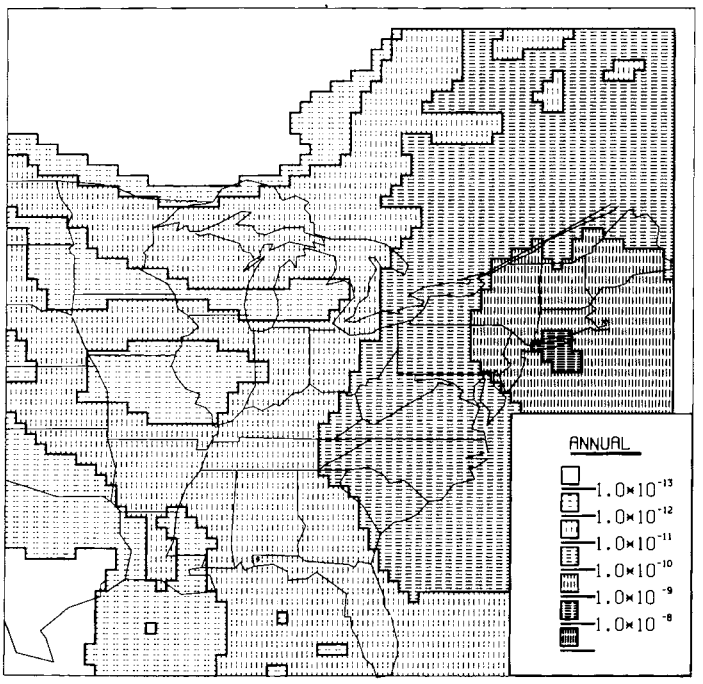

FIGURE 2.16. Surface Air Concentrations for 1975 for Simulated Release from BNL of 1 Ci/sec with No Deposition. Height of release was 62 m. Lines of concentrations are for Ci/m^3.

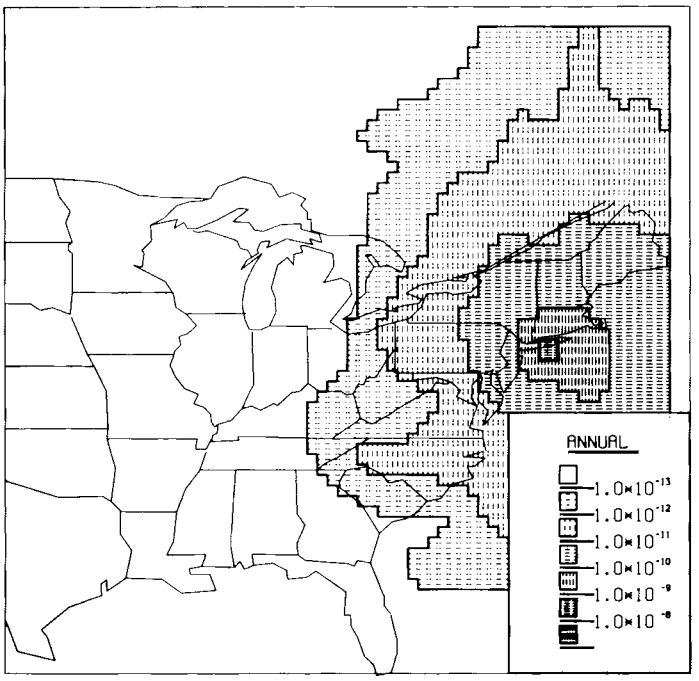

FIGURE 2.17. Surface Air Concentrations for 1975 for Simulated Release from BNL of 1 Ci/sec with a Dry Deposition Velocity of 1 cm/sec (See Figure 2.16)

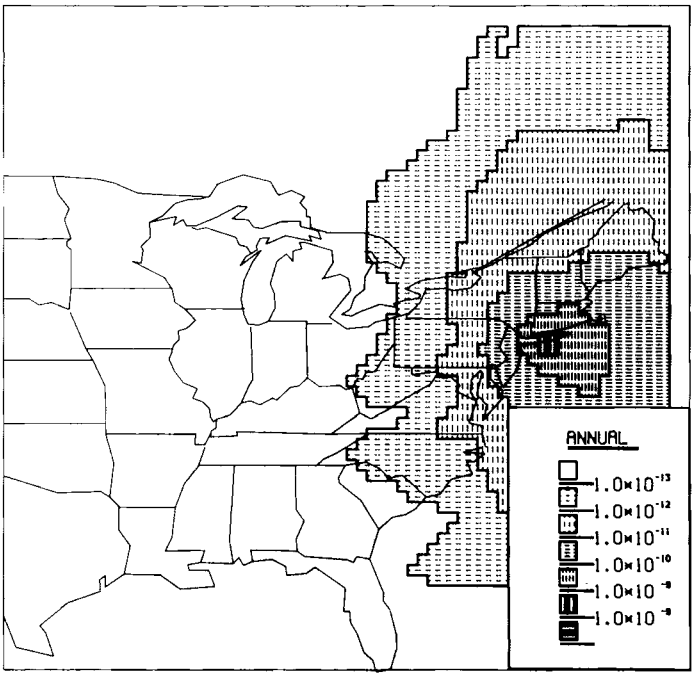

FIGURE 2.18. Surface Air Concentrations for 1975 fro Simulated Release from BNL of 1 Ci/sec with a Dry Deposition Velocity of 1 cm/sec and Washout Ratio of 5 x 10^5 with the Use of Hourly Precipitation (See Figure 2.16)

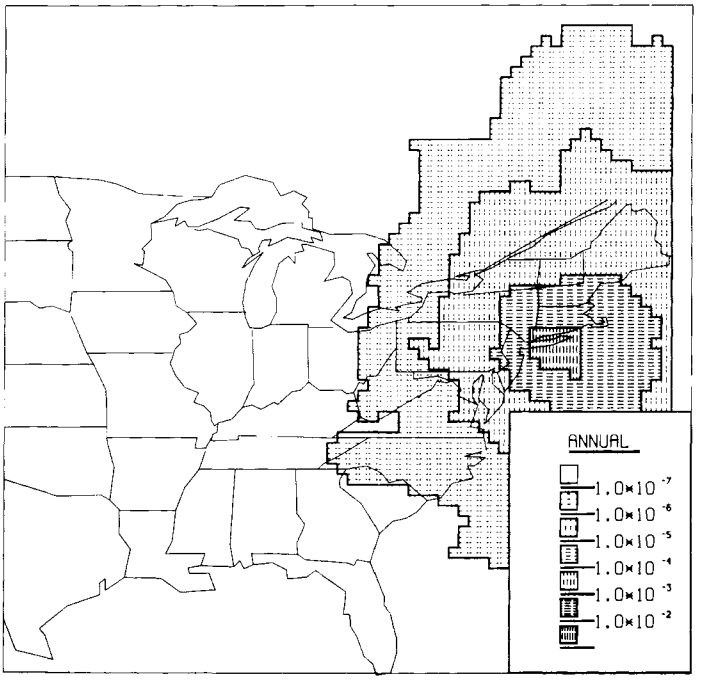

FIGURE 2.19. Ground Deposition for 1975 from a Simulated Release from BNL of 1 Ci/sec with a Dry Deposition Velocity of 1 cm/sec. Lines of deposition are for Ci/m^2 (See Figure 2.16)

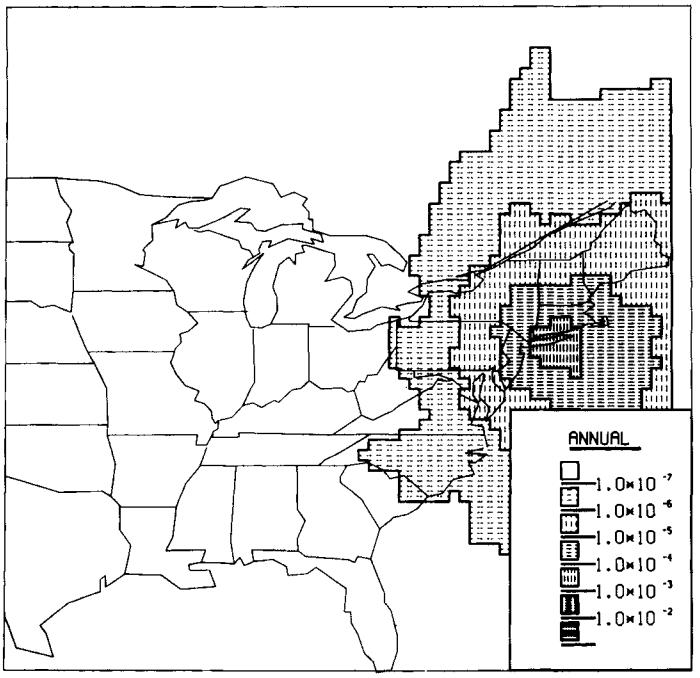

FIGURE 2.20. Ground Deposition for 1975 from a Simulated Release from BNL of 1 Ci/sec with a Dry Deposition Velocity of 1 cm/sec and a Washout Ratio of 5 x 10^5 with the Use of Hourly Precipitation (See Figure 2.16)

TESTING AND DOCUMENTATION OF PROGRAMS USED TO TRANSFORM CLIMATOLOGICAL PRECIPITATION DATA TO A GEOGRAPHICALLY GRIDDED FORMAT

T. D. Fox

A procedure was developed for converting climatological hourly precipitation data into a form suitable for input to regional atmospheric transport and removal models. The procedure involves a rearrangement of the original data by date rather than by station, followed by the use of a spatial averaging scheme to interpolate data from randomly spaced stations to a regularly spaced grid. The procedure has been tested and documented for general use.

It has been shown that the use of actual time-varying fields of precipitation, rather than climatologically averaged fields, in atmospheric transport and removal models can produce important differences in results (Wendell and Powell 1976). A procedure was developed to produce fields of hourly precipitation on a regularly spaced regional grid (Wendell and Hane 1976). Such a procedure requires time-concurrent data from many stations over a wide region. However, climatological precipitation data is arranged in month- or year-long series for each reporting station. A sequence of computer program steps has been created to rearrange climatological precipitation data in this way (Fox and Wendell 1977). This sequence has been incorporated with the original procedure into a system of CDC[a]-7600 FORTRAN computer programs for producing fields of gridded hourly precipitation data. The system has been tested, documented and is ready for general use.

The system consists of a main three-step sequence of computer programs and five auxiliary programs, which perform utility functions on the data. The system's eight program elements are organized by their major functions in Table 2.2.

The main conversion sequence (shown in Figure 2.21) transforms the original climatological data through two intermediate forms into the gridded output data. The original input data[b] is binary-coded-decimal (BCD) card climatological hourly precipitation data from the National Climatic Center (NCC), Ashville, North Carolina. These data are arranged by station, a year's worth of data for each station.[c] This type of arrangement is called station-file or STA-FILE.

TABLE 2.2. Eight Program Elements Procedure Arranged by Major Function.

Main Sequence Conversion Steps	Auxiliary Programs: Printing	Auxiliary Programs: Extraction/ Combination
PAK	CHEK	EXT
SRT	RGR	COMP
GRI		SPL

The first conversion program (PAK) converts this BCD data to a packed binary format to reduce space and access-time requirements. The result of PAK is packed binary data in the STA-FILE arrangement.

The need of atmospheric models for spatially distributed, time-concurrent data requires that the data be sorted with respect to time. The combination of programs called SRT sorts the packed STA-FILE data according to date and produces packed binary data arranged so that data for all stations are collected together for each day. This arrangement is called synoptic file[d] or SYN-FILE, because it emulates the more typical arrangement of weather data compiled for synoptic analysis.

The packed SYN-FILE data becomes input to GRI, the precipitation gridding program. GRI uses all precipitation reports for a given hour to produce a regular grid of average precipitation estimates. It does this for each hour for a specified period of time. The output is a file of hourly gridded precipitation "maps."

(a) Control Data Corporation.
(b) "Original" only in terms of entry to this system. An initial conversion of the NCC data may be needed to make it compatible with the user's hardware and software facilities.
(c) Arrangements may be made with NCC to obtain recent monthly STA-FILE data.
(d) This is not strictly a synoptic file arrangement in that all data for a given hour are not grouped together. This hourly grouping takes place within GRI, when the time zone data are included.

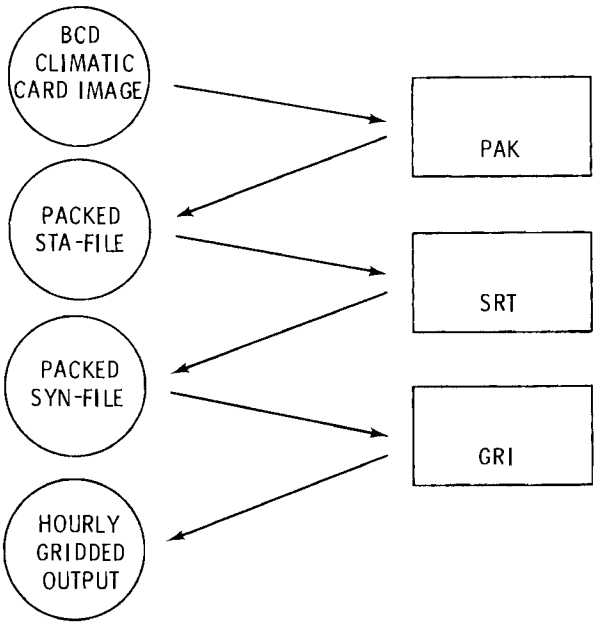

FIGURE 2.21. System Data Flow

The five auxiliary programs may be used to inspect or manipulate aggregates of data in the packed SYN-FILE or gridded formats. CHEK prints out specified days' data for all stations from a file in the packed SYN-FILE format. EXT extracts a specified subset of the packed SYN-FILE data and may also be used to splice two data sets covering different but overlapping time periods to form a chronologically continuous set. CMB combines packed SYN-FILE data sets of the same time period but from different sets of states. RGR prints out gridded data for a portion of the grid at specified hours. Finally, SPL is used to splice gridded data sets from overlapping time periods to form a chronologically continuous set. CMB combines packed SYN-FILE data sets of the same time period but from different sets of states. RGR prints out gridded data for a portion of the grid at specified hours. Finally, SPL is used to splice gridded data sets from overlapping time periods to form a single chronological continuous data set.

THE EFFECT OF USING TIME-AVERAGED PRECIPITATION FOR THE ESTIMATION OF WET DEPOSITION IN A REGIONAL SCALE MODEL

W. E. Davis

A study has been performed to determine why the use of average precipitation causes an increase in wet deposition over the wet deposition caused by the use of hourly precipitation. Results of this study are presented along with additional results from a study using the average precipitation turned on and off for set periods to calculate wet deposition.

Recently, it was restated that the use of mean precipitation rates was sufficient in wet removal parameterizations for long-term assessments using regional scale models (Slinn 1978). This study addressed the problem encountered in making such an assumption. The problem was discussed in a previous work by Wendell, Powell and Drake (1976) and more fully in Wendell, Powell and McNaughton (1977). They demonstrated that the use of long-term precipitation averages rather than an hour-by-hour rate caused higher deposition. This study explored why the difference occurs. Two PNL assessment models have been used to examine the effects of time averaging. The first is a single-layer model (Davis, Eadie and Powell 1978; Wendell, Powell and McNaughton 1977). The second is a multi-layer model (Davis and Wendell 1976). Both of these models are used to evaluate the impact of the release of a pollutant on the regional scale. In PNL's assessment models a series of hourly contaminant puffs are released and advected by hourly time steps using interpolated wind components from gridded windfields. As the puffs are transported they are allowed to grow both in the vertical and horizontal dimensions. In addition, the model based on isentropic considerations estimates the vertical motion by conserving the potential temperature modified by estimates of diabatic influences, i.e., radiational heating and cooling, heating resulting from mixing and heating resulting from the release of latent heat. When precipitation occurs, both models calculate wet removal of the contaminant.

Two study periods were selected: one for a spring period of April 1 to 15, 1974, and a second for a winter period in January 1975.

The following assumptions were made in order to run the two computer models. A release height of 62 m was used, and a mean depth of the mixing layer of 1000 m was assumed. A release rate of 1 Ci/sec was assumed for the hourly releases from the Savannah River Plant in South Carolina. The data used to compute gridded 1/2° latitude x 1/2° longitude hourly precipitation (68 x 64) came from the use of station file data of more than 3000 hourly reporting stations in the United States. The wind data used was upper air data averaged over a layer 100 to 1000 m above surface and interpolated to a 2° latitude x 2° longitude grid using a $1/\text{distance}^2$ weighting. The winds were used to advect the puff in hourly steps, and the gridded precipitation was used in calculating wet deposition in hourly increments. Wet deposition for the two time periods was calculated for 1/2° latitude x 1/2° longitude grid elements with no dry deposition.

In the April study only cumulative values of wet deposition were calculated for the total period. In January, a more in-depth study was made with PNL's single-layer model. Hourly arrays of air concentration values were written out in order to compare the contribution by the mean and fluctuation from the mean. The calculations were carried out for a series of washout rations (W), where $W = 5 \times 10^4$, 5×10^5, and 5×10^6 (Engelmann 1970) for both hourly precipitation and monthly average values for precipitation. The results of the January 1975 study are shown in Table 2.3.

The results clearly indicate the importance of B in offsetting deposition from the use of average values, A, for both 5×10^5 and 5×10^6. Not shown in the table is that the average air concentration was larger as a result of using hourly precipitation. This caused the increase in A with increasing washout ratios. For a washout ratio of 5×10^4, the total deposition from hourly and average precipitation was about equal.

Table 2.4 shows the effect of time-averaging on the total deposition for both time periods using both the single-layer and multilayer models. Also shown are results of a technique for estimating removal using the percent of time rain occurs during the month and mean number of

TABLE 2.3. Comparison (in percent of total released) of Deposition.

Washout Ratio	Total Deposition from Average Precipitation	Mean (A)	Fluctuations (B)	Hourly Total Deposition
5×10^4	24%	24%	6%	30%
5×10^5	82%	116%	-64%	52%
5×10^6	100%	158%	-95%	61%

TABLE 2.4. Total Deposition (in percent of total released) Using Different Averaging Times.

Type of Model	W	Averaging Times	Total Deposited
PERIOD 1: April 1-15, 1974			
Single Layer	5×10^5	1 hr	52
Single Layer	5×10^5	6 hr	56.6
Single Layer	5×10^5	360 hr	75
Eight Layer	5×10^5	1 hr	41.6
Eight Layer	5×10^5	6 hr	44.3
Eight Layer	5×10^5	12 hr	47.4
Eight Layer	5×10^5	24 hr	51
PERIOD 2: January 1-31, 1975			
Single Layer	5×10^4	1 hr	29.9
Single Layer	5×10^4	744 hr	23.8
Single Layer	5×10^4	10%(a)	25.7
Single Layer	5×10^5	1 hr	52
Single Layer	5×10^5	6 hr	57.1
Single Layer	5×10^5	744 hr	82
Single Layer	5×10^5	10%(a)	51.5
Single Layer	5×10^6	1 hr	61.1
Single Layer	5×10^6	744 hr	99.9
Single Layer	5×10^6	10%(a)	53.6

(a)Seven hours of 10x average precipitation every 72 hr.

hours of duration of rain during a month. The basic approach is that the average rain is turned on for 7 hr every 72 hr, and during the remainder of the 72 hr, precipitation is assumed to be zero. During the 7 hr, the precipitation is 10 times the average rate. This technique provided the best estimate of the wet deposition through the use of hourly precipitation.

An important point shown in Table 2.4 is that as the washout ratio increases, the amount of deposition by hourly precipitation approaches a limit of approximately 61% of that released, which reflects the fraction of puffs encountering precipitation. However, when average precipitation for the month was used, the limit was 100% of the puffs. Thus, the error in estimating deposition by the average rate precipitation increases for increasing washout ratio.

The final comparison shown in Table 2.4 is between the eight-layer model and the single-layer model for the period from April 1 to 15, 1974. The eight-layer model generally produced much lower depositions than the single-layer model. In the eight-layer model, when precipitation occurred, saturation of the puff was checked. If saturation did not occur, a washout ratio of W/10 was used to present below-cloud scavenging. This explains the difference in deposition results between the two models. In a previous study this approach was not used, and greater deposition occurred in the eight-layer model for hourly and 6-hr average precipitation. The same effect, increasing deposition with increased averaging time by the eight-layer model, can be seen in Table 2.4.

A comparison of wet deposition from the single-layer PNL model with an eight-layer PNL model showed much less deposition occurring in the eight-layer model. This difference was attributed to the calculation of wet deposition using a washout ratio that was a factor of 10 smaller when saturation of the puff did not occur and rain was occurring.

The results of this study showed why large differences can occur in estimating wet deposition when monthly averages of precipitation are used rather than shorter-term averages. In general, the larger the washout ratio, the larger the difference. A second method was tested using an on/off switch of 7 hr of precipitation every 72 hr. For the periods studied, this technique produced deposition results closer to the values produced by hourly precipitation than those produced by average precipitation. More work is necessary to test this technique for convective rainfall during summer months.

REDISTRIBUTION OF A LAYER OF HTO BY RAINFALL

M. Terry Dana and W. E. Davis

A uniform layer of HTO, when encountering a warm or cold front with rainfall, may be simultaneously lifted by frontal air motions over the front and lowered by reversible HTO scavenging. Illustrative calculations show that under typical conditions a layer of HTO bordering the ground may move through a front without rising. The attendant rainfall in this case causes a decay in the concentration which may be significant over the time of frontal pass through.

Theoretical work has shown that the gas-scavenging process is reversible and that a plume of gas may be redistributed by this mechanism (Hales 1972). Gas scavenged within an elevated plume will be desorbed from raindrops at lower levels, thus effectively lowering the plume. This problem of plume "washdown" was solved approximately by Slinn (1974) for idealized conditions. In this report, the effect is illustrated for a linearly soluble gas (solubility not dependent on concentration) such as HTO. Of particular interest is the interaction of washdown of a layer with vertical motions of the layer over a warm or cold front.

Consider a layer of HTO gas of concentration χ_o that is uniform with height throughout the layer. Assuming that the layer overall is descending by the effect of reversible scavenging, the flux F defines a washdown velocity w:

$$F \equiv w\chi_o \quad (w < o) \tag{1}$$

This flux downward can also be expressed as the product of c, the rain water concentration at the bottom of the layer, and J, the rainfall rate (constant with height). Thus,

$$w = cJ/\chi_o \tag{2}$$

When the liquid-phase concentration is in equilibrium with the gas-phase concentration,

$$c = H^*\chi_o \quad (\text{equilibrium}) \tag{3}$$

where H* is the solubility written as a "washout ratio" (mass of HTO per unit volume water/mass HTO per unit volume air). For the moment, assume that (3) holds at the bottom of the layer. Then (2) becomes

$$w = H^*J \tag{4}$$

Slinn (1974) arrived at the same conclusion for a Guassian plume, but his w represents the speed of lowering the plume's center of mass, and does not depend on reaching equilibrium conditions.

Although the above approach involves redistribution of an elevated layer, the present application is to the case where the layer is initially on the ground but is elevated by encounter with a front. Thus, the layer ascent over the front is compared to the descent by washdown. To illustrate, assume that the layer remains the same thickness vertically, that the temperature is constant with height everywhere, that rainfall begins at the instant that lifting begins, and that the speed v of lifting is constant in time.

Before w is compared with v, the assumption (4) (equilibrium conditions at the bottom of the layer) must be examined. For the "top hat" distribution shown in Figure 2.22, the linear gas-scavenging theory provides the following expression for c as a function of height z and raindrop radius a (Hales, Wolf and Dana 1973):

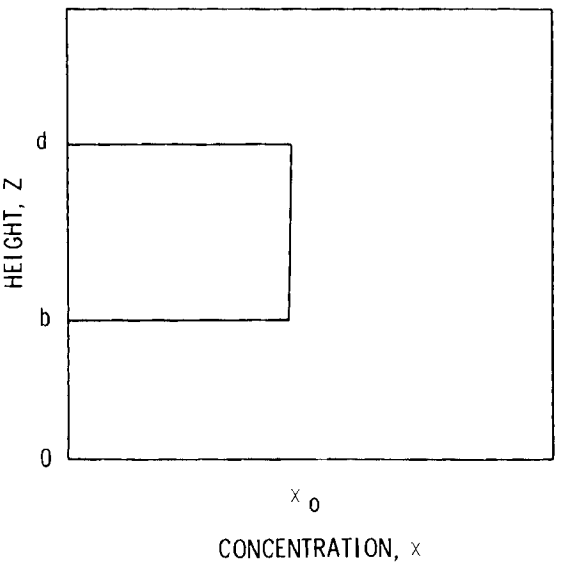

FIGURE 2.22. Top Hat Distribution of HTO Layer.

$$c(a,z) = H^{*}\chi_{o} \{\exp [\beta(b - z)] - \exp [\beta(d - z)]\} \quad (5)$$

where

$$\beta = \frac{3ky}{V_t a}\left(\frac{RT}{pH^{*}}\right)$$

V_t is the terminal velocity of fall of the raindrop (<o)

K_y is an overall mass transfer coefficient

R is the gas constant (82.057 cm^3 atm/°K mole)

T is the temperature (K)

p is the pressure (atm).

The term in curly brackets, call it δ, is clearly the fraction of equilibrium c reached at height z. If the term with b that describes desorption below the layer is ignored,

$$c(a,z) \simeq H^{*}\chi_{o}\,\delta(d - z) \quad (6)$$

Values of δ at the bottom of the layer (z = b) are listed in Table 2.5 for a typical frontal mass mean raindrop radius of a = 0.05 cm and for various layer thicknesses as a function of T. H* is a function of T only, and those values and the values of K_y are derived from Hales (1972). Thus, for HTO and typical conditions, a correction to (4) need only be made for low T and thin layers.

TABLE 2.5. Fraction of Equilibrium Concentration Reached at Layer Base (a = 0.05 cm).

T (K)	H^{*}[a]	δ at (d-b) Listed		
		0.5 km	1 km	2 km
273	2.3×10^5	0.52	0.77	1
283	1.2×10^5	0.76	0.94	1
293	6.5×10^4	0.94	1	1
303	3.4×10^4	0.996	1	1

[a]Dimensionless

Returning to the relative values of v and w, consider two cases: 1) a warm front with v = 0.2 km/hr and J = 0.3 cm/hr for three hours, and J = 0.1 cm/hr for the next three hours; and 2) a cold front with v = 1.0 km/hr and J = 1.2 cm/hr for one hour, and J = 0 later. In both cases, say that the layer thickness is 1 km. Table 2.6 lists net upward velocities v + w for these cases.

Negative upward velocities are meaningless here because the layer cannot be lowered below ground level. But they do illustrate the "potential" lowering of the layer, or more specifically, the distinct possibility that the HTO layer will pass through the front unlifted.

All the time that precipitation is falling and the base of the layer is at or

TABLE 2.6. Net Vertical Velocities of Layer and Rainfall Depletion (d-b = 1 km).

A. CASE 1—Warm Front

T (K)	Velocities, km/hr[a]		k,[a] hr^{-1}	χ/χ_o at time shown	
	w	v + w		3 hr	6 hr
273	-0.53	-0.33	0.53	0.20	0.12
283	-0.34	-0.14	0.34	0.36	0.26
293	-0.20	0	0.20	0.55	0.45
303	-0.10	+0.10	0.10	0.74	0.67

[a]First three hours; for second three hours: w → w/3, k → k/3

B. CASE 2—Cold Front[a]

T (K)	Velocities, km/hr		k,[a] hr^{-1}	χ/χ_o at time shown
	w	v + w		1 hr
273	-2.1	-1.1	2.1	0.12
283	-1.4	-0.41	1.4	0.25
293	-0.78	+0.22	0.78	0.46
303	-0.41	+0.59	0.41	0.66

[a]w and K values for one hour only

near the ground, the plume will be depleted by scavenging. If an exponential decay is assumed.

$$X(t) = X_o \exp(-kt) \quad (7)$$

where k is the scavenging or "washout" coefficient, it is easy to see that for equilibrium scavenging

$$k = \frac{-H^*J}{d - b} = \frac{-w}{d - b} \quad (8)$$

Values of k and the depletion at various times are listed in Table 2.6.

Some assumptions were made to obtain these results. Most unusual perhaps are the assumptions that the temperature is constant with height and that ascension does not compress or expand the layer. A single raindrop size was used, a typical mass mean for frontal rainfall. Condensation within the layer was not considered, so that scavenging of HTO-saturated cloud drops is not included. All these limitations can be handled with more detailed calculations. The problem of the redistributed "shape" of χ (χ was assumed to be depleted uniformly) was not solved; this is not a severe limitation, however, as long as equilibrium conditions are predominant (e.g., thick HTO layers and warm temperatures).

COOLING TOWER DRIFT: COMPREHENSIVE CASE STUDY

N. S. Laulainen and S. L. Ulanski

A comprehensive experiment to study drift from mechanical drift cooling towers was conducted during June 1978 at the PG&E Pittsburg Power Plant. The data from this study will be used for validation of drift deposition models. Preliminary results show the effects of tower geometry and orientation with respect to the wind and to single- or two-tower operation. The effect of decreasing relative humidity during a test run can also be seen.

INTRODUCTION

A comprehensive experiment to study emmisions, transport and downwind deposition of drift from a mechanical draft cooling tower was conducted at the PG&E oil-fired Pittsburg Power Plant at Pittsburg, California, from June 12 to 26, 1978. The purpose of the study was to develop a data base to be used for validation of drift deposition models.

The study was designed to measure the characteristics of the drift droplets emitted from the tower, the ambient meteorological conditions responsible for the transport and dispersion of the drift, and the downwind and near-surface air concentrations of the drift. The source characteristics, including updraft air temperature and velocity profiles, and the meteorological data are to be used as inputs to the models; the measured deposition patterns are to serve as comparisons to model outputs.

Source characterization measurements were performed by Environmental Systems Corporation (ESC of Knoxville, Tennessee) under sponsorship of the Electric Power Research Institute (EPRI). Measurements of meteorological and surface deposition were carried out by PNL. Other limited comparison tests were also performed by other organizations. Calfran Industries (Springfield, Massachusetts), also under EPRI sponsorship, measured drift droplet size distributions using a photographic technique; these measurements were to be compared to the ESC-derived size distributions and drift emission rates. Xonics (Van Nuys, California) provided limited remote wind profile measurements made with a Doppler acoustic radar system for comparison with measurements made by PNL's tethered-balloon system.

Experimental

A total of eight test runs plus a limited test were carried out during the June drift study at Pittsburg, California. Downwind deposition measurements were coordinated with ESC's source measurements on seven different tests. An eighth test was conducted with no concurrent source measurements. Limited droplet measurements were made on the fan deck of a single tower to examine

near-field deposition during a ninth and final test. The tests were divided into two-tower operation (three tests), tower 7-2 (western-most two tests), and tower 7-1 (three tests).

Meteorological conditions were not nearly as ideal as previous June climatology would indicate. The winds, though persistently from SW to W to NW, were more intense during the morning hours than usual. Only two or three runs were made where the winds could be classified as 10 mph or less. The other tests were carried out under winds ranging from 10 to 15 mph.

Meteorological data was collected at two levels from an instrumented 10-m tower upwind of the cooling towers from June 16 to 25, 1978. Temperature (dry- and wet-bulb), u, v, and w components of the wind were recorded continuously onto a seven-track magnetic tape at 5-min intervals over the experimental period.

A tethered-balloon system provided vertical profiles of temperature, moisture, and horizontal wind speed and direction within the vicinity of the cooling towers as well as in the upwind direction. Profiling was performed from the surface up to as high as 400 m on one occasion. The bulk of the profiles extended up to only 100 m. During the experimental period, the tethered-balloon system was flown on only seven days (June 15, 16, 17, 21, 23, 24, and 25). Its operation was limited by high winds (>10 m s^{-1}). The system, which was interfaced with an HP-97 calculator, provided print-outs of time, pressure, height, temperature, relative humidity, mixing ratio, wind speed and direction, and potential temperature.

During the last three days of the experiments, a Doppler acoustic sounder determined the wind profile in the boundary layer. A monostatic acoustic sounder also operated continuously from June 16 to 25. Data were recorded on a strip chart recorder. Automatic time-lapse camera systems were used to conduct plume photography during the experiment. In general, visible plume lengths were very short during the test period.

The strategy for measuring cooling tower drift emissions was based on pretest drift emission observations. Intensive measurements of a single cell during a specific test run and limited measurements of reference cells on each tower were made. Droplet size distributions were determined using sensitive papers (SP) and a light-scattering, droplet-counting system (PILLS). ESC acquired other plant and cooling tower operational parameters.

Downwind drift deposition patterns were determined using sensitive papers (SP) and deposition pans. Untreated filter papers were also exposed. These papers can be examined either as additional deposition receptors for further chemical analysis or developed for CL^- ion using Ag NO_3. (The papers treated in this manner should be similar to the SP's.) At selected locations a rotating arm sampler with sensitive papers attached was used to determine near-surface air concentrations of drift. Canal and basin water samples were regularly collected during test runs.

Data Analyses and Reductions

Of the eight test runs, five to six are of sufficient quality to warrant intensive analyses. Chemical and droplet analyses have been nearly completed for the 6-16 test; only partial analyses (droplet) of the 6-17 have been completed. Some drift deposition data interpretation has been carried out. Two types of analyses are conducted: 1) chemical analysis of bulk deposition samples and 2) droplet size distribution analysis of sensitive papers.

Mineral ion species, including Na^+, K^+ and NH_4^+, Cl^-, NO_3^- and SO_4^{--}, are obtained routinely with the positive and negative ion chromatographs (IC); Ca^{++} and Mg^{++} are determined by atomic absorption spectroscopy. Deposition pan samples and canal and basin water samples are analyzed using these techniques. Samples are recovered from the deposition pans using 10 ml of double-distilled, deionized water. Canal and basin water samples are usually diluted by a factor of 100 to 1000 before being analyzed on the IC's.

Drift droplet size distributions are obtained from the sensitive papers with an automated scanning and sizing device, the Quantimet 720 system. The system is interfaced with a mini-computer that allows the measured stain sizes to be converted to droplet sizes, binned according to size category, and number and volume size distributions stored on cassette tape for hard copy retrieval.

The results of the chemical and droplet analyses are then converted to deposition rates, from which the downwind deposition patterns are obtained. It is apparent from preliminary analysis of the 6-16 test that because of the wind and dust conditions at the site during the experiment, larger background values of mineral ion deposition are present in the data than originally anticipated. Fortunately, the sampling procedure allowed for enough outside-the-plume stations that, with suitable statistical procedures, it should be possible to

eliminate most of the influence of this variable background component.

Ratios of mineral ion mass deposition may be a convenient method for distinguishing drift from nonsoil, background aerosol, as the ratios for drift material should be similar to those of basin and/or canal water. The problem of soil contamination is not as straightforward, because the soil has been exposed to drift deposition and, more important, canal water from water trucks used in PG&E's dust abatement efforts. The upwind stations should be useful for evaluating the nonsoil background; the soil samples collected near many of the sampling stations may be useful for qualitative estimates of soil/dust contamination.

The 6-16 data also seem to show the screening effect caused by the electrical switchyard superstructures on the downwind deposition pattern. Since, in several of the test runs, the plume moved in a direction of few interferences, a quantitative estimate of drift interception by the switchyards may be possible (see Figure 2.23).

Drift distribution patterns are expected to show the effects of tower geometry and orientation with respect to the wind and single- or both-tower operation. For the most part, winds were along the long axis of the towers, which themselves were aligned end-to-end. Visual examination of the sensitive papers shows cross-plume differences in droplet size distribution and magnitude of deposition rate--an observation which is at least consistent with the above remarks.

Aside from the obvious effect of wind in determining the downwind drift distribution pattern, the effect of rising temperature and decreasing relative humidity during the course of a test run can also be seen on the sensitive papers. Thus, changes in

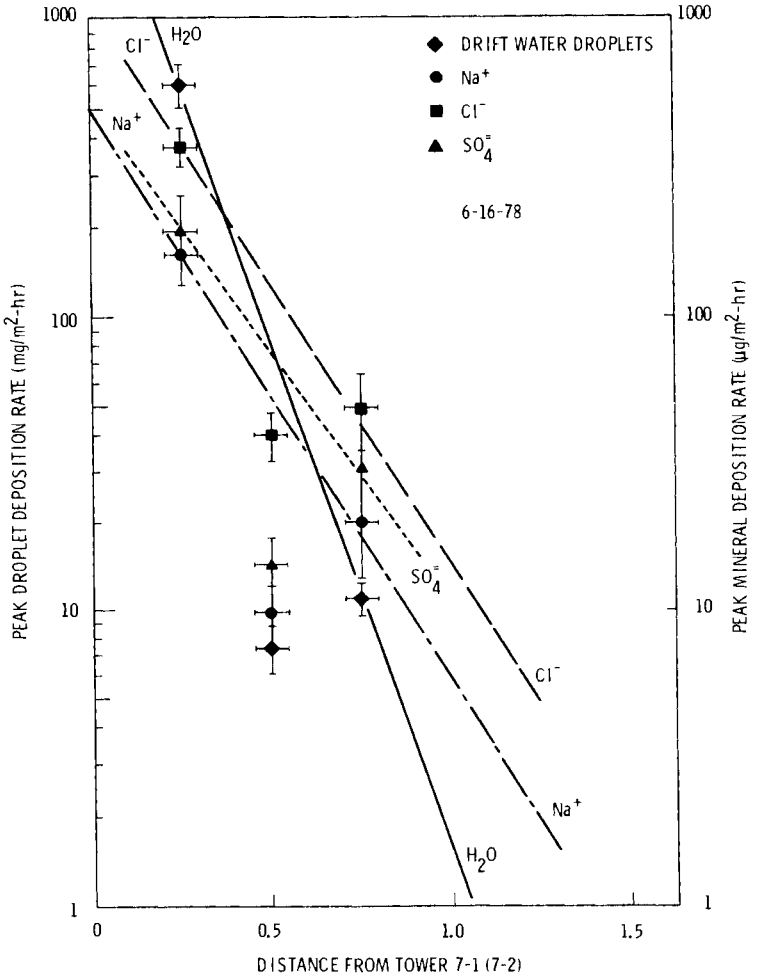

FIGURE 2.23. Quantitative Estimate of Drift Interception by Switchyards.

droplet evaporation rates are important factors in determining droplet size distribution and mineral deposition rates. To make these determinations, the meteorological observations (e.g., from the PG&E station, the tethered-balloon system and the 10-m meteorology tower) should be averaged, where practical, over intervals compatible with the actual sampling times.

Acknowledgements

The following people contributed to the success of the field effort: Owen Abbey, Don Glover, Roger Schreck and John Thorp. The efforts of Steve Harris and Jane Rothert in analyzing drift samples are appreciated, as are the efforts of Lee Daniel in sizing droplets.

A LAGRANGIAN-SIMILARITY DIFFUSION-DEPOSITION MODEL

T. W. Horst

A Lagrangian-similarity diffusion model has been incorporated into the surface-depletion deposition model. This model predicts vertical concentration profiles far downwind of the source that agree with those of a one-dimensional gradient-transfer model.

The surface-depletion model of Horst (1977) is a method for correcting an atmospheric diffusion model for dry deposition. It requires only a deposition velocity v_d and an expression for $D(x,z,h)$, the cross-wind-integrated airborne contamination at location (x,z) caused by a unit point source of nondepositing material at $(x = 0, z = h)$. Since the surface-depletion model uses a negative area source or sink of material at ground level to account for deposition, $D(x,z,0)$ is an essential element of the model.

The surface-depletion model has been improved by replacing the Pasquill-Gifford Gaussian plume formula for $D(x,z,0)$ with a Lagrangian similarity description. The latter theory predicts the vertical spread $\bar{z}$ of a contaminant in terms of the friction velocity u_* and the Obukhov length L,

$$d\bar{z}/dt = u_* k/\phi(\bar{z}/L) \qquad (1)$$

where ϕ is a function of atmospheric stability. $D(x,z,0)$ is assumed to be

$$D(x,z,0) = D(x,0,0) \exp\left[-(z/b\bar{z})^n\right] \qquad (2)$$

with $D(x,0,0)$ determined by the requirement of continuity. A gradient-transfer solution to the convective-diffusion equation predicts that $n = 2 - p$, if the eddy diffusivity is proportional to z^p ($p > 1$ for unstable conditions, $p = 1$ for neutral conditions, and $p < 1$ for stable conditions). Observations of atmospheric diffusion from a ground-level source, however, favor $n = 1.5$ for neutral conditions, $n < 1.5$ for unstable conditions, and $n > 1.5$ for stable conditions (Horst 1978a).

The new version of the surface depletion model has been tested with the vertical profiles of airborne contamination $C(z)$ predicted far downwind of the source. These profiles are independent of the source location (Horst 1978b) and are a function only of u_*, z/L, and the deposition $v_d C(z_d)$. One-dimensional gradient-transfer theory predicts that

$$C(z) - C(z_d) = \frac{v_d C(z_d)}{u_* k} \int_{z_d}^{z} \frac{\phi(z'/L)\, dz'}{z'} \qquad (3)$$

The best agreement between the surface depletion model and equation (3) is found with a value of $n = 1$ in neutral conditions, $n < 1$ in unstable conditions, and $n > 1$ in stable conditions. As might be expected, this agrees with the gradient-transfer solution to the convective-diffusion equation rather than with the observational data on vertical diffusion.

RADIOACTIVE FALLOUT FROM CHINESE NUCLEAR WEAPONS TEST OF MARCH 15, 1978

C. W. Thomas

Pacific Northwest Laboratory (PNL) has measured the radionuclide concentration of short-lived debris from a radioactive cloud, produced by a nuclear weapons test conducted by the People's Republic of China on March 15, 1978. Analysis with a 40 cfm Sierra impactor showed that a large portion of the radioactivity was associated with relatively large particles. Surface air samples showed significant concentrations of ^{124}Sb. Samples of rain water from New York State showed that radioactivity arrived on the east coast at about the same time as peak debris levels were observed on the west coast. Highest concentrations of ^{131}I occurred along the Washington State-Canadian border.

On March 15, 1978, the People's Republic of China tested a low-yield nuclear device. News media reported that this device was substantially less than 20 kiloton (AP 1978). The trajectory analysis predicted that the leading edge of the radioactive cloud would arrive on the west coast of the state of Washington on March 19, 1978 (Air Resources Laboratory 1978). Fallout from this test was detected on air filter samples collected at Quillayute, Sequim and Richland, Washington, and at Colstrip, Montana. As with other tropospheric detonations, air concentration and deposition of short-lived radionuclides were significant.

The first measurable concentration of short-lived radionuclides associated with this test was collected on a filter that sampled atmospheric aerosols from March 17, 1978 at 1313 hr through March 18, 1978 at 1205 hr at Colstrip, Montana, and from March 19, 1978 at 1820 hr through March 20, 1978 at 1655 hr at Quillayute, Washington. The radionuclide concentration of short-lived debris was first detected in Richland, Washington, on air samples collected from March 21, 1978 at 0736 hr through March 22, 1978 at 0726 hr. The initial ^{131}I concentration at both Colstrip and Quillayute was about two to three orders of magnitude less than the peak concentrations which occurred a day or so later. At Richland, Washington, the initial concentration was nearly as high as the peak concentration. This suggests that the radioactive debris arrived near the end of the first sampling period at Colstrip, Montana, and Quillayute, Washington. It may have arrived near the beginning of the sampling period at Richland, Washington. Comparing the arrival times of the fallout indicates that the debris peaked at about the same time at Colstrip, Quillayute, Sequim and Richland, and suggests that initial material which reached Colstrip during the March 17 through March 18 sampling period was associated with a more rapidly moving air mass.

The physical form of the short-lived radionuclides was obtained from the analysis of debris collected on the stages of a 40 cfm Sierra impactor, which had operated for two time periods. The first sample (Table 2.7) was taken from March 20 at 1420 hr through March 22 at 1025 hr, and the second sample from March 23 at 1256 hr through March 27 at 1006 hr. These observations were that a large portion of the radioactivity was associated with relatively large particles. Between 49% and 63% of the radionuclides produced in this test were associated with particles of greater than 1.3 μm in diameter. This is a substantially different distribution than that observed for radionuclides of stratospheric origin such as ^{7}Be and ^{144}Ce. Both ^{7}Be and ^{144}Ce showed only about 15% and 20% of their radioactivity associated with particles greater than 1.3 μm. When nuclear testing debris has remained in the stratosphere for some time, which is the case for the ^{144}Ce, or when radionuclides are formed in the stratosphere, which is the case for ^{7}Be, the radionuclides are associated with comparatively small particles, even though they descend through the relatively large particle distribution in the troposphere to the earth's surface (Thomas and Perkins 1977).

No significant difference was noted in the radionuclide-particle-size distribution for the first and second time periods, apparently because both samples were associated with material from the first circumnavigation of the earth.

Significant amounts of 2.7-day ^{122}Sb and 60.2-day ^{124}Sb were produced during this detonation. Both of these radionuclides are produced during detonation by n,γ activation of stable ^{121}Sb and ^{123}Sb. Surface-air concentration of 715 dpm/10^3 SCM and 3 dpm/10^3 of ^{122}Sb and ^{124}Sb, respectively, were measured in samples taken at Richland, Washington.

TABLE 2.7. Particle Size Distribution of Radionuclides in Initial Fallout from the Chinese Nuclear Test of March 15, 1978.[a]

	Percent in Each Size Range					
	10 μm	4.9-10 μm	2.7-4.9 μm	1.3-2.7 μm	0.6-1.3 μm	0.6 μm
^{144}Ce	<1.9	<4.8	5.2	14.4	29.4	44.3
^{99}Mo	1.7	13.5	19.7	22.8	21.2	21.2
^{141}Ce	1.4	12.1	21.0	24.1	23.0	18.3
^{132}Te	1.1	11.6	21.5	25.9	24.2	15.7
^{239}Np	1.9	14.3	22.3	24.2	21.8	15.5
^{131}I	1.3	10.8	18.3	19.6	18.7	31.3
^{7}Be	<1.4	<3.8	3.9	5.5	17.4	68.0
^{103}Ru	1.0	9.0	17.5	21.4	25.2	25.9
^{140}Ba	1.2	10.5	18.6	21.7	25.1	22.8
^{95}Zr	<2.1	12.8	18.6	17.6	24.8	24.0

[a]Aerosol sampling period March 20, 1978 at 1420 hr through March 22, 1975 at 1025 hr.

Samples of rain water from Brighton, New York, showed that radioactivity had arrived over the east coast during the sampling period of March 21 at 0800 hr through March 22 at 0800 hr. This was approximately the same time that the peak radioactive debris was observed in surface air samples at Richland, Washington. The earlier arrival in New York State is apparently associated with a faster-moving higher-elevation air mass from which debris was scavenged by the rain.

To aid in determining the areal distribution of short-lived debris, grass samples were collected along the west coast of the United States from Los Angeles, California, to the Canadian border adjacent to Washington State. The sampling locations and the observed ^{131}I concentrations in distintegrations per minute per kilogram of grass (wet weight) are shown in Table 2.8. It is evident that the fallout distribution along the west coast was greatest near the Washington State-Canadian border. The highest levels were observed in samples taken north of Seattle, Washington, and reached concentrations that were comparable to fallout levels measured on the east coast in October 1976, following the September 26, 1976 nuclear test. Based on the Federal Radiation Council Report No. 5 (1964) and the factors for radioactive uptake and transfer of ^{131}I, a dose to a 2-g child's thyroid was calculated (Thomas, Soldat, Silker and Perkins 1976). The highest potential infant thyroid dose, assuming an intake of 1 L of milk per day from a cow being fed entirely on pasture grass, was 350 mrem based on a sample taken at Laurel, Washington.

The physical and chemical forms of ^{131}I were measured with a special iodine sampler (Ludwick 1964). This sampler contained a particle filter followed by a charcoal-impregnated filter for removal of inorganic iodine species and a 10-cm-long compartmental charcoal bed for collection of organic iodides such as methyl iodide. The observed data indicated that 80% of the ^{131}I was associated with particles, and that the 20% remaining was in the gaseous form and was divided roughly between reactive and organic species.

TABLE 2.8. Concentration of ^{131}I on Grass from West Coast of the United States.

Location	^{131}I, dpm/kg (wet wt)	Location	^{131}I, dpm/kg (wet wt)
Blaine, Wash.	6985	Azalea, Ore.	93
Laurel, Wash.	25132	North Grants Pass, Ore.	57
Bellingham, Wash.	10474	South Grants Pass, Ore.	247
Mt. Vernon, Wash.	194	South Medford, Ore.	77
Everett, Wash.	346	South Henley, Calif.	74
North Seattle, Wash.	276	Edgewood, Calif.	356
Seattle, Wash.	199	Delta, Calif.	202
Mercer Island, Wash.	130	Hooker, Calif.	55
Ellensburg, Wash.	3616	Corning, Calif.	64
Sequim, Wash.	263	Astoris, Calif.	73
Kennewick, Wash.	541	Ourmega, Calif.	49
Fife, Wash.	119	North Sacramento, Calif.	58
Maytown, Wash.	320	Stockton, Calif.	81
Toledo, Wash.	301	Westley, Calif.	44
Ridgefield, Wash.	143	North Los Bemos, Calif.	58
Milwaukie, Ore.	156	South Los Bemos, Calif.	31
Canby, Ore.	178	North Avenal, Calif.	32
Salem, Ore.	148	North Bakersfield, Calif.	36
Buena, Vista, Ore.	399	South Bakersfield, Calif.	47
Walker, Ore.	109	Frazier, Calif.	262
North Roseburg, Ore.	186	South Newhalb, Calif.	82
South Roseburg, Ore.	268		

3.0 Oil Shale

OIL SHALE

- **MAP3S Modeling Studies**
- **DOE/RL Special Studies**
- **Air Pollution Dry Deposition**

The primary oil shale regions of the country are in the Rocky Mountain West, where any airborne pollutants will be emitted, transported, transformed and deposited over very complex terrain under meteorological conditions that are, at best, extremely complicated. This complexity dictates the development of a set of complex models and innovative field techniques.

PNL has initiated a modest effort in the development of windfield models for complex terrain. Other activities include the development of a tracer technique to measure dry deposition of pollutants over complex terrain, insolulation and turbidity measurements over rough topography, aerosol and visibility measurements, and deposition measurements of ambient airborne soil.

A DIRECT METHOD OF ADJUSTING WINDFIELDS OVER COMPLEX TERRAIN

C. H. Huang and R. L. Drake

In this preliminary study, a generalized, mass-consistent model was developed to study the airflow over complex terrain in a conformal space (terrain-following coordinate system). The methodology used in this model offers flexibility, because it is not based on potential flow approaches or restricted to a particular space. Thus, the nature and physics of the airflow over complex terrain can be easily realized through numerical experiments with the model.

In general, two methods have been used for computing mass-consistent windfields: one is an indirect method based on variational techniques (Sasaki 1958; Sherman 1978); the other is a direct method that solves the continuity equation in two-dimensional space (Endlich 1967; Liu and Goodin 1976). However in this study, a methodology that is a generalization of mass-consistent models was developed for obtaining windfields over complex terrain.

In simulating air concentration over complex terrain, mass consistent windfields are desirable; otherwise, air concentrations calculated from a transport and diffusion model may be invalid, because when evaluating median- and long-range transport and diffusion for air quality, the advection term is usually larger than the diffusion term. Thus, the mass consistent models and their methods of solution have been actively pursued in recent years (e.g., see the Livermore Region Air Quality models, Sherman 1978).

Sasaki (1958) developed a variational technique, which was used in a Lawrence Livermore mass-consistent model, MATHEW (Sherman, 1978). The technique minimizes the variance of the difference between the observed and the analyzed values, and conserves the mass within the computational volume. However, in the indirect method the computed windfield at an observational station often differs significantly from the actual data (Liu and Goodin 1976). This result arises from the model being strongly dependent on the Lagrangian multipliers, λ. As a result, the computed windfields may bear little resemblance to the actual wind data. In order to remedy this deficiency, Endlich (1967) suggested a heuristic direct model to reduce the value of divergence. His model is essentially two dimensional and is similar to Liu and Goodin's method for computing two-dimensional windfields (1976). This heuristic method presents difficulties when applied to three-dimensional airflow in a conformal coordinate system over complex terrain.

In this study three-dimensional mass-consistent windfields were computed directly by employing a "modified" Newton method (Huang and Nickerson 1972 and 1974). This model is more flexible than models of the MATHEW-type and the physical constraints are more easily realized than in other models. In the model the convergence makes this methodology for computing three-dimensional windfields over complex terrain in a conformal space possible, which distinguishes it from the existing models in current practice.

If only limited measurements are available, the observed data need to be interpolated horizontally to the grid points in a domain of interest. This interpolation combines a surface-fitting method and the weighted-averaging method of interpolation, according to the distance between actual data stations and the grid point (Barnes 1967). The values of variables at grid points are estimated by summing the weighted values of the individual data. After horizontal wind components have been evaluated at every grid point, wind speed at a reference-level is vertically extrapolated from one surface to another by using the wind profile power law.

Based on the theoretical analysis of convergence, a generalized, direct method for adjusting windfields was developed (Huang and Nickerson 1972). The mass-consistent model computes windfields over

complex terrain in a terrain conformal coordinate system, using a "modified" Newton's method. This method does not involve the iterative solution of the Poisson equation, which is time consuming. Our method is expected to reduce the formulation and the effort.

The continuity equation in a sigma system for nondivergent windfields was solved by using the modified Newton's method of optimum displacement by point.

In this preliminary investigation, the five levels of the sigma system are used to illustrate the methodology of the numerical scheme. The grid size in the volume of interest is 15 x 11 x 5 with the horizontal and lateral grid sizes of $\Delta x = \Delta y = 1$ km and the height at the top of the boundary layer, 1 km. In the first case studied, flat terrain was assumed in carrying out the numerical integrations. The initial windfields at each grid point were interpolated and extrapolated from four observation stations. The value of maximum divergence was reduced by an order of 10^{-14}.

In the second case, the airflow over a simple Gaussian mountain was studied. The initial wind-field generated for the sigma surface at level two in the presence of the Gaussian mountain is shown in Figure 3.1. The adjusted windfield at level two after the 50th iteration is shown in Figure 3.2. The results indicate that the wind speed increases over the mountaintop. When the upstream airflow encounters the mountain, it converges and then deflects around the mountain. The deflected airflow increases in wind speed, as seen by comparing wind vectors in Figure 3.2 with those in Figure 3.1. After the airflow passes over the top of the mountain, it diverges and the airflow decelerates on the lee side of the mountain.

In the long-term assessment of air quality, solving a set of primitive hydrodynamic equations, especially in the data sparse areas, is not economical; however, a mass-consistent windfield model is practical, used in conjunction with a transport and diffusion equation. Currently, more case studies for various atmospheric and terrain conditions are underway, and the diabatic effects will be incorporated into the model. The analysis of the effectiveness of the model is also under investigation.

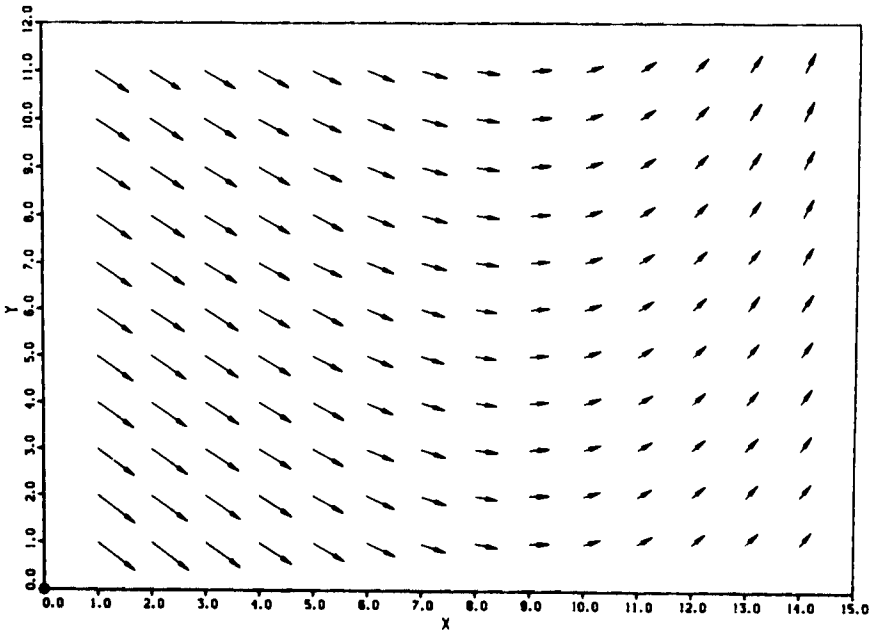

FIGURE 3.1. Initial Windfield at Level 2 ($\sigma = 0.25$) in the Presence of Gaussian Mountain ($\Delta x = \Delta y = 1$ km).

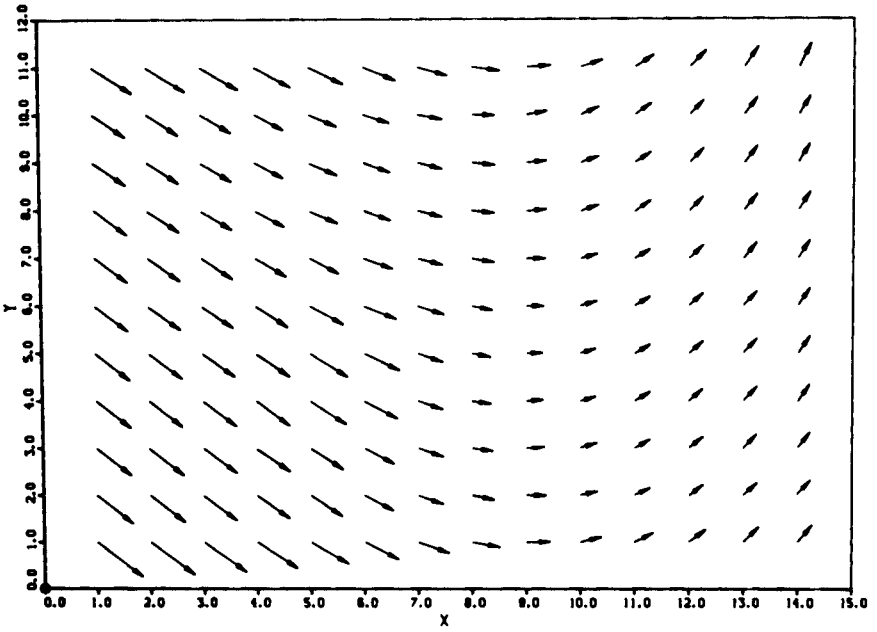

FIGURE 3.2. Mass Consistent Windfield at Level 2 (σ = 0.25) and at 50th Iteration Over Gaussian Mountain.

AEROSOL AND VISIBILITY MEASUREMENTS IN MOUNTAINOUS TERRAIN

M. M. Orgill, D. R. Drewes, and S. R. Garcia

This study is an initial effort to collect information on the relationship between aerosols and visibility in mountainous terrain and the occurrence of air pollutants from fossil-fuel energy sources. Airborne instruments were used as the primary means of obtaining data.

Past studies have shown that visibility may be reduced downwind of urban or industrial sources using fossil energy (Auer, Jr. 1977). The Air Quality Act and its amendments (EPA 1977, 1978) have declared the maintenance of good visibility as a national goal, especially in regions where excellent visual quality has been the general rule, e.g., Mandatory Class I Areas. Visibility or horizontal visual range is generally good in the mountainous western states, especially in wilderness areas. However, with the expected increased use of fossil fuel to meet energy demands in the western states, background levels of pollutants and the transport of pollutants to distant regions should be monitored in order to ascertain whether the provisions of the Clear Air Act can be met.

An effort to obtain preliminary data was conducted on June 16, 21 and 22, 1978 by three aircraft sampling flights in mountainous terrain downwind of Portland, Seattle and Spokane. Data were obtained using an integrating nephelometer (Charlson et al. 1967), high-volume filter sampler, and a DAS 32 Data Acquisition System. The integrating nephelometer measures the scattering extinction coefficient, the sum of molecular scattering and particle scattering (b_s). This scattering coefficient is a useful parameter for estimating visual range and fine particle mass loading. The relationship

of b_{scat} and visual range is

$$L_v = \frac{3.9}{b_{scat}} \quad (1)$$

For the experimental flights, the nephelometer was adjusted so that the background (molecular scattering) was zero for clear air. In this case, the instrument read b_{sp}, or the particle scattering extinction coefficient:

$$b_{sp} = b_{scat} - \text{molecular scat} \quad (2)$$

$$b_{sp} = b_{scat} - 0.15 \times 10^{-4} m^{-1}(a)$$

The high-volume filter sampler was used to give information on the chemical nature of the light scattering particles. IPC filters were used in the high volume sampler and were analyzed by x-ray flourescence analysis for 16 trace elements.

Figure 3.3 shows a time series plot of the particle scattering extinction coefficient (b_{sp}), temperature, relative humidity, and altitude for two of the seven experimental flights. In these cases as well as in the other flights, the prevailing visibility at surrounding National Weather Service observation stations was 24 km (15 mi) or more; therefore, the flights were conducted during "clean air" atmospheric conditions. Generally, the experimental flights were flown around 300 m (1000 ft) to 457 m (1500 ft) above the terrain.

Table 3.1 shows a breakdown of 16 trace elements as obtained from the filter samples for the seven experimental flights. At the bottom of the table is an estimate of the average visual range for the flights as calculated from Equation (1). The lowest average visual range was calculated for June 21. On this day, hazy conditions were present in the upper and lower Kittitas Valley during the experimental sampling, and the second sampling period was concluded about two hours before a dust storm was observed in the Spokane area. The remainder of the sampling flights were made during cloudy conditions, but with generally good visibility. However, the nephelometer data showed the presence of an urban plume downwind of the Seattle area and local sources of light scattering particles in the Columbia River Gorge, Willamette Valley and the Middle Fork of the Willamette River.

The significance, if any, of these results will have to await the collection of more data of this nature, but in greater detail and under different weather conditions. Future data collection flights are planned for the Pacific Northwest area, and data obtained from other areas where potential energy resources are being exploited (such as the oil shale tracts in Colorado, Utah and Wyoming and the geothermal sites in California) would be of interest.

(a) sea level value

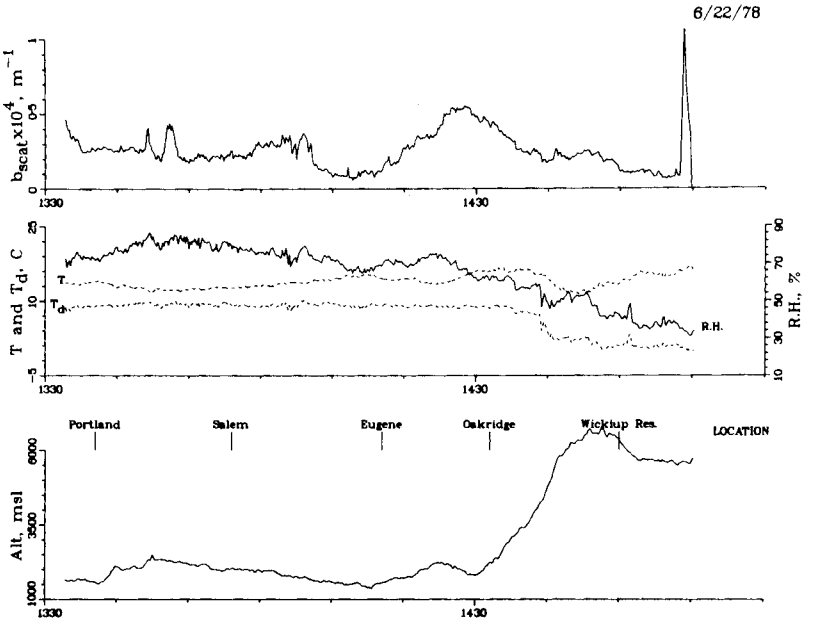

A

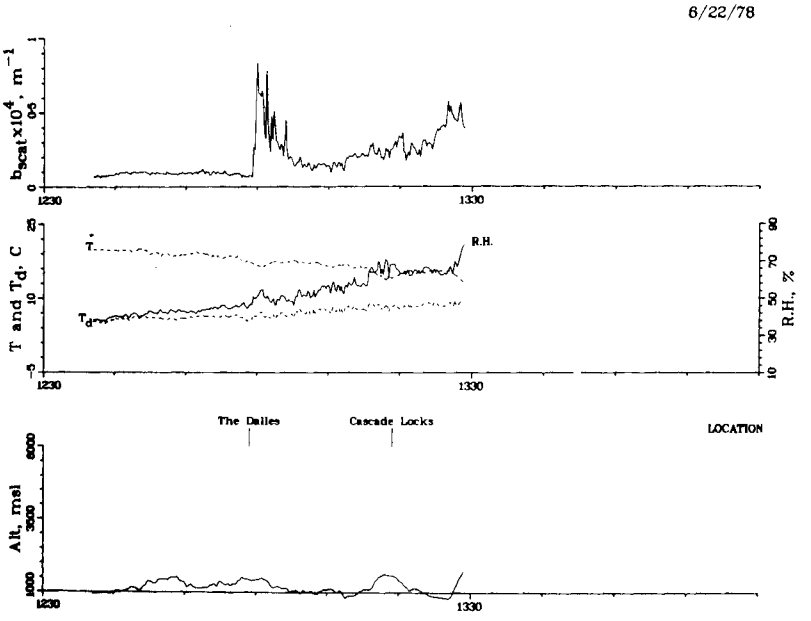

B

FIGURE 3.3. Time-Series Plot of the Particle Scattering Extinction Coefficient (b_{sp}), Temperature, Relative Humidity and Altitude for Experimental Flights in The Columbia Gorge and Oregon.

TABLE 3.1. Trace Elements (ng/m³) and Average Visual Range for Sampling Flights for June 16, 21 and 22, 1978.

Date	June 16			June 21		June 22	
Sampling Sites	Hood Canal E. of Olympic Mountains	Seattle Foothills	Upper & Lower Kittitas Valley	Upper Kittitas Valley and Wenatchee	Priest Riv. Lk. Coeur d'Alene Sandpoint (Spokane-D.W.)	Columbia Gorge	East Willamette Valley
As	<2.6	5.6	3.4	4.4	9.9	3.6	2.5
Br	6.3	11.1	3.9	5.5	7.4	5.1	6.5
Ca	299.8	452.0	534.1	1478.4	1673.1	1935.0	477.8
Cl	642.0	643.1	865.9	422.4	222.7	199.3	363.1
Cr	62.7	33.9	46.3	76.8	116.6	75.1	35.2
Cu	142.1	57.3	77.3	44.9	57.1	78.9	44.5
Fe	1017.7	871.4	1077.4	3264.0	4182.7	4489.2	887.2
K	<54.6	<43.8	64.1	823.2	1202.2	1253.9	96.1
Mn	29.1	12.8	24.8	72.0	110.2	97.5	23.9
Ni	18.2	13.8	17.7	22.5	31.6	27.2	9.4
Pb	19.4	30.9	14.8	25.4	45.2	20.6	17.5
Rb	<4.4	<3.4	<5.1	4.4	6.8	10.4	<2.0
S	547.8	1034.5	611.4	734.4	440.4	1091.3	608.8
Ti	92.2	137.0	126.9	384.0	443.2	561.2	88.7
V	<9.6	<7.9	11.5	6.2	10.2	24.9	7.3
Zn	25.5	19.6	23.7	21.1	38.2	30.8	16.6
Sampling Time, min	30	43	31	87	74	53	74
Sample Volume, m³	32.3	47.3	33.4	93.6	79.6	57.0	80.7
Average Visual Range, mi	77	69	85	44	57	70	60

INSOLATION AND TURBIDITY MEASUREMENTS AT HANFORD

N. S. Laulainen, E. W. Kleckner, J. J. Michalsky and J. M. Thorp

From observations obtained at the Rattlesnake Observatory and the Hanford Meteorological Station, the redistribution of solar radiation as a result of aerosols in the lowest 1 km of the earth's atmosphere has been examined using several types of solar radiation measuring instruments. Large turbidity excursions are observed with high values associated with stagnant air masses and low values associated with frontal passage. Turbidities show variations in color dependence that arise because of changes in particle size distribution.

An experiment to examine differential turbidity effects on insolation measured at the earth's surface was initiated during the summer of 1977 and continued through the summer of 1978. Several types of solar-radiation measuring instruments were employed during the study at the Rattlesnake Observatory (RSO) at 1090 m MSL and at the Hanford Meteorological Station (HMS) at 220 m MSL. Nearly simultaneous observations were frequently made at both observing sites with occasional instrument comparison at the same site.

The rationale for the experiment was: the first kilometer or so of the atmosphere above the surface is generally the most turbid and aside from clouds, solar radiation is attenuated and diffused largely through scattering and absorption by suspended atmospheric particles. Thus, characterizing turbidity and redistribution of solar radiation in this portion of the atmosphere is an important consideration in using solar energy and in evaluating potential inadvertent climate modification as a result of aerosols.

The Hanford area provides a unique opportunity for such characterization because of the nearly 1-km altitude difference between RSO and HMS and because of the large variability of atmospheric dust, smoke and haze in the Central Columbia Basin region (Laulainen 1978).

Total insolation on a horizontal surface was measured with pyranometers. A precision Eppley (Model PSP) thermopile unit was located at HMS and was used to compare the portable field units. A silicon-cell pyranometer with a rotating shadow band provided both total insolation and diffuse sky radiation. Direct solar measurements were made with a 10-channel sunphotometer, a 6-channel active cavity radiometer (ACR), and the 7-channel mobile automated scanning photometer (MASP) unit. The sunphotometer used in this study employed a silicon photovoltaic cell as a detector, which is sensitive to radiation in the spectral range 0.4 to 1.2 μm. The ACR was sensitive to radiation over the entire solar spectrum (0.3 to ∿4 μm). The MASP unit, operating in a direct sun-looking mode, also used a silicon cell as a detector.

Calibrations of the portable field pyranometers were difficult to maintain. Moreover, mechanical failures of a few of these instruments occurred. The unit assigned to RSO was damaged beyond repair during late fall 1977, so that comparative insolation data between RSO and HMS are only available for July through September 1977. Direct solar measurements can be made only for a cloud free line-of-sight.

The ACR and sunphotometer were compared at the same site on three separate occasions, twice at HMS (14 August 1978 and 14 September 1978) and once at RSO (6 July 1977). The turbidities derived from observations with each of these instruments are compared in Figure 3.4.

Turbidities at HMS during 1977 and 1978 are shown in Figure 3.5. Variations are similar to those reported earlier (Laulainen 1978). The turbidities show large excursions that are related to the synoptic meteorology. A stagnant air mass, for example, allows smoke and haze to accumulate in the basin leading to rather high turbidities. Abrupt turbidity decreases usually occurred after frontal passage.

The aerosol layer redistributes the direct solar beam primarily through scattering of radiation. As the turbidity increases, so does the diffuse component of insolation. The increase in diffuse radiation, however, does not compensate entirely for the loss from the direct beam, since some of the radiation is back-scattered or reflected into space while other parts of it are absorbed by the particles. The ratio of absorption to back-scattering determines whether the aerosol layer acts to cool or to warm the surface. The redistribution of radiation also can have a significant effect on solar collector performance. On cloud-free days, diffuse radiation accounted for 10 to 20% of the total insolation, depending upon the turbidity.

Because light scattering is particle-size dependent, the spectral quality of solar radiation is affected by size distribution of the aerosol layer. Spectral turbidities can be approximated by a simple power law dependence on wavelength over the visible spectrum, i.e., $\tau \sim \lambda^{-\alpha}$ where τ is the optical depth or turbidity, λ is the wavelength and α is the Ångström wavelength exponent. Typical values of α are found in the range 0.5 to 2.5 with occasional values in the -1 to 0 range at background sites (Middleton 1968).

Fresh aerosols originating from gas-to-particle conversion or from combustion products tend to have a predominance of fine particles smaller than 0.1 μm in diameter and consequently have larger values of α, e.g. in the range 1.5 to 2.5. As the aerosols age the size distribution becomes larger, typically in the range of 0.1 to 1.0 μm, by coagulation and condensational growth processes. The value of α tends to decrease as the aging continues and values in the range 0.5 to 1.5 are common. Mechanically generated aerosols are generally larger than 1 or 2 μm; these particles have essentially neutral optical

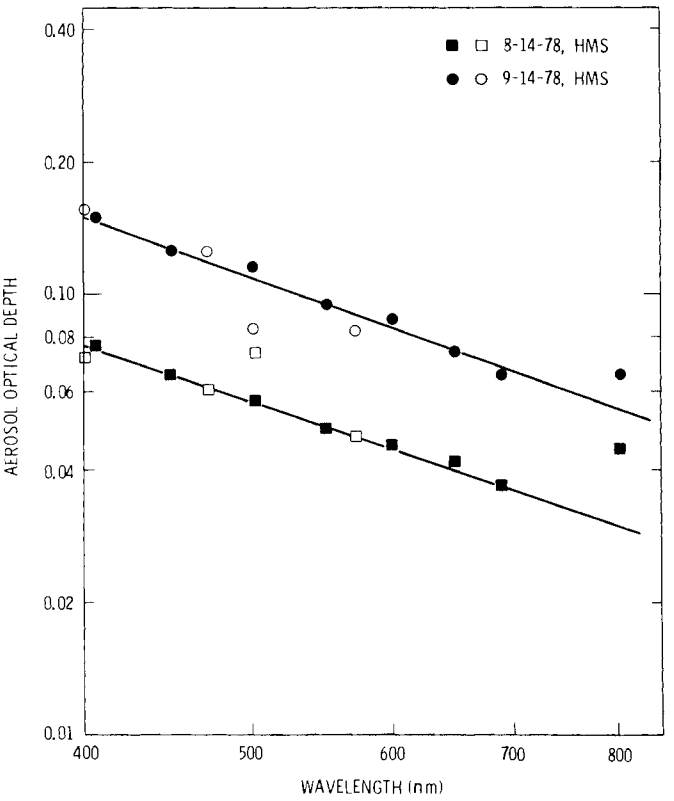

FIGURE 3.4. Comparison of Turbidities Derived from Observations Using the ACR and Sun-Photometer.

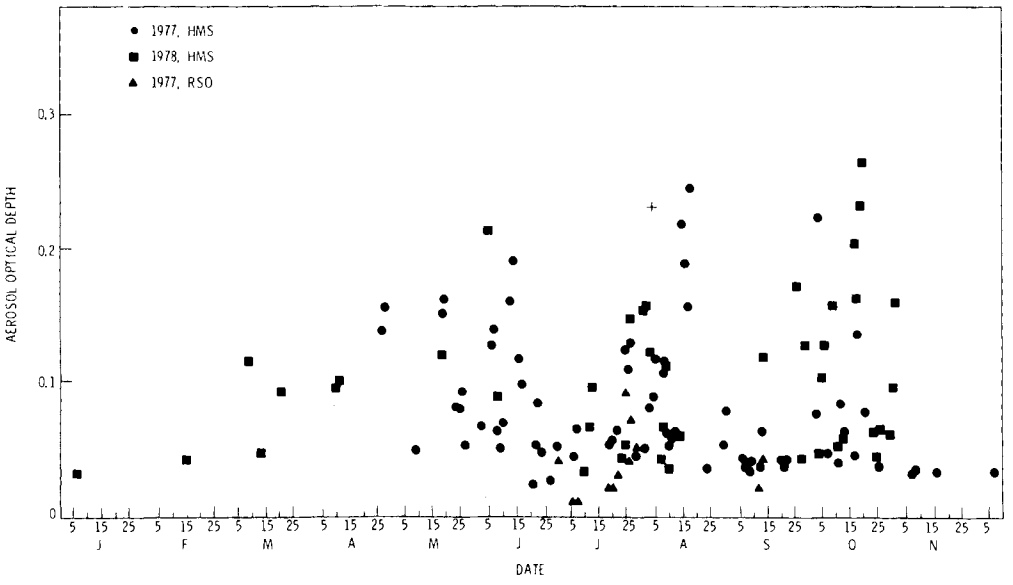

FIGURE 3.5. Turbidities at Hanford Meteorological Station During 1977 and 1978.

properties; i.e., $\alpha \sim 0$. Certain well-aged aerosols, which are nearly monodispersed, may have a wavelength exponent of $\alpha < 0$.

An example of changes in the turbidity wavelength dependence during a 2-wk period in August 1977 is shown in Figure 3.6. A hot, stagnant air mass covered eastern Washington for most of this period. Smoke accumulated in this air mass and accounted for much of the turbidity increase. The values of α changed from 0.9 to 1.5 at the beginning of this period to 1.6 to 1.9 at the time of highest turbidities. With passage of a cold front on 23 August, the turbidities associated with the clean, cool air mass dropped dramatically and α returned to a value of $\sim$1.4. Blowing dust occurred during part of the day on 4 August; in this case, the value of α was near 0.35.

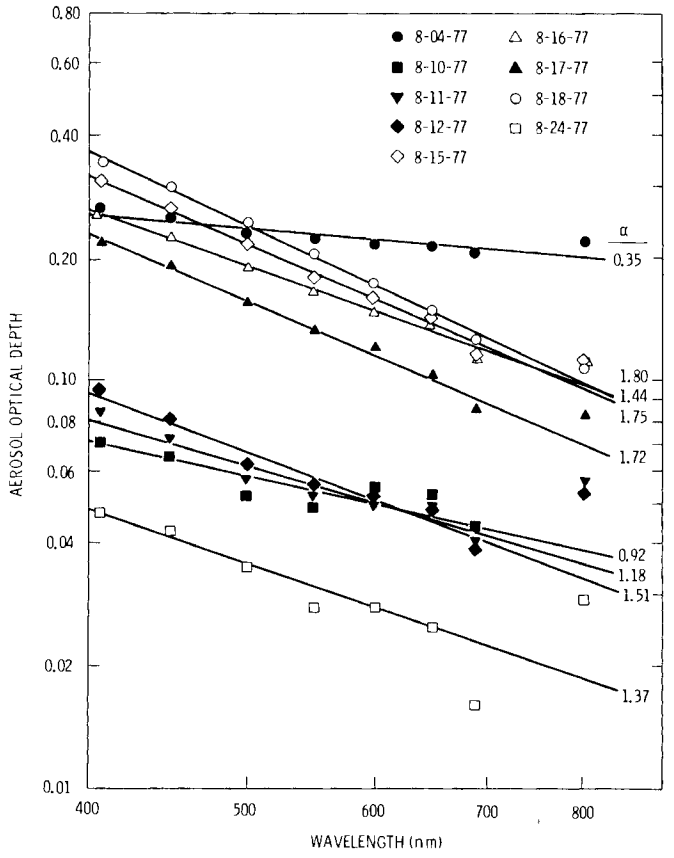

FIGURE 3.6. Changes in the Turbidity Wavelength Dependence During a Two-Week Period in August, 1977

The vertical distribution of the aerosol has an important effect on the magnitude of the redistribution of solar radiation. To examine this effect, nearly simultaneous turbidity and insolation observations at both HMS and RSO were made on several occasions. The results of some of these observations obtained with the same sunphotometer are compared in Figure 3.7. Additional comparisons obtained with the sunphotometer and ACR are shown in Figure 3.5. For very clean, clear days differences between RSO and HMS are very slight, while for hazy days the difference can be quite large, depending upon the depth of the mixed layer. Daily total insolation differences between RSO and HMS are of the order of only a few percentages for clean, clear days (mostly because of differences in molecular scattering between those two elevations), whereas differences of 10 to 20% occur for the hazy days. Insolation differences at HMS from day to day appear to be related to aerosol optical depth (turbidity) at λ = 600 nm by the approximate relation

$$Q = Q_{max} \cdot \exp(-a\,\tau) \qquad (1)$$

where Q_{max} is the maximum probably daily insolation, and a is a constant that has a value between 1 and 2.5 for cloud-free days.

In summary, the experiment showed that turbidity differences between RSO and HMS

can produce significant insolation differences between these two stations. It is important, however, to have independent methods of measuring turbidity and diffuse radiation in order to interpret the insolation measurements properly, expecially spectral diffuse-to-direct relationships. Future studies should incorporate radiative transfer modeling calculations to examine these relationships on a theoretical bases.

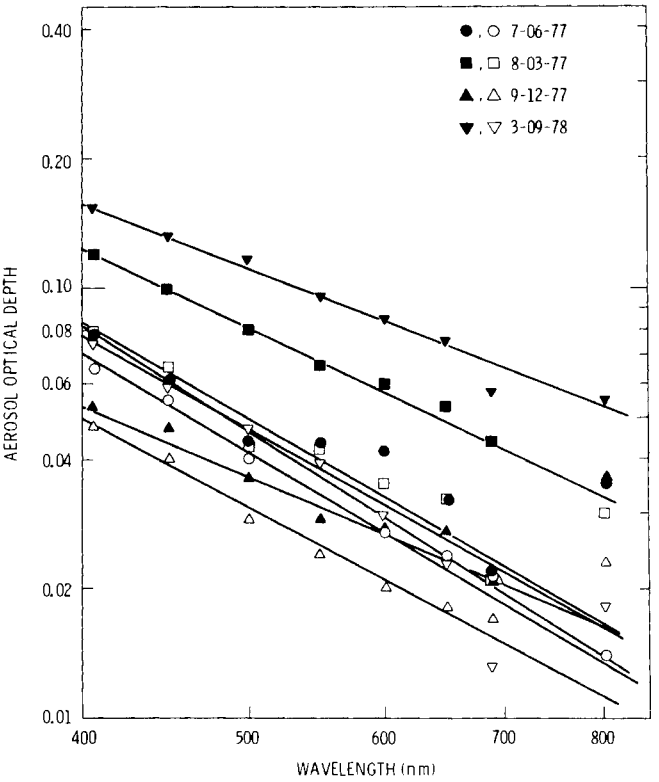

FIGURE 3.7. Results of Turbidity and Insolation Observations at Hanford Meteorological Station and Rattlesnake Observatory

DEVELOPMENT OF A DUAL-TRACER REAL-TIME PARTICLE DRY-DEPOSITION MEASUREMENT TECHNIQUE FOR SIMPLE AND COMPLEX TERRAIN

G. A. Sehmel, W. H. Hodgson and J. A. Campbell

Detectors are being developed and tested for measuring the airborne concentrations of lithium particles and SF_6 gas in real time. The airborne lithium detector sill be used for real-time measurements of both particle dry-deposition velocities and resuspension rates. Both the lithium and SF_6 detectors will be used for measuring dry deposition in field experiments.

A dual-tracer real-time experimental technique for measuring dry deposition particles and reactive gases over environmental surfaces is being developed (Sehmel 1978). This measuring technique uses depositing lithium-traced particles and nondeposition SF_6 gas and is based upon a concept of real-time measurement of both particles and gas at two or more distances downwind from a single dual-tracer release site. Deposition removal is calculated from the relatively more rapid downwind decrease of airborne tracer particle concentration referenced to the decrease of the tracer gas concentration.

Two approaches will be considered for measuring dry deposition in future field utilization of these detectors. The first approach, described by standard meteorological transport and diffusion equations, measures the dual-tracer airborne-concentration vertical profiles at two or more distances downwind from a source. The amount of particle deposition can then be inferred from the relative change in particle to SF_6 gas concentrations from the upwind to downwind sampling locations. This modeling approach includes measurements of both atmospheric stability and wind speed parameters.

In many practical applications, airborne pollutant concentrations are predicted using meteorological transport and diffusion models developed from data obtained over level terrain. Even after a long history of model development for level terrain, great uncertainty exists in model predictions (Crawford et al. 1978). Often, this level-terrain data base is used for predictions over complex terrain, which creates a problem of validation. Thus, the development of validated general models to adequately describe transport and diffusion over complex terrain may be in the distant future. Consequently, a more pragmatic approach for predicting the decrease of airborne concentrations at respirable heights may be a most useful method for several more years. In the second approach downwind changes of particle concentrations at respirable heights will be determined and compared to downwind changes of nondepositing SF_6 tracer gas. This more empirical approach may develop a useful data set of predicting downwind concentrations at respirable height.

Currently detectors are being tested, developed, and evaluated for measuring airborne nondepositing SF_6 gas and depositing lithium-traced particle concentrations in real time. Considerable difficulty with both detectors has been experienced.

For the lithium particle detector, the detector airflow system was modified to reduce particle deposition within the sampling line between the sample inlet and actual sensing volume. Initially, over 90% of the particles were lost in the entry lines, but with the present modifications, over 90% of the material is being sensed. Reproducibility and precision between detectors still present difficulties; however, the electronics are being modified to adjust detector sensitivity. At the present time, precision between detectors is within a factor or two, although increased precision and accuracy are desired.

The lithium particle detector was used in initial field experiments to determine if lithium-traced particle resuspension could be measured with the detector. Although detector response is still being improved, these initial field experiments showed that airborne concentrations from wind resuspension are measureable. Real-time measurements of airborne concentrations will permit evaluation in controlled field experiments of the often quoted weathering half-time for resuspension.

The prototype real-time SF_6 detector was based upon Lovelock's design (1975). Considerable difficulties have been experienced with both that design and the as-build prototype detector. Improvements have been made in the detector electronics; however, the prototype detector is not responding satisfactorily. Further improvement and testing of both the SF_6 real-time and lithium particle detectors are in process.

PARTICLE DRY-DEPOSITION EXPERIMENT USING AMBIENT AIRBORNE SOIL

G. A. Sehmel

Airborne solid concentrations were measured simultaneously at sampling towers upwind and 305-m downwind of a site. When the wind speed and wind direction were identical at each site, isokinetic air samplers on the sampling towers were automatically activated. The fraction of the airborne solid plume remaining after the 305-m fetch ranged from 0.53 to 1.07.

An airborne concentration profile is the variation of the concentration of airborne solids, $\mu g/m^3$, as a function of height. Concentration profiles depend upon many parameters, including deposition and resuspension; however, if all other parameters are constant, deposition will deplete the airborne concentration near the air-surface interface. When resuspension occurs, airborne concentrations will increase near the air-surface interface. For the total wind speed range (3 to 17 m/sec) investigated, particle dry deposition was expected to increase with increasing wind speed. However, if resuspension occurred, concentration profiles were confounded because of simultaneous deposition and resuspension. Resuspension was expected to increase more rapidly above wind speeds of 5 to 7 m/sec.

A field experiment (Sehmel 1978a) was completed to directly measure airborne concentration profiles along a 305-m fetch. The experimental design anticipated a uniform airborne plume that would decrease along the 305-m fetch. If mainly fallout radionuclides were measured, the airborne radionuclides plume would be uniform in the crosswind direction.

The experiment was conducted just within the southwest perimeter of the Hanford area near Horn Rapids dam. The vegetation cover mainly consisted of cheatgrass and sparse sagebrush. Between sampling towers, elevation changes were within ± 1.6 m. In the 233° direction, the surface elevation was nearly constant for 80 m, while the Yakima River was approximately 2.4 km upwind and 34 m below the upwind sampling tower.

Reasons for selecting this site were:

- Equipment security,
- A reasonably uniform fetch near an existing electrical power line and along the prevailing direction for maximum wind speeds,
- A minimal influence on analyzed samples from nuclide releases from the Hanford area.

Air sampling was conducted with both isokinetic air samplers (Sehmel 1978b) and particle cascade impactor-cowl systems (Sehmel 1978a). To date, only the isokinetic samples have been analyzed. For these isokinetic samplers, there is a rough separation between nonrespirable and respirable particles. Nonrespirable particles settled by gravity within the isokinetic sampler inlet. All particles not settling out were collected on a 20 x 25-cm glass fiber filter.

Isokinetic air samplers on upwind and downwind air-sampling towers were automatically turned on only if wind speed and direction were within a pre-selected range at both sampling towers. The meteorological sensing instrumentation was located at a 30-m elevation. A wind direction increment of 233 ± 45° at each tower was selected for automatically controlling the air samplers.

Concentrations profiles were determined by isokinetic sampling (1.1 m^3/sec) at seven heights (0.3, 1, 2, 3, 5, 9 and 20 m) and at three wind speed increments (3 to 5, 5 to 7 and 7 to 11 m/sec).

Samples were analyzed only for solids content. Nonrespirable particles were collected by brushing particles from each isokinetic inlet to determine the total inlet sample weight. For each 5- to 7-m/sec sample, brushed samples were subsequently sieved into size increments. Before weighing, filter-collected samples were equilibrated with laboratory air with relative humidity of less that 50%.

Airborne concentrations ($\mu g/m^3$) were calculated for solids collected on the filter as well as total solids collected on the isokinetic inlet plus filter. In addition, for the 3- to 5-m/sec wind speed increment isokinetic-inlet samples, airborne solids concentrations were calculated for three nonrespirable size ranges, i.e., 20 to 37, 37 to 63 and 63- to 105-μm dia. Only in these diameter ranges were there sufficient solids collected for calculating the concentration profile for the entire 0.3- to 20-m sampling height range. The accuracy for the concentrations is estimated to be within ± 20 $\mu g/m^3$.

Airborne solids concentrations for upwind and downwind towers are shown as a function of sampling height in Figure 3.8. Upwind and downwind concentration profiles are shown by solid lines and dashed lines, respectively. Airborne solids concentrations determined from only filter collection are shown in three sections on the left side of the figure. The upper section is for the 3- to 5-m/sec wind-speed increment, whereas the lower section is for the 7- to 11-m/sec wind-speed increment.

For the 3- to 5-m/sec wind-speed increment, airborne concentrations are nearly independent of either sampling height or upwind and downwind locations. These concentrations are approximately 100 $\mu g/m^3$. Airborne concentrations for the 5- to 7-m/sec wind-speed increment increased and were between 250 and 500 $\mu g/m^3$. However, at this intermediate wind speed, concentration profiles were nonuniform in relation to both sampling weight and sampling tower. For the highest wind-speed increment, 7 to 11 m/sec, significant differences occurred between upwind and downwind vertical concentration profiles. With only one exception, airborne concentrations decreased 70 to 120 $\mu g/m^3$ between sampling towers. This decrease suggests that deposition occurred between upwind and downwind sampling towers.

Airborne concentration profiles for total collection on both the isokinetic sampler inlet plus filter are shown on the right side of Figure 3.8. For the 3- to 5-m/sec wind-speed increment, total airborne solids concentrations ranged (except at the 20-m sampling height) from 110 to 230 $\mu g/m^3$. For the 5- to 7-m/sec wind-speed increment, total airborne concentrations ranged from 420 $\mu g/m^3$ to 1.2 $\mu g/m^3$. With only one exception at the 5-m sampling height, the total airborne concentration was greater

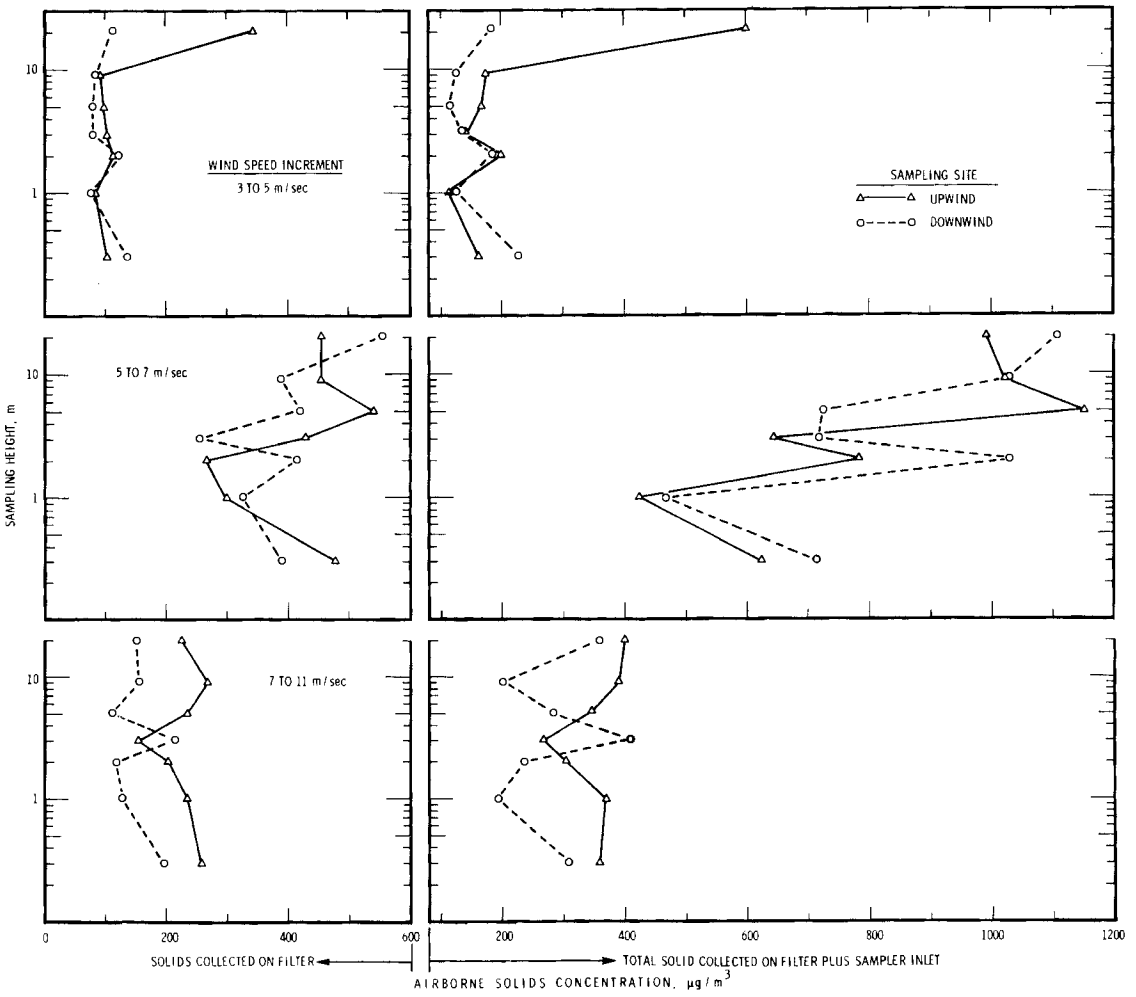

FIGURE 3.8. Airborne Solids Concentration During Identical Wind Speed Increments and Direction 233 + 45° at an Upwind Site and a Sampling Site 305 m Downwind Along 233°

downwind than upwind. This increased concentration suggests that either resuspension occurred along the 305-m fetch or the airborne plume was nonuniform in the crosswind direction. For the highest wind-speed increment, of 7 to 11 m/sec, the total airborne solids concentration (except at 3 m) ranged from 40 to 190 $\mu g/m^3$ less at the downwind sampling site. This decrease suggests that deposition occurred along the fetch.

As can be seen, the largest airborne concentrations were measured during the 5- to 7-m/sec wind-speed increment. Although prior results have nearly always indicated an increased airborne concentration with increasing wind speed, the maximum concentration at the intermediate wind speed might be attributed to an upwind source occurring during different meteorological conditions elsewhere than at the sampling towers.

For the 3- to 5-m/sec wind-speed increment, airborne solids concentrations are shown in Figure 3.9 for three nonrespirable particle diameter sizes. For all three wind-speed increments, concentration profiles were nearly identical, with some deviation, at both upwind and downwind sampling heights. Airborne solids concentrations are greatest for the 20- to 37-m size increment.

Nonuniform concentrations as a function of height are indicated by all of the vertical concentration profiles in Figure 3.9. Most profiles show an inconsistent trend between upwind and downwind sampling towers. In order to quantitate these trends for total airborne solids, the vertical concentration profiles were integrated; i.e., $\int \chi dz$ up to 20-m sampling height. To make the integration, an average wind-speed increment (5- to 7-m/sec) was assumed constant with height. In addition, airborne concentrations were assumed to be constant below 0.3 m.

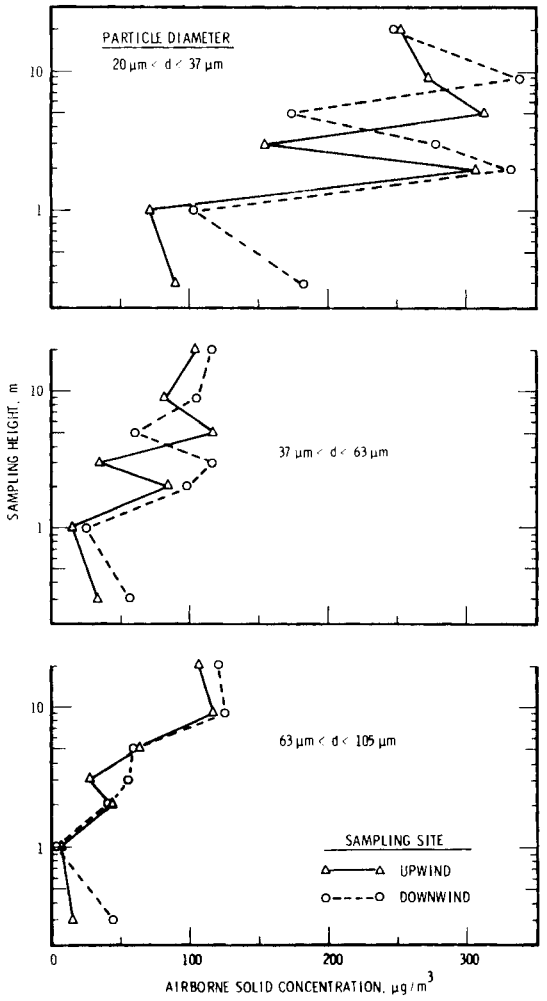

FIGURE 3.9. Airborne Solids Concentration for Nonrespirable Particle Diameter During Identical Wind Speed Increments and Direction 233 + 45° at an Upwind Site and a Sampling Site 305 m Downwind Along 233°

Changes in the total airborne solids χ, $\mu g/m^3$, within the lower 20 m are shown in Table 3.2. The ratio of the downwind integral to the upwind integral,

$$\text{Ratio} = \int_{\circ}^{20\ m} (\chi_{downwind}/\chi_{upwind})\ dz,$$

ranged from 0.53 to 1.07.

This experiment is continuing with the isokinetic air samplers. In addition, particle cascade impactor-cowl systems, still in operation from the first experiment, will be used to determine changes in airborne respirable concentrations below 1 m.

TABLE 3.2. Ratio of Airborne Solids Concentration Profiles Integrated to 20-m Height

Wind Speed m/sec	Ratio: Downwind/Upwind				
			Particle Diameter Range, μm		
	Filter	Filter + Inlet	20 to 37	37 to 63	63 to 105
3 to 5	0.60	0.53			
5 to 7	0.96	1.00	1.07	0.87	0.91
7 to 11	0.63	0.75			

4.0 References

REFERENCES

Alkezweeny, A. J., J. A. Young, R. N. Lee, K. M. Busness and J. M. Hales. 1977. "Transport and Transformation of Pollutant in the Lake Michigan Area." Paper presented at the Fourth Joint Conference on Sensing of Environmental Pollutants, November 10, 1977, New Orleans, Lousiana.

Associated Press. March 17, 1978. "AP News Release." Tri-City Herald.

Air Resources Laboratory. March 17, 1978. Air Trajectory Bulletin, NOAA, Silver Springs, Maryland.

Auer, A. H. Jr. 1977. "The Evolution of Visibility Deterioration and Aerosol Spectra in the St. Louis Urban Plume." J. Air Pollut. Control Assoc. 27:1188-1191.

Baes, C. F., H. E. Goeller, J. S. Olson and R. M. Rotty. 1976. The Global Carbon Dioxide Problem. ORNL-5194, Oak Ridge National Laboratory, Oak Ridge, Tennessee.

Barnes, S. L. 1967. "A Technique for Maximizing Details in Numerical Weather Map Analysis." J. Appl. Meteor. 3:396-409.

Calvert, J. G. 1976. "Hydrocarbon Involvement in Photochemical Smog Formation in Los Angeles Atmosphere." Environ. Sci. and Tech. 10:256-262.

Charlson, R. J., H. Horvath and R. F. Pueschel. 1967. "The Direct Measurement of Atmospheric Light-Scattering Coefficient for Studies of Visibility and Pollution." Atmos. Environ. 1:469-478.

Crawford, T. V. et al. 1978. "Atmospheric Transport of Radionuclides." In Proceedings of a Workshop on the Evaluation of Models Used for the Environmental Assessment of Radionuclide Releases, pp. 5-32. CONF-770901, available from National Technical Information Service, Springfield, Virginia.

Dana, M. T., J. M. Hales, W. G. N. Slinn and M. A. Wolf. 1973. Natural Precipitation Washout of Sulfur Compounds from Plumes. Environmental Protection Agency Report EPA-R3-73-047, Meteorology Laboratory National Environmental Research Center, Triangle Park, North Carolina 27711.

Davis, W. E., W. J. Eadie and D. C. Powell. 1978. "Technical Progress in the Alternate Fuel Cycle Program." In Pacific Northwest Laboratory Annual Report for 1977 to the DOE Assistant Secretary for Environment, Part 3, Atmospheric Sciences, pp. 2.21-2.24. PNL-2500 PT 3, Pacific Northwest Laboratory, Richland, Washington 99352.

Davis, W. E. and L. L. Wendell. 1976. "Some Effects of Isentropic Vertical Motion Simulation in a Regional Scale Quasi-Langrangian Air Quality Model." Paper presented at the Third Symposium on Atmospheric Turbulence Diffusion and Air Quality, October 19-22, 1976, Raleigh, North Carolina.

Desjardins, R. L. and E. R. Lemon. 1973. "Limitations of an Eddy Correlation Technique for the Determination of the Carbon Dioxide and Sensible Heat Fluxes." Boundary-Layer Meteorol. 5:475-488.

Droppo, J. G. 1977. "Proof Test of a System to Measure the Dry Deposition of Sulfur Aerosols in the Plume from a Northwest Fossil Fuel Power Plant." In Pacific Northwest Laboratory Annual Report for 1976 to the ERDA Assistant Administrator for Environmental Safety, Part 3, Atmospheric Sciences, BNWL-2100 PT 3, Pacific Northwest Laboratory, Richland, Washington 99352.

Droppo, J. G. and J. M. Hales. 1976. "Profile Methods of Dry Deposition Measurement." In Proceedings Atmospheric-Surface Exchange of Particulate and Gaseous Pollutants (1974), pp. 192-211. ERDA Symp. Series, CONF-740921. Richland, Washington 99352.

Dyer, A. J. 1974. "A Review of Flux-Profile Relationships." Boundary-Layer Meteorol. 1: 363-372.

Dyer, A. J. and B. B. Hicks. 1970. "Flux-Gradient Relationships in the Constant Flux Layer." Quart. J. Roy. Meteorol. Soc. 96: 715-721.

Endlich, R. M. 1967. "An Iterative Method for Altering the Kinematic Properties of Wind Fields." J. Appl. Met. 6:837-844.

Engelmann, R. J. 1970. "Precipitation Scavenging (1970)." Proceedings. AEC Symposium Ser. No. 22, Washington, DC.

Engelmann, R. J., and G. A. Sehmel, eds. 1976. Proceedings of the Atmospheric-Surface Exchange of Particulate and Gaseous Pollutants--1974 Symposium. Energy Research and Development Administration Symposium Series. CONF-740921, National Technical Information Service, Springfield, Virginia.

Environmental Protection Agency. November 3, 1977. "1977 Clean Air Act Amendments to Prevent Significant Deterioration." Federal Register 42(212):57459.

Environmental Protection Agency. September 1978. Guidelines for Air Quality Maintenance Planning and Analysis. Vol. 1 of Designation of Air Quality Maintenance Areas. EPA-450/4-74-001, Research Triangle Park, North Carolina.

Federal Radiation Council. July 1964. Background Material for the Development of Radiation Protection Standards. Staff Report No. 5.

Fox, T. D. and L. L. Wendell. 1977. "Precipitation Data Base Manipulation for Use in Regional Transport and Removal Models. "In Pacific Northwest Laboratory Annual Report for 1976 to the ERDA Assistant Administrator for Environment and Safety, Part 3, Atmospheric Sciences, pp. 191-192. BNWL-2100 PT 3, Pacific Northwest Laboratory, Richland, Washington 99352.

Galbally, I. E. 1971. "Ozone Profiles and Ozone Fluxes in the Atmospheric Surface Layer." Quart. J. Roy. Meteorol. Soc. 97: 18-29.

Garland, J. A. 1976. "Dry Deposition of SO_2 and Other Gases." In Proceedings of Atmospheric-Surface Exchange of Particulate and Gaseous Pollutants (1974), pp. 212-227. ERDA Symp. Series, CONF-740921, Richland, Washington, 99352.

Hales, J. M. Scavenging of Gaseous Tritium Compounds by Rain. BNWL-1959, Pacific Northwest Laboratory, Richland, Washington 99352.

Hales, J. M. 1972. "Fundamentals of the Theory of Gas Scavenging by Rain." Atmos. Environ. 6:635-659.

Hales, J. M. and S. L. Sutter. 1973. "Solubility of Sulfur Dioxide in Water at Low Concentrations." Atmos. Env. 7:997-1001.

Hales, J. M., M. A. Wolf and M. Terry Dana. 1973. "A Linear Model for Predicting the Washout of Pollutant Gases from Industrial Plumes." AI Ch EJ 19:242-247.

Hall, D. N. B. 1970. Kitt Peek National Observatory Contribution No. 564. Unpublished disertation, Harvard University.

Hicks, B. B. and M. L. Wesely. 1978. "Recent Results for Particle Deposition Obtained by the Eddy-Correlation Method." Paper presented at AI ChE 85th National Meeting, June 1978, Philadelphia, Pennsylvania.

Hidy, G. M. 1975. Design of the Sulfate Regional Experiment (SURE). EC-125, Electric Power Research Institute, Palo Alto, California.

Holzworth, G. C. 1964. "Estimates of Mean Maximum Mixing Depths in the Contiguous United States." Mon. Weather Review 92:235-242.

Horst, T. W. 1977. "A Surface Depletion Model for Deposition from a Gaussian Plume." Atmos. Environ. 11:41-46.

Horst, T. W. 1978a. "Lagrangian Similarity Modeling of Vertical Diffusion from a Surface Source." In Pacific Northwest Laboratory Annual Report for 1977 to the DOE Assistant Secretary for Environment, Part 3, Atmospheric Sciences, pp. 2.16-2.17. PNL-2500 PT 3, Pacific Northwest Laboratory, Richland, Washington 99352.

Horst, T. W. 1978b. "The Dependence of Deposition Velocity on Distance Downwind of a Point Source of Atmospheric Contamination." In Pacific Northwest Laboratory Annual Report for 1977 to the DOE Assistant Secretary for Environment, Part 3, Atmospheric Sciences, p. 1.29. PNL-2500 PT 3, Pacific Northwest Laboratory, Richland, Washington 99352.

Huang, C. H., and E. C. Nickerson. 1972. "Numerical Simulation of Wind, Temperature, Shear Stress, and Turbulent Energy over the Nonhomogeneous Terrain." TR-CED 71-62Ch, Fluid Dynamics and Diffusion Laboratory, Colorado State University, Fort Collins, Colorado.

Huang, C. H., and E. C. Nickerson. 1974. "Stratified Flow over Nonuniform Surface Conditions: Mixing Length Model." Boundary-Layer Meteorology, 5:395-417.

Johnson, W. B., D. E. Wolf and R. L. Mancuso. 1978. "Long-Term Regional Patterns and Transfrontier Enchanges of Airborne Sulfur Pollution in Europe." Atmos. Env. 12:511-528.

Keeling, C. D., R. B. Bacastow, A. E. Bainbridge, C. A. Ekdahl, R. R. Guenther, L. S. Waterman and J. F. S. Chin. 1976. Tellus 28:538.

Kempthorne and R. R. Allmaraz. 1965. "Propagation of Errors." In Methods of Soil Analysis, Pt. 1, Physical and Mineralogical Properties Including Statistics of Measurement and Sampling," ed. C. A. Black, p. 18. American Society of Agronomy, Madison, Wisconsin.

Kopczynski, S. L., W. A. Lonneman, T. Winfield and R. Seila. 1975. "Gaseous Pollutants in St. Louis and Other Cities." J. Air Pollut. Control Assoc. 25:251-255.

Laulainen, N. S. 1978. "Turbidity Variations at Hanford Since July 1974." In Pacific Northwest Laboratory Annual Report for 1977 to the DOE Assistant Secretary for Environment, Part 3, Atmospheric Sciences, pp. 3.1-3.3. PNL-2500 PT 3, Pacific Northwest Laboratory, Richland, Washington 99352.

Lazrus, A., E. Lorange and J. P. Lodge, Jr. 1978. "New Automatic Microanalysis for Total Inorganic Fixed Nitrogen and for Sulfate Ion in Water." Adv. Chem. Ser. 73: 164-171.

Liu, C. and W. Goodin. 1976. An Iterative Algorithm for Objective Wind Field Analysis." Monthly Weather Rev. 104:784-792.

Lovelock, J. E. 1975. "Solute Switching and Detection by Synchronous Demodulation in Gas Chromatography." J. Chrom. 112:29-36.

Ludwick, J. D. 1964. "Investigation of the Nature of ^{131}I in the Atmosphere." In Hanford Radiological Sciences Research and Development Annual Report for 1963, p. 3.58. HW-81746 (AEC), available from National Technical Information Center, Springfield, Virginia.

MacCracken, M. C. 1978. "Simulation of Regional Precipication Chemistry." Paper presented at EPRI Workshop on Acid Precipitation, August 22-25, 1978, Alta, Utah.

MAP3S Precipitation Chemistry Network Participants. 1977. The MAP3S Precipitation Chemistry Network: First Periodic Summary Report (September 1976-June 1977). PNL-2402, Pacific Northwest Laboratory, Richland, Washington 99352.

Middleton, W. E. 1968. Vision Through the Atmosphere. University of Toronto Press, Toronto, Canada.

Mohler, O. C., A. K. Pierce, R. R. McMeth and L. Goldberg. 1950. Photometric Atoms of the Near-IR Solar Spectrum - λ8468-λ25242. University of Michigan Press, Ann Arbor, Michigan.

National Academy of Sciences. 1977. Ammonia. Assembly of Life Sciences, Washington, DC.

Powell, D. C., D. J. McNaughton, L. L. Wendell and R. L. Drake. 1978. Available Trajectory Model for Multistate Assessment of Air Pollution from Sulfur Compounds. PNL-2734, Pacific Northwest Laboratory, Richland, Washington 99352.

Saltzmann, B. E. 1954. "Colorimetric Microdetermination of Nitrogen Dioxide in the Atmosphere." Anal. Chem. 26:1949-1955.

Sasaki, Y. 1958. "An Objective Analysis Based on the Variational Method." J. Meteor. Soc., Japan 36:77-88.

Scott, B. C. 1978. "Parameterization of Sulfate Removal by Precipitation." J. Appl. Meteor. 17:1375-1389.

Scott, W. D. and P. V. Hobbs. 1967. "The Formation of Sulfate in Water Droplets." J. Atmos. Sci. 24:54-57.

Sehmel, G. A. 1977. "Offsite Plutonium Resuspension Near Hanford." In Pacific Northwest Laboratory Annual Report for the DOE Assistant Secretary for the Environment, Part 3, Atmospheric Sciences, pp. 2.4-2.5. PNL-2500 PT 3, Pacific Northwest Laboratory, Richland, Washington 99352.

Sehmel, G. A. 1978a. "Dual Tracer Deposition Experiment." In Pacific Northwest Laboratory Annual Report for 1977 to the DOE Assistant Secretary for the Environment, Part 3, Atmospheric Sciences, PNL-2500 PT 3, Pacific Northwest Laboratory, Richland, Washington 99352.

Sehmel, G. A. 1978b. "Isokinetic Air Sampler." In Pacific Northwest Laboratory Annual Report for 1977 to the DOE Assistant Secretary for the Environment, Part 3, Atmospheric Sciences, pp. 1.32-1.34. PNL-2500 PT 3, Pacific Northwest Laboratory, Richland, Washington 99352.

Sehmel, G. A. 1978c. "Field Particle Deposition Measurement by a Mass Balance Using Ambient Radioactive Particles and Airborne Soil." In Pacific Northwest Laboratory Annual Report for 1977 to the DOE Assistant Secretary for the Environment, Part 3, Atmospheric Sciences, pp. 213-215. PNL-2500 PT 3, Pacific Northwest Laboratory, Richland, Washington 99352.

Sehmel, G. A. 1978d. "Airborne Plutonium-239 Transport Measured from the 125-m Hanford Meteorological Tower." In Pacific Northwest Laboratory Annual Report for 1977 to the DOE Assistant Secretary for the Environment, Atmospheric Sciences, pp. 2.9-2.11. PNL-2500 PT 3, Pacific Northwest Laboratory, Richland, Washington 99352.

Sehmel, G. A. and W. H. Hodgson. 1978. A Model for Predicting Dry Deposition of Particles and Gases to Environmental Surfaces. PNL-SA-6721, Pacific Northwest Laboratory, Richland, Washington 99352.

Sehmel, G. A. and F. D. Lloyd. 1978. "Wind Resuspension Experiments." In Pacific Northwest Laboratory Annual Report for 1977 to the DOE Assistant Secretary for the Environment, Part 3, Atmospheric Sciences, pp. 2.1-2.3. PNL-2500 PT 3, Pacific Northwest Laboratory, Richland, Washington 99352.

Shendriker, A. D. and J. P. Lodge, Jr. 1975. "Microdetermination of Ammonia by the Ring Oven Technique and its Application to Air Pollution Studies." Atmos. Envir. 9:431-435.

Sherman, C. 1978. "A Mass-Consistent Model for Wind Fields Over Complex Terrain." J. Appl. Meteor. 17:312-319.

Slade, D. H. 1968. Meteorology and Atomic Energy--1968. TID-24190, available from National Technical Information Service, Springfield, Virginia.

Slinn, W. G. N. 1975. "In-Cloud Scavenging of Aerosol Particles." In Pacific Northwest Laboratory Annual Report for 1974 to the USAEC Division of Biomedical and Environmental Research, Part 3, Atmospheric Sciences, pp. 114-118. BNWL-1950 PT 3, Pacific Northwest Laboratory, Richland, Washington 99352.

Slinn, W. G. N. 1977. "The Redistribution of a Gas Plume Caused by Reversible Washout." Atmos. Environ. 8:233-239.

Slinn, W. G. N. March-April, 1978. "Parameterization for Resuspension and for Wet and Dry Deposition of Particles and Gases for Use in Radiation Dose Calculations." Nuclear Safety 19(2):205-219.

Thomas, C. S. and R. W. Perkins. 1977. "Transuranic Elements in the Atmosphere. BNWL-1881, Pacific Northwest Laboratory, Richland, Washington 99352.

Tomas, C. W., J. K. Soldat, W. B. Silker and R. W. Perkins. 1976. Radioactive Fallout from Chinese Nuclear Weapons Test, September 26, 1976. BNWL-2164, Pacific Northwest Laboratory, Richland, Washington 99352.

Tong, E. Y. and R. B. Batchelder. 1978. Aerometric Data Compilation and Analysis for Regional Sulfate Modeling. Teknekron, Inc., Waltham, Massachusetts.

U.S. Energy and Research Administration. March 1977. "Standards for Radiation Protection." In ERDA Manual of Operations, Chapter 0524.

Wendell, L. L. and C. E. Hane. 1976. "Preparation of Hourly Maps of Gridded Precipitation Data for Use in Precipitation Scavenging Calculations." In Pacific Northwest Laboratory Annual Report for 1975 to the USERDA Division of Biomedical and Environmental Research, Part 3, Atmospheric Sciences, pp. 229-232. BNWL-2000 PT 3, Pacific Northwest Laboratory, Richland, Washington 99352.

Wendell, L. L. and D. C. Powell. 1976. "An Examination of the Effects of Real-Time versus Time-Averaged Precipitation Data on SO_2 and SO_4 Removal in the Regional Assessment Model." In Pacific Northwest Laboratory Annual Report for 1975 to the USERDA Division of Biomedical and Environmental Research, Part 3, Atmospheric Sciences, pp. 224-229. BNWL-2000 PT 3, Pacific Northwest Laboratory, Richland, Washington 99352.

Wendell, L. L., D. C. Powell and R. L. Drake. 1976. "A Regional Scale Model for Computing Deposition and Ground-Level Air Concentrations of SO_2 and Sulfates from Elevated and Ground Sources." In Proceedings of the Third Symposium on Turbulence, Diffusion and Air Quality, pp. 318-324. American Meteorological Society, Boston, Massachusetts.

Wendell, L. L., D. C. Powell and D. J. McNaughton. 1977. "A Multi-Source Comparison of Real-Time versus Time-Averaged Precipitation Data on SO_2 and Sulfate Particulate Removal in a Regional Assessment Model." Presented at the Joint Conference on Applications of Air Pollution Meteorology, November 20-December 2, 1977, Salt Lake City, Utah.

Wesely, M. L., B. B. Hicks, W. P. Dannevich, S. Frisella and R. B. Husar. 1977. "An Eddy-Correlation Measurement of Particulate Deposition from the Atmosphere." Atmos. Environ. 11:561-563.

Wesely, M. L. and B. B. Hicks. 1977. "Some Factors that Affect the Deposition Rates of Sulfur Dioxide and Similar Gases on Vegetation." J. Air Poll. Control Assoc. 27:1110-1116.

Whitby, R. A. and E. R. Altwicker. 1976. "Acetylene in the Atmosphere: Sources, Representative Ambient Concentrations and Ratios to Other Hydrocarbons." Atmos. Environ. 12:1289-1296.

Publications and Presentations

PUBLICATIONS AND PRESENTATIONS

PUBLICATIONS

Alkezweeny, A. J., "Measurement of Aerosol Particles and Trace Gases in METROMEX." J. Appl. Meteor. 17(5):609-614, May 1978.

Dana, M. T., N. A. Wogman and M. A. Wolf, "Rain Scavenging of Tritiated Water (HTO): A Field Experiment and Theoretical Considerations." Atmos. Environment, 12(6/7): 1523-1529, 1978.

Doran, J. C., "Limitations on the Determination of Deposition Velocity." Boundary Layer Meteor., 10:365-371, 1977.

Doran, J. C. and T. W. Horst, "Long-Range Travel of Airborne Material Subjected to Dry Deposition" and a "Surface Depletion Model for Deposition from a Gaussian Plume." Atmos. Environment, 11(12):1246-1247, 1977.

Doran, J. C., T. W. Horst and P. W. Nickola, "Variations in Measured Values of Lateral Diffusion Parameters." J. Appl. Meteor, 17(6):825-831, June 1978.

Doran, J. C., T. W. Horst and P. W. Nickola, "Experimental Observations of the Dependence of Lateral and Vertical Dispersion Characteristics on Source Height." Atmos. Environment, 12:2259-2263, 1978.

Hales, J. M., "Wet Removal of Sulfur Compounds from the Atmosphere." Atmos. Environment, 12(1-3):389-400, 1978.

Hane, Carl E., "The Application of a 2-D Convective Cloud Model to Waste Heat Release from Proposed Nuclear Energy Centers." Atmos. Environment, 12(9):1839-1848, 1978.

Hane, Carl E., "Scavenging of Urban Pollutants by Thunderstorm Rainfall: Numerical Experimentation." J. Appl. Meteor, 17(5): 699-710, May 1978.

Horst, T. W., "Comments on a General Gaussian Diffusion-Deposition Model for Elevated Point Sources." J. Applied Meteor., 17(3):415-416, March 1978.

Horst, T. W., "Estimation of Air Concentrations Due to the Suspension of Surface Contamination." Atmos. Environment, 12(4): 797-802, 1978.

Laulainen, N. S., A. J. Alkezweeny and J. M. Thorp, "Simultaneous Aerosol Size Distribution and Turbidity Measurements over St. Louis during METROMEX 1975." J. Appl. Meteor., 17(5):615-626, May 1978.

Miller, D. F., A. J. Alkezweeny, J. M. Hales, R. N. Lee, "Ozone Formation Related to Power Plant Emissions." Science, 202(4373):1186-1189, December 15, 1978.

Ramsdell, J. V., "Wind Shear Fluctuations Downwind of Large Surface Roughness Elements." J. Appl. Meteor., 17(4):436-443, April 1978.

Ramsdell, J. V., The Impact of a Hanford Nuclear Energy Center on Cloudiness and Insolation. PNL-2452, Pacific Northwest Laboratory, Richland, WA, July 1978.

Ramsdell, J. V. and D. I. Diebel, Meteorological Evaluation of Multiple Reactor Contamination Probabilities for a Hanford Nuclear Energy Center. PNL-2352, Pacific Northwest Laboratory, Richland, WA, March 1978.

Sandusky, W. F., "Diffusion Climatology at Selected Nuclear Facility Sites." Nuclear Safety, 19(3):366-367, May-June 1978.

Scott, B. C., "Parameterization of Sulfate Removal by Precipitation." J. Appl. Meteor, 17:1375-1389, 1978.

Scott, B. C., "The Impact of the Proposed Atikohan Electric Generating Facility on the Wet Deposition of Sulfur in the Boundary Water Canal Area." PNL-SA-7021, Workshop Report on Deposition, Madison, WI, April 11, 1978.

Sehmel, G. A., Panel Member, Proceedings of a Workshop on the Evaluation of Models Used for the Environmental Assessment of Radionuclide Releases. CONF-779 901, available from National Technical Information Service, Springfield, VA. 1978.

Sehmel, G. A., Panel Member, Ecologist/ Meteorologist Workshop - 1976. CONF-7608116, available from National Technical Information Service, Springfield, VA. February 1978.

Sehmel, G. A., "Plutonium Concentrations in Airborne Soil at Rocky Flats and Hanford Determined During Resuspension Experiments." Airborne Radioactivity, (Selected papers from the 1977 ANS Winter Meeting) pp. 81-102, 1978.

Simpson, C. L. and Staff, Pacific Northwest Laboratory Annual Report for 1977 to the DOE Assistant Administrator for Environment, Part 3, Atmospheric Sciences. PNL-2500, PT 3, Pacific Northwest Laboratory, Richland, WA, February 1978.

Slinn, W. G. N., et al., "Some Aspects of the Transfer of Atmospheric Trace Constituents Past the Air-Sea Interface." Atmos. Environment, 12(12):2055-2087, 1978.

Woolridge G. L. and M. M. Orgill, "Airflow, Diffusion and Momentum Flux Patterns in a High Mountain Valley." Atmos. Environment, 12(4):803-807, 1978.

PRESENTATIONS

Bander, T. J., D. S. Renne and W. F. Sandusky, "An Analysis of Tritium Releases to the Atmosphere by a Controlled Thermonuclear Reactor." PNL-SA-6879, presented at the Symposium on the Behavior of Tritium in the Environment, IAEA, San Francisco, CA, October 16-20, 1978.

Dana, M. T., "Rain Chemistry in the Vicinity of the Centralia Steam-Electric Plant." PNL-SA-7113, presented at the Workshop on Acid Precipitation in the West, Corvallis, OR, August 10, 1978.

Dana, M.T., "Seasonal Trends of SO_2, $SO_4^=$, NH_4^+ and NO_3 in Precipitation: MAP3S Precipitation Chemistry Network." PNL-SA-6932, presented at the MAP3S Precipitation Chemistry Network Meeting, Ithaca, NY, May 11-12, 1978.

Droppo, J. G., "Dry Removal of Air Pollutants by Vegetation Canopies." PNL-SA-5973, presented at the WMO International Symposium on Forest Meteorology, Ottawa, Ontario, Canada, August 21-25, 1978.

Droppo, J. G. "Ozone Field Studies Adjacent to a HVdc Test Line." PNL-SA-7046, presented at 18th Hanford Biology Symposium, Richland, WA, October 16-18, 1978.

Droppo, J. G.,"Revised Method of Computing Energy Balances over Vegetation Canopies." PNL-SA-6205, presented at the Fifth Conference on Fire and Forest Meteorology, American Meteorological Society, Atlantic City, NJ, March 14-16, 1978.

Droppo, J. G. and J. C. Doran, "Dry Deposition of Atmospheric Ozone." PNL-SA-6887, presented at the 59th AAAS Annual Meeting, Pacific Division, American Meteorological Society, Seattle, WA, June 13-17, 1978.

Hadlock, R. K., "Acoustic Sounding at Hanford." PNL-SA-6644, presented at the 4th Symposium on Meteorological Observations and Instrumentation, American Meteorological Society, Denver, CO, April 10-14, 1978.

Laulainen, N. S., E. W. Kleckner and J. J. Michalsky, "Differential Insolation and Turbidity Measurements." PNL-SA-6680, presented at the 3rd Conference on Atmospheric Radiation, American Meteorological Society, Darris, CA, June 28, 1978.

Laulainen, N. S., "Experiment Design for a Case Study of Drift from a Mechanical Draft Cooling Tower." PNL-SA-6679, presented at the 1978 Symposium on Cooling Tower Environment, Baltimore, MD, May 2-4, 1978.

Pennell, W. T. and M. A. LeMone, "An Intercomparison of Turbulence Measurements from Aircraft." PNL-SA-6497, presented at the MAP3S Precipitation Chemistry Network Meeting, Ithaca, NY, May 11-12, 1978.

Renne, D. S., "A Comparison of Atmospheric Stability Between a VAlley and Maountain Site." PNL-SA-6578, presented at the Fifth Conference on Fire and Forest Meteorology, Atlantic City, NJ, March 14-16, 1978.

Rothert, J. E., "Use of Ion Chromotography for Trace Analysis of MAP3S Precipitation Samples." PNL-SA-7087, presented at the 22nd Conference on Analytical Chemistry, Gatlinburg, TN, October 10-12, March 14-16, 1978.

Sehmel, G. A., "Airborne ^{239}Pu and ^{241}Am Concentrations Measured from the 125-M Hanford Meteorological Tower." PNL-SA-6771, presented at the Nevada Applied Ecology Plutonium Information Conference, San Diego, CA, February 28-March 2, 1978.

Sehmel, G. A. and W. H. Hodgson, "A Model for Prediction Dry Deposition of Particles and Gasses to Environmental Surfaces." PNL-SA-6721, presented at the 85th AICHE National Meeting, Philadelphia, PA, June 4-8, 1978.

Author Index

AUTHOR INDEX

Organization Charts Distribution

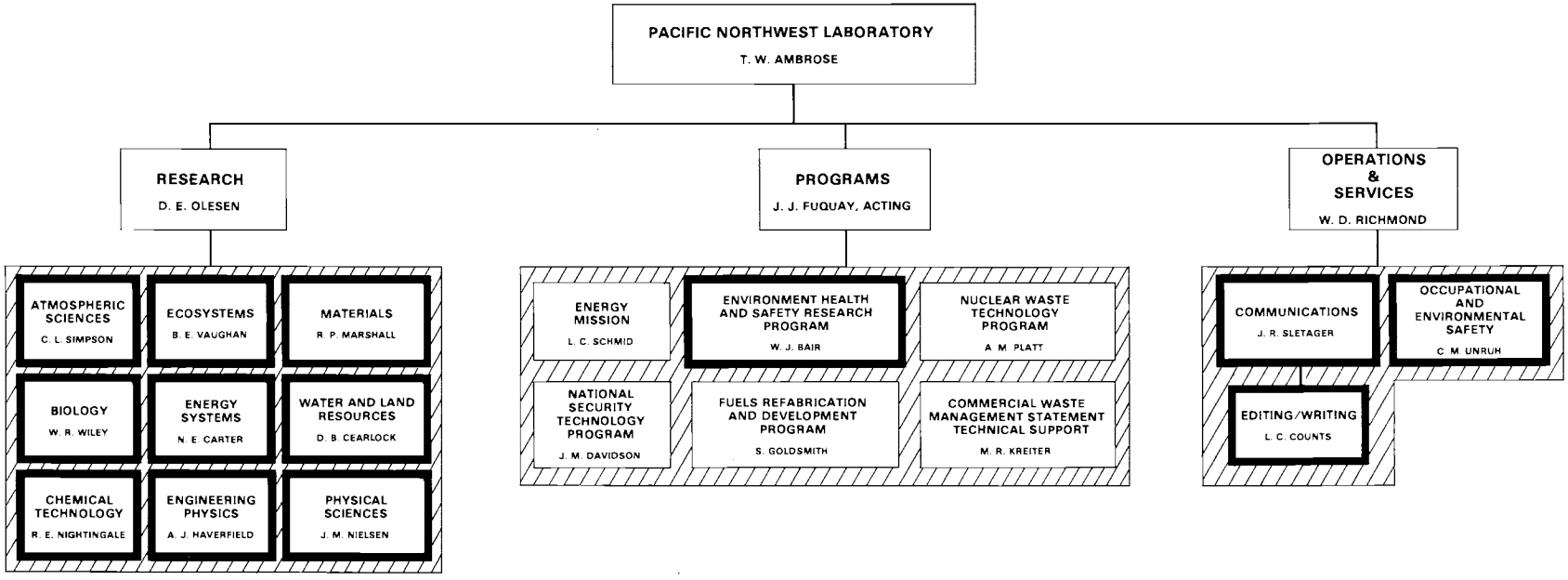

NOTE:

HEAVY BLACK LINES DENOTE ORGANIZATIONAL COMPONENTS IN WHICH ENVIRONMENT, HEALTH AND SAFETY RESEARCH IS BEING CONDUCTED.

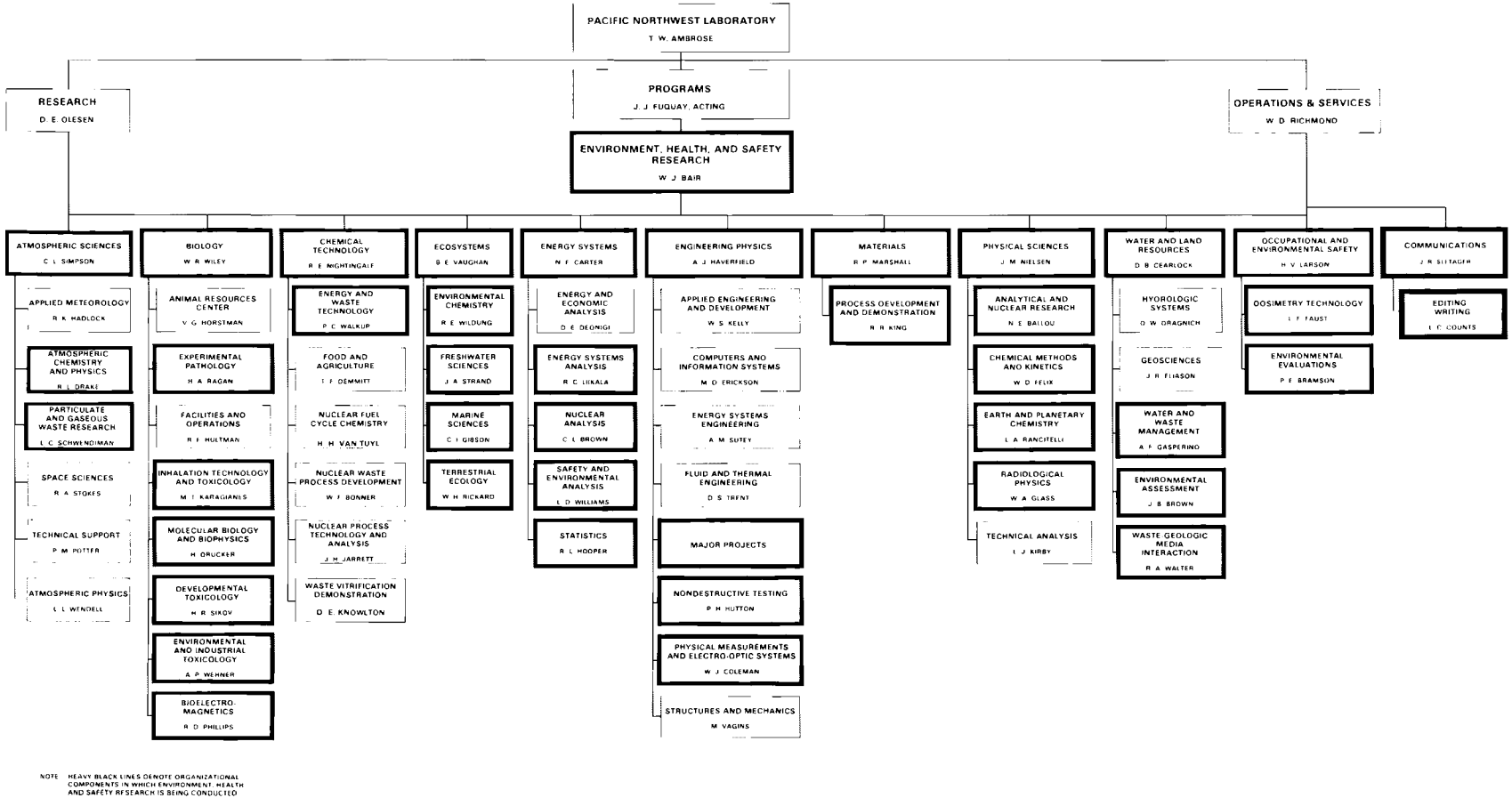

NOTE HEAVY BLACK LINES DENOTE ORGANIZATIONAL COMPONENTS IN WHICH ENVIRONMENT, HEALTH AND SAFETY RESEARCH IS BEING CONDUCTED

DISTRIBUTION

No. of Copies

OFFSITE

A. A. Churm, Director
Patent Division
DOE--Chicago Operations Office
9800 S. Cass Avenue
Argonne, IL 60439

Ralph E. Austin
Biomed/Environ.
Department of Energy
Federal/629A
Richland, WA 99352

W. R. Albers
Department of Energy
Office of Operational and Environmental Research
Washington, DC 20545

D. S. Ballantine
Department of Energy
Office of Biomedical and Environmental Research
Washington, DC 20545

R. W. Barber
Department of Energy
Office of Reactor Safety Research Coordination
Washington, DC 20545

N. F. Barr
Department of Energy
Division of Regional Assessments
Washington, DC 20545

R. W. Beadle
Department of Energy
Office of Biomedical and Environmental Research
Washington, DC 20545

M. A. Bell
Department of Energy
Office of Biomedical and Environmental Research
Washington, DC 20545

J. W. Benson
Department of Energy
Office of the Asst. Sec. for Environment
Washington, DC 20545

L. C. Brazley
Department of Energy
Washington, DC 20545

No. of Copies

J. Bresee
Department of Energy
Office of the Asst. Sec. for Energy Technology
Washington, DC 20545

W. A. Brobst
Department of Energy
Office of Environmental Control Technology
Washington, DC 20545

W. W. Burr, Jr.
Department of Energy
Office of Biomedical and Environmental Research
Washington, DC 20545

C. E. Carter
Department of Energy
Office of Biomedical and Environmental Research
Washington, DC 20545

R. A. Catlin
Department of Energy
Office of the Asst. Sec. for Environment
Washington, DC 20545

R. J. Catlin
Department of Energy
Office of NEPA Oversight
Washington, DC 20545

J. A. Coleman
Department of Energy
Office of Technology Impacts
Washington, DC 20545

R. A. Conaway
Department of Energy
Office of Program Coordination
Washington, DC 20545

R. C. Clusen
Department of Energy
Office of the Asst. Sec. for Environment
Washington, DC 20545

D. K. Craig
Department of Energy
Office of the Asst. Sec. for Environment
Washington, DC 20545

No. of Copies

R. L. Darneal
Department of Energy
Office of Biomedical and Environmental Research
Washington, DC 20545

L. J. Deal
Department of Energy
Office of Operational and Environmental Safety
Washington, DC 20545

J. M. Duetch
Department of Energy
Office of the Asst. Sec. for Energy Research
Washington, DC 20545

G. P. Dix
Department of Energy
Office of Operational and Environmental Safety
Washington, DC 20545

T. J. Dobry
Department of Energy
Office of the Asst. Sec. for Energy Technology
Washington, DC 20545

C. W. Edington
Department of Energy
Office of Biomedical and Environmental Research
Washington, DC 20545

G. C. Facer
Department of Energy
Office of Asst. Sec for Defense Programs
Washington, DC 20545

A. S. Fege
Department of Energy
Office of Biomedical and Environmental Research
Washington, DC 20545

C. W. Fisher
Department of Energy
Office of Asst. Sec. for Energy Administration
Washington, DC 20545

T. J. Gross
Department of Energy
Office of Biomedical and Environmental Research
Washington, DC 20545

No. of Copies

R. E. Grossman
Department of Energy
Office of NEPA Oversight
Washington, DC 20545

G. Hagey
Department of Energy
Office of Biomedical and Environmental Research
Washington, DC 20545

J. H. Harley
Environmental Monitoring Laboratory
376 Hudson Street
New York, NY 10014

J. Hock
Department of Energy
Office of the Asst. Sec. for Environment
Washington, DC 20545

H. H. Hollister
Department of Energy
Office of Biomedical and Environmental Research
Washington, DC 20545

P. W. House
Department of Energy
Office of Technology Impacts
Washington, DC 20545

J. S. Kane
Department of Energy
Office of Asst. Sec. for Energy Research
Washington, DC 20545

F. A. Koomanoff
Department of Energy
Office of the Asst. Sec. for Energy Technology
Washington, DC 20545

C. Kuhlman
Department of Energy
Office of the Asst. Sec. for Energy Technology
Washington, DC 20545

R. L. Leith
Department of Energy
Office of Program Coordination
Washington, DC 20545

F. A. Leone
Department of Energy
Office of NEPA Oversight
Washington, DC 20545

No. of Copies

3 W. J. Little, Jr.
Department of Energy
Office of Planning Coordination
Washington, DC 20545

3 J. L. Liverman
Acting Assistant Secretary
Department of Energy
Office of the Asst. Sec. for Environment
Washington, DC 20545

K. E. Lockridge
Department of Energy
Office of Planning Coordination
Washington, DC 20545

E. K. Loop
Department of Energy
Office of Biomedical and Environmental Research
Washington, DC 20545

R. Loose
Department of Energy
Office of the Asst. Sec. for Energy Technology
Washington, DC 20545

W. E. Lotz
Department of Energy
Office of the Asst. Sec. for Energy Technology
Washington, DC 20545

J. N. Maddox
Department of Energy
Office of Program Coordination
Washington, DC 20545

J. R. Maher
Department of Energy
Office of Biomedical and Environmental Research
Washington, DC 20545

D. Mayhew
Department of Energy
Office of the Asst. Sec. for Environment
Washington, DC 20545

W. J. McCool
Department of Energy
Office of Operational and Environmental Safety
Washington, DC 20545

No. of Copies

B. F. McCully
Department of Energy
Office of Program Coordination
Washington, DC 20545

W. A. Mills
Director
Division of Criteria and Standards
Office of Radiation Program
Environmental Protection Agency
Rockville, MD 20852

M. L. Minthorn, Jr.
Department of Energy
Office of Biomedical and Environmental Research
Washington, DC 20545

D. Monti
Department of Energy
Division of Technology Overview
Washington, DC 20545

H. Moses
Department of Energy
Office of Biomedical and Environmental Research
Washington, DC 20545

W. E. Mott
Department of Energy
Office of Environmental Control Technology
Washington, DC 20545

M. B. Neuworth
Department of Energy
Office of the Asst. Sec. for Energy Technology
Washington, DC 20545

D. E. Patterson
Department of Energy
Office of Biomedical and Environmental Research
Washington, DC 20545

3 W. H. Pennington
Department of Energy
Office of NEPA Oversight
Washington, DC 20545

R. W. Ramsey, Jr.
Department of Energy
Office of Environmental Control Technology
Washington, DC 20545

No. of Copies

D. M. Ross
Department of Energy
Office of Operational and Environmental Safety
Washington, DC 20545

A. A. Schoen
Department of Energy
Office of Biomedical and Environmental Research
Washington, DC 20545

D. E. Shaw
Department of Energy
Office of Management Coordination
Washington, DC 20545

G. Shepherd
Department of Energy
Office of Biomedical and Environmental Research
Washington, DC 20545

R. D. Shull
Department of Energy
Division of Environmental Impacts
Washington, DC 20545

N. F. Simpson
Department of Energy
Office of Program Coordination
Washington, DC 20545

D. H. Slade
Department of Energy
Office of Biomedical and Environmental Research
Washington, DC 20545

H. F. Soule
Department of Energy
Office of the Asst. Sec. for Energy Technology
Washington, DC 20545

R. J. Stern
Department of Energy
Office of the Asst. Sec. for Environment
Washington, DC 20545

J. Swinebroad
Department of Energy
Office of Biomedical and Environmental Research
Washington, DC 20545

No. of Copies

E. J. Vallario
Department of Energy
Office of Biomedical and Environmental Research
Washington, DC 20545

A. R. Vincent
Department of Energy
Office of Planning Coordination
Washington, DC 20545

B. W. Wachholz
Department of Energy
Division of Policy Analysis
Washington, DC 20545

H. P. Wald
Department of Energy
Office of the Asst. Sec. for Federal Energy Regulatory Commission
Washington, DC 20545

S. Weinstein
Department of Energy
Office of the Asst. Sec. for Environment
Washington, DC 20545

W. W. Weyzen
Department of Biomedical and Environmental Research
Washington, DC 20545

J. C. Whitnah
Department of Energy
Office of the Asst. Sec. for Environment
Washington, DC 20545

T. Williams
Department of Energy
Division of Policy Analysis
Washington, DC 20545

E. Willis
Department of Energy
Office of the Asst. Sec. for Energy Technology
Washington, DC 20545

R. W. Wood
Department of Energy
Office of Biomedical and Environmental Research
Washington, DC 20545

No. of Copies

C. I. York
Department of Energy
Office of Biomedical and Environmental Research
Washington, DC 20545

F. R. Zintz
Department of Energy
Office of Biomedical and Environmental Research
Washington, DC 20545

Chief, Environmental and Sanitary Engineering Branch
Department of Energy
Washington, DC 20545

Robert F. Abbey, Jr.
Office of Nuclear Regulatory Research
U.S. Nuclear Regulatory Commission
Washington, DC 20545

J. S. Ball
Bartlesville Energy Research Center
Department of Energy
P.O. Box 1398
Bartlesville, OK 74003

E. W. Bean
Rocky Flats Area Office
DOE--Albuquerque Operations Office
P.O. Box 928
Golden CO 80401

A. W. Decora
Laramie Energy Research Center
Department of Energy
P.O. Box 3395
University Station
Laramie, WY 83071

P. B. Dunnaway
DOE--Nevada Operations Office
P.O. Box 14100
Las Vegas, NV 89114

B. M. Erickson
DOE--Schenectady Naval Reactors Office
P.O. Box 1069
Schenectady, NY 12301

D. M. Gardiner
DOE--Chicago Operations Office
9800 South Cass Avenue
Argonne, IL 60439

No. of Copies

M. E. Gates
DOE--Nevada Operations Office
P.O. Box 14100
Las Vegas, NV 89114

Dom M. Geraghty
Energy Analysis & Environment Division
Electric Power Research Institute
3412 Hillview Avenue
P.O. Box 10412
Palo Alto, CA 94303

G. H. Gronhovd
Grand Forks Energy Research Center
Department of Energy
Box 8213, University Station
Grand Forks, ND 58202

C. Jackson
DOE--San Francisco Operations Office
133 Broadway
Wells Fargo Building
Oakland, CA 94616

C. Hakkarinen
Environment Assessment Department
Electric Power Research Institute
3412 Hillview Avenue
P.O. Box 10412
Palo Alto, CA 94303

G. R. Hilst
Energy Analysis & Environment Division
Electric Power Research Institute
3412 Hillview Avenue
P.O. Box 10412
Palo Alto, CA 94303

J. A. Lenhard
DOE--Oak Ridge Operations Office
P.O. Box E
Oak Ridge, TN 37830

Mei-Kao Lin
Systems Applications, Inc.
950 Northgate Drive
San Rafael, CA 94903

Charles Miller
Environment Sciences/ Bldg. 2001
Oak Ridge National Laboratory
P.O. Box X
Oak Ridge, TN 37830

No. of Copies

A. A. Pitrolo
Morgantown Energy Research Center
Department of Energy
P.O. Box 880
Morgantown, WV 26505

R. Ray
DOE--Nevada Operations Office
P.O. Box 14100
Las Vegas, NV 89114

W. Reese
DOE--Savannah River Operations Office
P.O. Box A
Aiken, SC 29801

J. R. Roeder
DOE--Albuquerque Operations Office
P.O. Box 5400
Albuquerque, NM 87115

J. H. Spickard
DOE--Idaho Operations Commission
550 Second Street
Idaho Falls, ID 83401

J. F. Stevens
Dayton Area Office
DOE--Albuquerque Operations
P.O. Box 66
Miamisburg, OH 45342

I. Wender
Pittsburgh Energy Research Center
Department of Energy
4800 Forbes Avenue
Pittsburgh, PA 15213

27 DOE Technical Information Center

W. Singlevich
Air Force Technical Applications Center/ TD-4
Patrick Air Force Base
FL 32925

H. Mueller
Air Resources Laboratory
National Oceanic and Atmospheric Administration
Research Laboratories
P.O. Box 14985
Las Vegas, NV 89114

No. of Copies

L. Machta
Air Resources Laboratory
National Oceanic and Atmospheric Administration
8060 13th Street
Silver Spring, MD 20910

I. Van der Hoven
Air Resources Laboratory
National Oceanic and Atmospheric Administration
8060 13th Street
Silver Spring, MD 20910

L. Hodges
Ames Laboratory, U.S. ERDA
Iowa State University
Physics Bldg., Rm. A530
Ames IA 50010

P. Frenzen
Argonne National Laboratory
9700 S. Cass Avenue
Argonne, IL 60439

F. Gustafson
Argonne National Laboratory
9700 S. Cass Avenue
Argonne, IL 60439

W. K. Sinclair
Arginne National Laboratory
9700 S. Cass Avenue
Argonne, IL 60439

G. A. Briggs
Atmospheric Turbulence and Diffusion Laboratory
NOAA, Oak Ridge, TN 37830

F. I. Gifford
Atmospheric Turbulence and Diffusion Laboratory
NOAA, Oak Ridge, TN 37830

S. R. Hanna
Atmospheric Turbulence and Diffusion Laboratory
NOAA, Oak Ridge, TN 37830

I. Ophel
Atomic Energy of Canada Ltd.
Chalk River, Ontario, CANADA

R. V. Osborne
Atomic Energy of Canada Ltd.
Chalk River, Ontario, CANADA

Librarian, Bldg. 465
Atomic Energy Research Establishment
Harwell, Didcot
OXION OXII ORD, ENGLAND

No. of Copies

A. E. J. Eggleton
Atomic Energy Research Establishment
Harwell, Oxfordshire
OXIIORB, ENGLAND

D. H. Pierson
Atomic Energy Research Establishment
Harwell, Oxfordshire
OXIIORB, ENGLAND

G. H. Clark
Health Physics Research Section
A.A.E.C. Research Establishment
Private Mailbag, Sutherland
New South Wales 2232
AUSTRALIA

Librarian
Australian AEC
Post Office Coogee
New South Wales 2034
AUSTRALIA

U. C. Mishra
Head Air Monitoring Section
Bhabha Atomic Research Centre
Bombay-85 AS
INDIA

R. N. Sachdev
Air Monitoring Section
Bhabha Atomic Research Centre
Trombay, Bombay
400-085, INDIA

V. P. Bond
Brookhaven National Laboratory
Upton, Long Island
NY 11973

Librarian
Research Library, Reference
Brookhaven National Laboratory
Upton, Long Island,
NY 11973

C. B. Meinhold
Brookhaven National Laboratory
Upton, Long Island
NY 11973

No. of Copies

D. Beirman
Chief, Document Service Branch
Central Intelligence Agency
Attn: CRS/DPSD/DSB/IAS/409779/DB
Washington, DC 20505

W. Broecker
Columbia University
Lamong Geological Observatory
Palisades, NY 10964

Council on Environmental Quality
72 Jackson Place, N.W.
Washington, DC 20006

Librarian
Centre d'Etudes Nucléaires de Saclay
P.O. Box 2, Saclay
Fig-sur-Yvette (S&O)
FRANCE

M. Rzekiecki
Commissariat á l'Energie Atomique
Centre d'Etudes Nucléaires de Cadarache
BP n 13-St. Paul
Les Durance
FRANCE

Director
Commissiariat á l'Energie Atomique
Centre d'Etudes Nucléaires de Fontenay-aux-Roses (Seine)
FRANCE

Librarian
Commonwealth Scientific and Industrial Research Organization
314 Albert Street
P.O. Box 89
East Melbourne, Victoria
AUSTRALIA 3002

Director
Commonwealth Scientific and Industrial Research Organization
Aspendal, Victoria,
AUSTRALIA

No. of Copies

Capt. D. L. Moffett
Defense Nuclear Agency
HYBLA Valley Bldg.
6801 Telegraph Road
Alexandria, VA 23007

A. V. Dodd
Department of Army
U.S. Army Research Office
Environmental Sciences Division
Box CM Duke Station
Durham, NC 27706

M. P. Measures
Department of National Health and Welfare
Radiation Protection Division
Ottawa, CANADA

J. Shapiro
Department of Environmental Health Sciences
School of Public Health
Harvard University
Boston, MA 02115

L. Jeanmaire
D.P.S. - S.C.S.
B.P. 6, Fontenay-aux-roses
(Seine) FRANCE

J. F. Willing
Rockwell International
Rocky Flats Plant
Golden, CO 90401

C. M. Patterson
E. I. DuPont de Nemours and Company
Savannah River Plant
Aiken, SC 29801

Technical Information Service
Room 773A
Savannah River Laboratory
E. I. DuPont de Nemours and Company
Aiken, SC 29801

E. Wllauschek
ENEA (OECD) Health and Safety Office
38, Blvd. Suchet
Paris IVI,
FRANCE

R. C. Yoder
Rockwell International
P.O. Box 888
Golden, CO 80401

No. of Copies

T. V. Crawford
Environmental Transport
Savannah River Laboratory
E. I. DuPont de Nemours
Aiken, SC 29801

C. D. Kerns
Environmental Transport
Savannah River Laboratory
E. I. DuPont de Nemours
Aiken, SC 29801

D. D. Dominick
Environmental Protection Agency
Office of Categorical Programs
Washington, DC 20460

W. Mills
Environmental Protection Agency
Washington, DC 20460

D. Smith
Environmental Protection Agency
Washington, DC 20460

Environmental Protection Agency/NERC, Meteorology Laboratory
Research Triangle Park, NC 27711

Harold Barkhau
Air Pollution Technical Information Center
U.S. Environmental Protection Agency
Research Triangle Park, NC 27711

W. Cotton
Experimental Meteorology Laboratory
University of Miami Branch
NOAA P.O. Box 8044
Coral Gables, FL 33124

W. Woodley
Experimental Meteorology Laboratory
University of Miami Branch
NOAA P.O. Box 8044
Coral Gables, FL 33124

J. W. Winchester
Florida State University
Department of Oceanography
Tallahassee, FL 32306

No. of Copies

K. Edvarson
Forsvarets Forskingsanstalt
Research Institute of Nation Defense
Avdelning 4, Stockholm 80
SWEDEN

R. G. Semonin
Illinois State Water Survey
Box 232
Urbana, IL 61801

J. W. McCaslin
INEL, Aerojet Nuclear
550 Second Street
Idaho Falls, ID 83401

C. F. Junge
Institut für Chemie
65 Mainz
Saarstrasse 23,
Postfach 3060
WEST GERMANY

S. Beilke
Umveltbundesomt-Pilotstation Frankfurt
6 Frankfurt/Main
Feldbergstrasse 45,
WEST GERMANY

H. W. Georgii
Institut für Meteorologie und Geophysik der Johann Wolfgang Geothe Universitat
600 Frankfurt am Main
Feldbergstrasse 47,
WEST GERMANY

H. Daw
Director, Division of Health, Safety and Waste Management
International Atomic Energy Agency
Vienna 1, Kaerntnerring 11,
AUSTRIA

J. Z. Minczewski
International Atomic Energy Agency
Vienna 1, Kaerntenerring 11,
AUSTRIA

Director, Division of Health Safety and Waste Management
International Atomic Energy Agency
Vienna, 1, Kaerntnerring 11,
AUSTRIA

No. of Copies

E. L. Alpen
Lawrence Berkley Laboratory
University of California
Building 90, Room 2056
No. 1 Cyclotron Road
Berkely, CA 94720

Librarian
Lawrence Radiation Laboratory
University of California
Technical Information Dept., L-3
P.O. Box 808
Livermore, CA 94550

M. L. Mendelsohn
University of California
Lawrence Livermore Laboratory
P.O. Box 808
Livermore, CA 94550

L. Anspaugh
Lawrence Livermore Laboratory
University of California
P.O. Box 808
Livermore, CA 94550

R. E. Heft
Lawrence Livermore Laboratory
University of California
P.O. Box 808
Livermore, CA 94550

J. B. Knox
Lawrence Livermore Laboratory
University of California
P.O. Box 808
Livermore, CA 94550

S. Barr
Los Alamos Scientific Laboratory
University of California
P.O. Box 1663
Los Alamos, NM 87544

J. W. Healy
Los Alamos Scientific Laboratory
University of California
P.O. Box 1663
Los Alamos, NM 87544

Librarian
Los Alamos Scientific Laboratory
P.O. Box 1663
Los Alamos, NM 87544

No. of Copies

G. L. Voelz
University of California
Los Alamos Scientific Laboratory
P.O. Box 1663
Los Alamos, NM 87545

Dr. Roger O. McClellan
Inhalation Toxicology Research Institute
Lovelace Foundation for Medical Education and Research
P.O. Box 5890
Albuquerque, NM 87115

H. W. Kirby
Mound Laboratory
Monsanto Research Corporation
Miamisburg, OH 45345

David Rall, Director
NIEHS
P.O. Box 12233
Research Triangle Park, NC 27709

P. La Fleur
National Bureau of Standards
Nuclear Reactor Laboratory
Gaithersburg, MD 20760

W. R. Ney
Executive Director
National Council on Radiation Protection and Measurements
7910 Woodmont Avenue
Suite 1061
Washington, DC 20014

J. Z. Holland
National Oceanic and Atmospheric Administration
North Bethesda Office Center
11420 Rockville Heights
Rockville, MD 20852

NRC Advisory Committee on Reactor Safeguards
Washington, DC 20555

R. Alexander
Nuclear Regulatory Commission
Washington, DC 20545

No. of Copies

2 J. J. Davis
Assistant Director of Research
Nuclear Regulatory Commission
Washington, DC 20545

W. Cool
Nuclear Regulatory Commission
Washington, DC 20545

S. I. Auerbach
Oak Ridge National Laboratory
P.O. Box X
Oak Ridge, TN 37830

J. A. Auxier
Oak Ridge National Laboratory
P.O. Box X
Oak Ridge, TN 37830

G. D. O'Kelley
Oak Ridge National Laboratory
P.O. Box X
Oak Ridge, TN 37830

C. R. Richmond
Oak Ridge National Laboratory
P.O. Box X
Oak Ridge, TN 37830

K. A. Smith
Sandia Laboratories
P.O. Box 5800
Albuquerque, NM 87115

J. T. Goll
Hydrology-Meteorology Branch
USNRC
Washington, DC 20555

D. Lal
Physical Research Laboratory
Nvrangpura
Ahmedabad-9, INDIA

P. K. Kuroda
University of Arkansas
Department of Chemistry
Fayetteville, AR 72701

R. C. Srivastava
University of Chicago
Laboratory for Atmospheric Probing
Geophysical Sciences
5734 S. Ellis Avenue
Chicago, IL 60637

No. of Copies

F. I. Badgley
University of Washington
Department of Atmospheric Sciences
Seattle, WA 98195

Leo Bustad, Dean
College of Veterinary Medicine
Washington State University
Pullman, WA 99163

J. E. Tillman
University of Washington
Department of Atmospheric Sciences
Seattle, WA 98195

E. Held
U.S. NRC Directorate Regulatory Standards
Washington, DC 20545

E. P. Hardy, Jr.
DOE Health and Safety Laboratory
376 Hudson Street
New York, NY 10012

J. H. Harley
DOE Health and Safety Laboratory
376 Hudson Street
New York, NY 10012

P. W. Krey
DOE Health and Safety Laboratory
376 Hudson Street
New York, NY 10012

C. W. Sill
U.S. DOE Idaho Operations Office
Idaho Falls, ID 93401

B. Baskin
Wayne County Department of Health
Air Pollution Control Division
1311 E. Jefferson
Detroit, MI 48207

Librarian
World Meteorological Organization
Geneva, 20
Case Postale No. 5, CH-1211
SWITZERLAND

No. of Copies

Paul Michael
Meteorology Group
Brookhaven National Laboratory
Upton, NY 11975

H. W. Hoffman
Oak Ridge National Laboratory
P.O. Box Y
Oak Ridge, TN 37830

R. J. Engelmann
Environmental Research Laboratories
National Oceanic and Atmospheric Administration
Boulder, CO 80302

J. Davis
Nuclear Regulatory Commission
5650 Nicholson Lane
Rockville, MD 20854

J. D. Macdougall
University of California San Diego
P.O. Box 1529
La Jolla, CA 92037

J. W. Keizur
Sandia Laboratories
P.O. Box 5800
Albuquerque, NM 87115

W. G. N. Slinn
Air Resources Center
Oregon State University
Corvallis, OR 97331

M. A. Wolf
Air Resources Center
Oregon State University
Corvallis, OR 97331

A. N. Dingle
Department of Atmospheric and Oceanic Science
University of Michigan
Ann Arbor, MI 48104

T. Lyons
School of Environmental & Life Sciences
Murdock University
Murdock,
WESTERN AUSTRALIA 6153

No. of Copies

V. V. Shirvaikar
Meteorology Group
Environmental Studies Section
Bhabha Atomic Research Centre
Bombay-85 AS, INDIA

C. Miller
Oak Ridge National Laboratory
Building 2001, P.O. Box X
Oak Ridge, TN 37830

J. K. Munro, Jr.
Oak Ridge National Laboratory
P.O. Box X
Oak Ridge, TN 37830

A. C. Chamberlain
Environmental and Medical Sciences Division
OX11 ORA
AERA Harwell, Oxfordshire
ENGLAND

Director
National Institute of Radiological Sciences
4-9-1, Anagawa
Chiba-Shi
JAPAN

Librarian
Australian AEC
Riverina Laboratory
P.O. Box 226
Denliquin
New South Wales
AUSTRALIA 2710

A. M. Marko
Director
Atomic Energy of Canada Ltd.
Biology and Health Physics Division
Chalk River Nuclear Laboratories
Chalk River, Ontario
K0J 1J0
CANADA

F. D. Sowby
International Commission on Radiological Protection
Clifton Avenue
Sutton, Surrey
ENGLAND

No. of Copies

G. W. Dolphin
National Radiological Protection Board
Harwell, Didcot
Oxfordshire OX11 ORQ
ENGLAND

J. Durham
U.S. Environmental Protection Agency
National Environmental Research Center
Research Triangle Park, NC 27711

J. D. Macdougall
Scripps Institution of Oceanography
Geological Research Division
P.O. Box 1529
La Jolla, CA 92037

B. B. Hicks
Atmospheric Physics Section
Argonne National Laboratory
9700 Cass Avenue
Argonne, IL 60439

J. E. Flinn
Battelle Memorial Institute
Columbus Laboratories
505 King Avenue
Columbus, OH 43201

Librarian
Battelle Memorial Institute
Columbus Laboratories
505 King Avenue
Columbus, OH 43201

R. S. Paul
Battelle Memorial Institute
Columbus Laboratories
505 King Avenue
Columbus, OH 43201

G. W. Duncan
Battelle Human Affairs Research Centers
4000 N.E. 41st Street
P.O. Box 5395
Seattle, WA 98105

No. of Copies

J. E. Rasmussen
Battelle Human Affairs
Research Centers
4000 N.E. 41st Street
P.O. Box 5395
Seattle, WA 98105

J. L. Hebert
Battelle Human Affairs
Research Centers
4000 N.E. 41st Street
P.O. Box 5395
Seattle, WA 98105

S.M. Nealey
Battelle Human Affairs
Research Center
4000 N.E. 41st Street
P.O. Box 5395
Seattle, WA 98105

C. Shorrock
Battelle-Geneva
Geneva Research Centre
7, Route de Drize
1227 Carogue-Geneva
SWITZERLAND

S. Hartwig
Battelle- Institute e.V
Am Romerhof 35
6000 Frankfurt am Main 90
GERMANY

Director
Joint Center for
Graduate Study
100 Sprout Road
Richland, WA 99352

No. of Copies

ONSITE

7 DOE Richland Operations Office

P.F.X. Dunigan
N. W. Fraser
J. L. Landon
H. E. Ransom
F. R. Standerfer
J. D. White

3 Rockwell Hanford Operations

D. J. Brown
R. D. Fox
R. E. Isaacson

3 Hanford Environmental Health Foundation

B. Breitenstein
P. A. Fuqua
W. D. Norwood

217 Pacific Northwest Laboratory

T. W. Ambrose
W. J. Bair (20)
N. E. Ballou
N. E. Carter
D. B. Cearlock
J. P. Corley
R. L. Drake (40)
C. E. Elderkin
J. W. Finnigan
J. C. Fox

No. of Copies

J. J. Fuquay
A. G. Gibbs
R. K. Hadlock (15)
J. M. Hales
A. J. Haverfield
D. L. Hessel
J. V. Larson
J. D. Ludwick
S. Marks
R. P. Marshall
J. M. Nielsen
R. E. Nightingale
D. E. Olesen
J. F. Park
H. M. Parker
P. R. Partch
R. W. Perkins
M. R. Peterson
P. M. Potter (10)
L. A. Rancitelli
W. D. Richmond
L. C. Schwendiman (20)
C. L. Simpson (40)
J. R. Sletager
R. A. Stokes (15)
W. L. Templeton
R. C. Thompson
C. M. Unruh
B. E. Vaughan
E. C. Watson
L. L. Wendell (10)
W. R. Wiley
J. A. Young
Biology Library (2)
Technical Information (5)
Publishing Coordination (2)